IL
NUOVO CIMENTO
ORGANO DELLA SOCIETÀ ITALIANA DI FISICA
SOTTO GLI AUSPICI DEL CONSIGLIO NAZIONALE DELLE RICERCHE

VOL. VIII, N. 3 *Serie nona* 1 Marzo 1951

Lo spettro di energia delle particelle emesse nella reazione ${}^6_3\mathrm{Li}(n,\alpha){}^3_1\mathrm{H}$.

U. FACCHINI, E. GATTI e E. GERMAGNOLI
Laboratori C.I.S.E. - Milano

(ricevuto il 1° Dicembre 1950)

Riassunto. — Lo spettro di energia dei prodotti della reazione nucleare

$$ {}^6_3\mathrm{Li} + {}^1_0n \rightarrow {}^4_2\mathrm{He} + {}^3_1\mathrm{H} + \mathrm{Q} $$

indotta da neutroni lenti, è stato ricavato per mezzo di una camera di ionizzazione a collezione di elettroni munita di griglia. Si sono ottenuti per le energie delle particelle α e ${}^3_1\mathrm{H}$ i valori

$$ E_\alpha = \frac{3}{7} Q = 2{,}059 \pm 0{,}010 \text{ MeV} $$

$$ E_{{}^3_1\mathrm{H}} = \frac{4}{7} Q = 2{,}745 \pm 0{,}013 \text{ MeV} $$

corretti per le perdite di energia per ionizzazione nello strato emittente. Questi sono in accordo coi valori ricavati dai range delle stesse particelle, in base alle curve range-energia di Jesse e Sadauskis.

1. – Come è noto, il nucleo ${}^6_3\mathrm{Li}$ in seguito a cattura di un neutrone lento dà luogo alla reazione nucleare

$$ {}^6_3\mathrm{Li} + {}^1_0n \rightarrow {}^4_2\mathrm{He} + {}^3_1\mathrm{H} + Q . $$

Poichè finora sono state eseguite misure precise soltanto del range dei prodotti di questa reazione [1] ci è apparsa interessante una determinazione indipendente della loro energia. Fra l'altro ciò permette di controllare due punti

[1] J. K. BÖGGILD e L. MINNHAGEN: *Phys. Rev.*, **75**, 782 (1949).

delle curve range-energia per particelle α e protoni date recentemente da JESSE e SADAUSKIS (2).

È stata utilizzata una camera di ionizzazione a collezione di elettroni, munita di griglia (3). Sull'elettrodo a tensione della camera vennero collocati insieme, adiacenti, uno strato di LiF, depositato mediante evaporazione nel vuoto sopra un dischetto di acciaio inossidabile lavorato otticamente, e uno

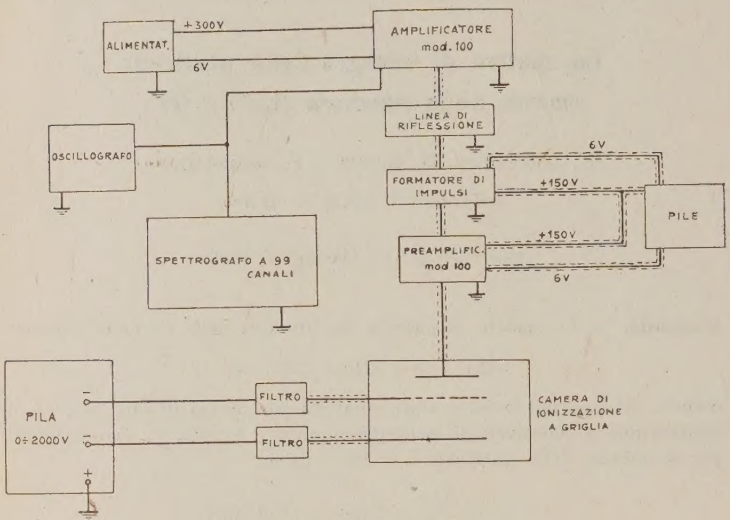

Fig. 1. – Schema di assieme del circuito.

di UO_3, ottenuto per deposizione elettrolitica. Entrambi gli strati erano dello spessore di circa 0,02 mg cm^{-2}: con strati così sottili l'assorbimento delle particelle entro il preparato ha qualche importanza solo per le particelle α del Li, come verrà discusso in seguito. Lo strato di UO_3 ha lo scopo di fornire particelle α di energia nota, onde permettere la taratura assoluta della scala di energia del sistema di misura.

La camera di ionizzazione, riempita a 6 atmosfere di Argon, purificato con circolazione su Calcio a 300 °C, venne collocata in una cavità in paraffina e sottoposta a un flusso di neutroni termici ottenuti da una sorgente di 500 mg di Raα + Be. I particolari della disposizione sperimentale sono riferiti nel lavoro più sopra citato (3).

In queste condizioni venne rilevato lo spettro di energia dei prodotti della scissione del Litio e quello delle particelle α dell'Uranio.

---

(2) W. P. JESSE e J. SADAUSKIS: *Phys. Rev.*, **78**, 1 (1950).
(3) U. FACCHINI e E. GATTI: *Nuovo Cimento*, **7**, 589 (1950).

2. – Diamo in fig. 1 lo schema di assieme del circuito utilizzato.

Il sistema di amplificazione comprende un preamplificatore e un amplificatore mod. 100, con tempo di salita di circa 0,6 μs e guadagno massimo di circa 10^6, collegati mediante una linea di riflessione con tempo di riflessione variabile tra 3 e 6 μs per la formazione dell'impulso. In tutte le misure si utilizzò un tempo di riflessione di 6 μs, cioè superiore al tempo di salita degli impulsi che era $1 \div 2$ μs per le particelle α, e di circa 4 μs per i tritoni. Le ampiezze degli impulsi vennero analizzate per mezzo dello spettrografo a 99 canali, descritto in una precedente nota [4].

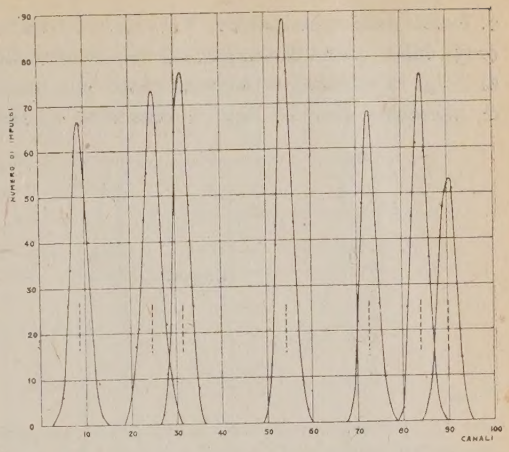

Fig. 2*A* Picchi ottenuti collegando la griglia della camera di ionizzazione ad un generatore di impulsi campione.

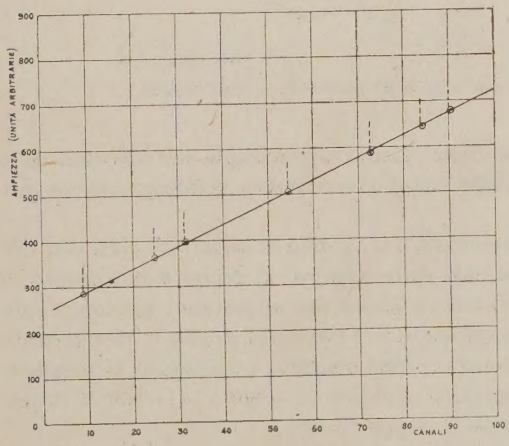

Fig. 2*B* Ampiezze degli impulsi campione misurate con uno strumento di classe 0,2 riportate in funzione del numero d'ordine del canale corrispondente dello spettrografo.

Per controllare la stabilità e la linearità del sistema di amplificazione e di registrazione, e per valutare l'entità della dispersione introdotta dal sistema stesso, prima e dopo di ogni misura la griglia della camera di ionizzazione venne connessa direttamente ad un generatore di impulsi ricavando così sull'elettrodo collettore impulsi artificiali di ampiezza variabile. Facendo variare questa in modo noto e lasciando inalterate le caratteristiche di ingresso della catena di amplificazione si definiva una scala di energie in corrispondenza

(4) E. GATTI: *Nuovo Cimento*, **7**, 655 (1950).

ai canali dello spettrografo. Tale scala è risultata lineare e la distorsione introdotta dalla catena di amplificazione e registrazione apparve in ogni caso inferiore al 3 °/₀₀; la stabilità è risultata entro tale limite anche per misure della durata di parecchie ore. Le figg. 2 illustrano il metodo di controllo qui descritto.

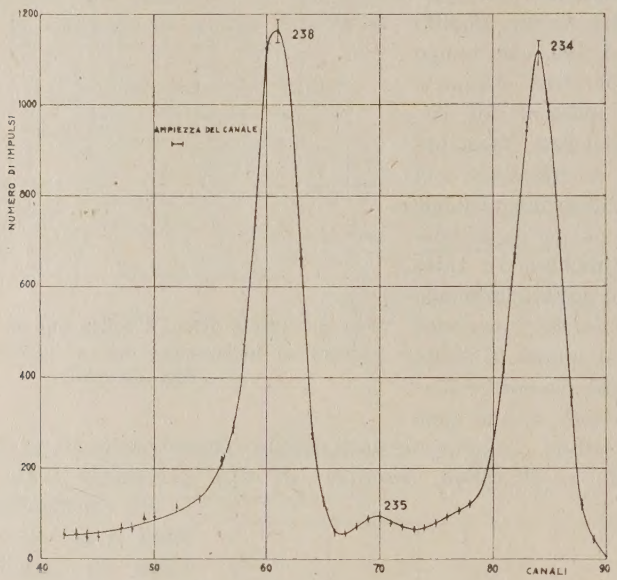

Fig. 3. – Spettro di energia delle particelle α dell'Uranio.

3. – Riportiamo in fig. 3 uno spettro ottenuto collocando sull'elettrodo della camera uno strato di solo UO_3, allo scopo di controllare il funzionamento dell'intero apparato.

In figg. $4A$ e $4B$ sono rappresentati due esempi di spettri ottenuti con LiF e UO_3 contemporaneamente presenti nella camera. Il primo è il risultato di una misura eseguita nelle condizioni di lavoro più opportune: tensioni applicate -1800 V sull'elettrodo emittente e -1200 sulla griglia e riempimento con Argon a 6 atmosfere. Il secondo è stato ottenuto dimezzando la pressione e di conseguenza riducendo le tensioni applicate a -900 V e -600 V rispettivamente per mantenere costante il rapporto E/p.

Confrontando i due spettri si osserva che le righe dovute alle particelle α dell'Uranio e del Litio non si sono sensibilmente spostate; la riga dei tritoni è invece distorta nel secondo caso poichè alla pressione di 3 atmosfere queste particelle non esauriscono il range nello spazio tra elettrodo emittente e griglia. Il confronto tra i due spettri prova l'indipendenza del guadagno dell'amplificatore dai tempi di salita, che sono funzioni delle lunghezze delle traiettorie,

e la sufficiente purezza dell'Argon, in quanto la presenza di impurità, se dotate di affinità elettronica, dovrebbe causare un sensibile spostamento di tutte le righe verso le basse energie nel primo caso rispetto al secondo.

Una correzione va apportata ai valori delle energie che si ottengono dagli spettri per tener conto dello spostamento dei massimi delle righe dovuto all'assorbimento delle particelle negli strati emittenti. La «forma della riga» calcolata considerando le particelle monoenergetiche generate uniformemente e isotropicamente nello strato venne pesata sopra una distribuzione gaussiana delle ampiezze degli impulsi intorno al loro valore più probabile, quale è data dalla catena di amplificazione e di registrazione. Si è assunta per tale distribuzione una deviazione standard di circa il 2,5%, quale è stata misurata usando gli impulsi artificiali.

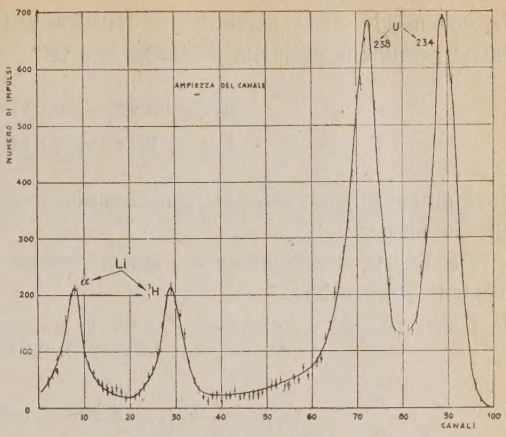

Fig. 4*A*. – Spettro di energia dei prodotti di scissione della reazione ${}^{6}_{3}\mathrm{Li}(n, \alpha){}^{3}_{1}\mathrm{H}$ e delle α dell'Uranio. Riempimento con Argon a 6 atm. Tensioni applicate: — 1 800 V all'elettrodo emittente — 1 200 V alla griglia.

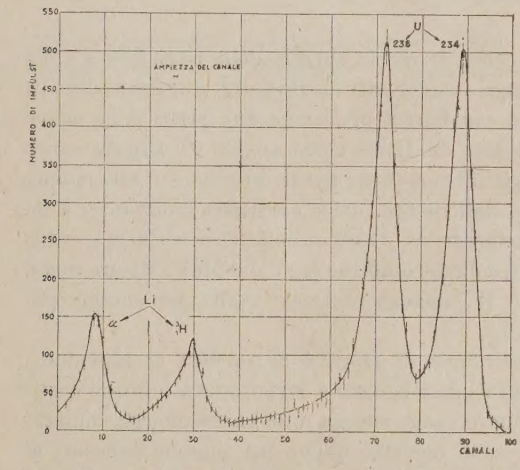

Fig. 4*B*. – Spettro di energia dei prodotti di scissione della reazione ${}^{6}_{3}\mathrm{Li}(n, \alpha){}^{3}_{1}\mathrm{H}$ e delleparticelle α dell'Uranio. Riempimento con Argon a 3 atm. Tensioni applicate: — 900 V all'elettrodo emittente e — 600 V alla griglia.

Si è ottenuto in definitiva che le energie ricavate dai massimi della curva spettrale vanno corrette del 3 ‰ per le particelle α dell'Uranio e per i tritoni, mentre per le α del Litio la correzione è più importante, ossia del 2%.

4. – Mediando i risultati relativi a 15 determinazioni, ottenute in varie condizioni di campo e pressione, e assumendo 4,180 MeV e 4,763 MeV

per le energia delle particelle α dell'Uranio [5] si sono ottenuti i seguenti valori per le energie delle particelle α e ${}^3_1H$.

$$E_\alpha = 2{,}051 \pm 0{,}017 \text{ MeV},$$
$$E_{{}^3_1H} = 2{,}748 \pm 0{,}014 \text{ MeV},$$

dove gli errori sono calcolati considerando lo scarto quadratico medio relativo alle 15 misure.

Da questi si ottengono i seguenti valori per l'energia Q liberata nella reazione ${}^6_3Li(n, \alpha){}^3_1H$:

$$Q_\alpha = \frac{7}{3} E_\alpha = 4{,}786 \pm 0{,}043 \text{ MeV},$$

$$Q_{{}^3_1H} = \frac{7}{4} E_{{}^3_1H} = 4{,}809 \pm 0{,}024 \text{ MeV},$$

da cui si hanno in definitiva i seguenti valori medi ponderati:

$$Q = 4{,}804 \pm 0{,}022 \text{ MeV},$$
$$E_\alpha = \frac{3}{7} Q = 2{,}059 \pm 0{,}010 \text{ MeV},$$
$$E_{{}^3_1H} = \frac{4}{7} Q = 2{,}745 \pm 0{,}013 \text{ MeV}.$$

Confrontando i valori da noi ottenuti per le energie delle particelle α e ${}^3_1H$ con i corrispondenti valori dei range determinati da BÖGGILD e MINNHAGEN [1] in camera di Wilson, si ritrovano con buona precisione due punti delle curve range-energia per le α e i protoni date da JESSE e SADAUSKIS [2]. Queste curve sono basate sull'ipotesi che l'energia W necessaria per la creazione di una coppia di ioni sia indipendente in Argon dall'energia della particella ionizzante. Tale ipotesi è stata controllata recentemente da JESSE e coll. [6] e verificata entro l'incertezza dello 0,5% per energie delle α comprese tra 5 e 9 MeV. Misure meno dirette fanno inoltre ritenere che W rimanga costante anche per energie più basse, e fino ad almeno 1 MeV [6].

Il fatto che sulle curve range-energia di JESSE e SADAUSKIS si adattano i punti ottenuti per mezzo dei risultati di BÖGGILD e MINNHAGEN e nostri costituisce un'ulteriore prova che le curve range-energia e le curve energia-ionizzazione ottenuta da JESSE e coll. sono corrette anche per energie inferiori ai 5 MeV.

---

[5] G. T. SEABORG e I. PERLMAN: *Rev. Mod. Phys.*, **20**, 585 (1948).
[6] W. P. JESSE, N. FORSTAT e J. SADAUSKIS: *Phys. Rev.*, **77**, 782 (1950).

Il valore di Q è pure stato calcolato da TOLLESTRUP e coll. (7) usando valori noti delle energie liberate in alcune reazioni nucleari. Detti autori ricavano per Q il valore

$$Q = 4{,}788 \pm 0{,}023 \text{ MeV},$$

che è in buon accordo con il nostro.

Ringraziamo il prof. BOLLA per l'interessamento dimostrato per il presente lavoro.

---

(7) A. TOLLESTRUP, W. A. FOWLER e C. C. LAURITSEN: *Phys. Rev.*, **76**, 428 (1950).

SUMMARY

The energy spectrum of ${}^{6}_{3}\text{Li}(\text{n}, \alpha){}^{3}_{1}\text{H}$ nuclear reaction has been determined by means of a gridded ionization chamber. The following values, corrected for energy losses in the emitting layers, have been obtained for the energies of α and ${}^{3}_{1}\text{H}$ particles:

$$E_{\alpha} = 2{,}059 \pm 0{,}010 \text{ MeV}$$
$$E_{{}^{3}_{1}\text{H}} = 2{,}745 \pm 0{,}013 \text{ MeV}$$

These values agree with known range values of the same particles, if Jesse and Sadauskis range-energy curves are used for the comparison.

A Further Theoretical Contribution to the Photodisintegration of H^3 and He^3 (*).

M. VERDE

Swiss Federal Institute of Technology - Zürich, Switzerland

(ricevuto il 1° Dicembre 1950)

Summary. — Integral formulae for the two averages $\bar{\sigma} = \int \sigma(E)\, dE$ and $\bar{E} = \frac{1}{\bar{\sigma}} \int E\, \sigma(E)\, dE$ in the electrical dipole transition from the ground state H^3 and He^3 are deduced. Some numerical values of $\bar{\sigma}$ are computed for three types of static potentials.

The theoretical possibilities for the choice of the nuclear potential are most directly restricted by the configurations of two nucleons. It is neverthless very important to check the validity of the potential derived from the two body experiments against the experiments involving three nucleons. One reason for this is that three-body problems are more sensitive than the corresponding two body problems to the dependence of the nuclear forces on the exchange of spin or space coordinates. Furthermore three-body problems should be able to give the most direct answer to the important question whether the nuclear potentials are simply additive or whether the so called « many-body » forces play no small part therein.

It is a fortunate circumstance that three nucleons, form two bound states (H^3 and He^3) and that these two nuclei should at present, at least in some countries, be available in reasonable quantities.

It is higly desirable that a systematic experimental investigation of these nuclei be carried out in order that profitable results may accrue from the efforts made on the theoretical plane.

(*) This paper was presented at the Oxford meeting for Nuclear Physics (September (1950).

We have already good experimental knowledge of the spins of H^3 and He^3, $J = 1/2$ for both nuclei, as well as of their magnetic moments which have been measured very accurately. It is still possible to improve our knowledge of H^3 and He^3 by means of experiments on the photo-disintegrations of these nuclei. We have data which refer to the inverse processes, namely to the formation of H^3 and He^3 by radiative capture of a nucleon from a deuteron in its ground state. We know that the cross-section for the capture of thermal neutrons by deuterons is extremely small, and also from a recent paper by LAURITSEN [1] and collaborators, that the γ rays emitted in the capture of protons by deuterons have, in the proton energy range between $0.5 \div 1.5$ MeV, an angular distribution according to practically a pure $\sin^2 \vartheta$ law.

There are some theoretical papers which attempt to deal with three-body problems, but most of them are unduly complicated owing to the fact that their authors fail to take into account all of the constants of motion. Generally they do not give sufficient importance to different symmetry classes of the eigenfunctions, despite the fact that for a long time, expecially by WIGNER, attention has been directed to this point. Furthermore, it often happens that one makes from the very beginning an assumption as to the form of the eigenstates – in saying so we refer to the so called group structure introduced by WHEELER. – This implies the loss of the general features of the phenomenon and the impossibility of generalising methods well established in the theory of two-body problems. It is to be recommended that use be made of the isotopic spin formalism, despite the fact that not only the experimentalists but also some theoreticians have an avversion to it. By using it, the different symmetry classes of the eigenfunctions which enter into the problem emerge from the very beginning. The theoretical treatment without isotopic spin formalism must of course become the same if one puts a posteriori into evidence the different components belonging to a given symmetry class. Often one of these components is by far the most important one and thus mainly responsible for a given phenomenon. Consequently restrictions like the resonating group structure may often, especially for bound states, be unjustfied and dangerous.

We are interested at first in the general aspect of the problem, and we shall put aside effects which have minor importance. It is to be assumed that the ground state is predominantly an S state. The spin is 1/2, as already mentioned, the isotopic spin must be also 1/2. The z component of the magnetic moment of a three nucleon system in an S state is [2]

$$\mu = \sum_1^3{}_k \sigma_z^{(k)} \left(\frac{1 + \tau_z^{(k)}}{2} \mu_P + \frac{1 - \tau_z^{(k)}}{2} \mu_N \right) = \frac{\mu_P + \mu_N}{2} \sigma_z^s + \frac{\mu_P - \mu_N}{3} \left(\frac{\sigma_z^{(s)} \tau_z^{(s)}}{2} + 2S \right),$$

(1) W. FOWLER *and al.*: *Phys. Rev.*, **76**, 1767 (1949).

(2) M. VERDE: *Nuovo Cimento*, **7**, 283 (1950); *Helv. Phys. Acta*, **23**, 453 (1950).

where

$$2S = \sigma_z' \tau_z' + \sigma_z'' \tau_z'' ,$$

$$\sigma_z^s = +1 , \quad \tau_z = \mp 1 \quad \text{for } H^3 \text{ respect. } He^3 .$$

S changes sign too with τ_z^s so that the magnetic moments of He^3 for a given state are obtained from those of H^3 changing μ_P in μ_N.

For H^3 is

$$\mu = \frac{2\mu_N + \mu_P}{3} + \frac{2}{3}(\mu_P - \mu_N) S .$$

In the case of $S = 1/2$, $T = 1/2$ all the three classes of the symmetric group of three elements are allowed. These classes are the totally symmetrical, the totally antisymmetrical, and a two-dimensional one (D).

We write for the most general eigenfunction in this state [3]

$$\psi = \psi^s \xi^a + (\psi' \xi'' - \psi'' \xi') + \psi^a \xi^s .$$

The ξ's are the eigenfunctions in the product space of the ordinary and the isotopic spin. ψ' and ψ'' transform under permutation of the coordinates according to the representation D. $(\xi'', -\xi')$ transform according to $-D$ and $(\psi'\xi'' - \psi''\xi')$ is totally antisymmetrical as it must be according to the Pauli principle. Now

$$\xi' * S \xi' = 0 , \quad \xi'' * S \xi'' = 0 , \quad \xi^s * S \xi^s = -1 , \quad \xi^a * S \xi^a = +1 .$$

For the magnetic moments one has respectively

$$\mu = \mu_P \qquad \text{for} \quad \psi^s ,$$

$$\mu = \frac{2\mu_N + \mu_P}{3} = -0{,}13\,\mu_P \qquad \text{for} \quad (\psi', \psi'')$$

$$\mu = -\frac{\mu_P}{3} + \frac{4}{3}\mu_N = -1{,}25\,\mu_P \qquad \text{for} \quad \psi^a ,$$

$\mu = 1.068\,\mu_P$ is the experimental value of the m.m. of the triton. That means that the ground state must be predominantly a completely symmetrical one; any admixture of two-dimensional or totally antisymmetrical states has the result to make a contribution in the wrong direction. The same considerations apply to the He^3 nucleus which has a m.m. $\mu = 1.11\,\mu_N$.

A remarkable fact is that ξ^a is an eigenfunction of S [3]. One has $S\xi^a = \xi^a$ for H^3. This is not the case for the other states. The immediate consequence of this circumstance is that a magnetic S-S dipole transition from a state totally symmetrical in space is forbidden. The observed very

---

[3] M. VERDE: *Helv. Phys. Acta*, 22, 339 (1949).

low capture cross section of deuterons by thermal neutrons is hence an other evidence in favour of the suspected prevalence of the symmetrical state [4].

The electric dipole moment which one needs for the cross section is proportional to

$$\sqrt{\hbar\omega}\,(\tau_z' r_z + \tau_z'' q_z)\,,$$

z- is the direction of polarisation of the γ-quantum.

The purpose of this paper is to give rigorous formulae for the integrated cross-section $\int_0^\infty \sigma(E)\,\mathrm{d}E$ and for the mean energy

$$\bar{E} = \frac{\int E\sigma(E)\,\mathrm{d}E}{\int \sigma(E)\,\mathrm{d}E}\,.$$

One has to generalize the sum rules which are well known for two-body problems.

Let us put

$$M_z = \tau_z' r_z + \tau_z'' q_z \qquad \text{and} \qquad P_z = \frac{\hbar}{i m_r}\,(\tau_z' p_{r_z} + \tau_z'' p_{q_z})\,,$$

where r_z and q_z are defined by

$$r_z = \frac{\sqrt{3}}{2}\,(\mathbf{r}_3 - \mathbf{r}_2)_z\,, \qquad q_z = \left\{ -\mathbf{r}_1 + \frac{1}{2}\,(\mathbf{r}_2 + \mathbf{r}_3) \right\}_z\,,$$

and p_{r_z}, p_{q_z} are the coniugate momenta, $m_r = (2/3)M_p$ is the reduced mass in our reference system.

One has

$$\frac{\hbar}{i}\,\dot{M}_z = [H, M_z]\,. \tag{2}$$

H being the Hamiltonian of the three-body problem, equal to the sum of the kinetic energy T and the potential energy W

$$H = T + W\,.$$

One has

$$[T, M_z] = \left[\frac{p_{r_z}^2 + p_{q_z}^2}{2m_r},\ (\tau_z' r_z + \tau_z'' q_z)\right] = \frac{1}{2m_r}\,\{\tau_z'[p_{r_z}^2, r_z] + \tau_z''[p_{q_z}^2, q_z]\} = \tag{3}$$

$$= \frac{\hbar}{i m_r}\,(\tau_z' p_{r_z} + \tau_z'' p_{q_z}) = P_z\,.$$

---

[4] I should like to add that S-S magnetic dipole transitions to or from a bound state which is totally symmetrical in space, are always forbidden, except in the case of deuterons, as has kindly been pointed out to me by Prof. WIGNER.

We put furthermore

$$S = [W, M_z] , \tag{4}$$

and remark as W and M_z are real symmetrical operators, that S is a real antisymmetrical operator.

For a given transition from the ground state 0, to a final state n, one has as consequence of (2), (3), (4):

$$-\hbar\omega_{0n} \cdot \langle 0 \mid M_z \mid n \rangle = \langle 0 \mid P_z + S \mid n \rangle . \tag{5}$$

$\hbar\omega_{0n}$ is the energy absorbed in the transition. We now multiply by $\langle n \mid M_z \mid 0 \rangle$ and sum over all final states

$$-\sum_n \hbar\omega_{0n} \mid \langle 0 \mid M_z \mid n \rangle \mid^2 = \langle 0 \mid (P_z + S) M_z \mid 0 \rangle . \tag{6}$$

We can further write

$$\langle 0 \mid P_z M_z \mid 0 \rangle = \frac{h}{im_r} \langle 0 \mid \tau_z'^2 p_{r_z} r_z + \tau_z''^2 p_{q_z} q_z + \tau_z' \tau_z'' p_{r_z} q_z + \tau_z'' \tau_z' p_{q_z} r_z \mid 0 \rangle . \tag{7}$$

It can readily be proved that

$$\tau_z'^2 = 2 \pm \tau_z'', \qquad \tau_z''^2 = 2 \mp \tau_z'', \qquad \tau_z' \tau_z'' = \tau_z'' \tau_z' = \pm \tau_z' , \tag{8}$$

the upper sign refers to H^3 and the lower to He^3. Than (6) becomes

$$\langle 0 \mid P_z M_z \mid 0 \rangle = \frac{2\hbar}{im_r} \langle 0 \mid p_z r_z + p_{q_z} q_z \mid 0 \rangle \pm \frac{2\hbar}{im_r} \langle 0 \mid \tau_z'(p_{r_z} q_z + p_{q_z} r_z) + \tau_z''(p_{r_z} r_z - p_{q_z} q_z) \mid 0 \rangle ,$$

and finally as the second average is identical zero

$$\langle 0 \mid P_z M_z \mid 0 \rangle + \text{c.c.} = -4 \frac{\hbar^2}{m_r} ,$$

$\langle 0 \mid S M_z \mid 0 \rangle$ being real, equation (5) reads:

$$\sum_n \hbar\omega_{0n} \mid \langle 0 \mid M \mid n \rangle \mid^2 = \frac{2\hbar^2}{m_r} - \langle 0 \mid S M_z \mid 0 \rangle .$$

For a ground state of the form (1), and for an interaction of the general type [3]

$$W = U^s O^s + U' O' + U'' O'' ,$$

the operator S is represented by the following matrix

$$S = \begin{pmatrix} ih\sigma_y X^a & m(\sigma_z X'' + \sigma_z X') \\ -m(\sigma_x X'' + \sigma_z X') & -ih\sigma_y X^a \end{pmatrix} , \tag{9}$$

σ_x, σ_y, σ_z being the usual PAULI spin matrices and the X are defined as follows

$$\begin{cases} X^a = r_z U' - q_z U' \\ X' = r_z U^s - q_z U' - r_z U'' \\ X'' = q_z U^s - r_z U' + q_z U'' \,. \end{cases}$$

X^a is totally antisymmetrical in the exchange of the coordinates and (X', X'') transform according to the representation D.

It is now a simple matter to write down the average $\langle 0 \mid S M_z \mid 0 \rangle$. The formula is a rather clumsy one, but greatly simplifies for a totally symmetrical ground state. One has

$$\langle 0 \mid S M_z \mid 0 \rangle = -(2m + \hbar) \langle 0 \mid (r_z^2 + q_z^2) U^s - 2 r_z q_z U' - (r_z^2 - q_z^2) U'' \mid 0 \rangle .$$

With additive forces [3]

$$U^s = U_{23} + U_{12} + U_{13} \qquad \begin{cases} U' = \dfrac{\sqrt{3}}{2} \cdot \{ U_{12} - U_{13} \} , \\ U'' = -U_{23} + \dfrac{1}{2} (U_{12} + U_{13}) , \end{cases}$$

and

$$\langle 0 \mid S M_z \mid 0 \rangle = -2(\hbar + 2m) \langle 0 \mid r^2 U_{23} \mid 0 \rangle ,$$

U_{23} is the radial dependence of the potential between the nucleons 2 and 3.

For the integrated cross section one has [2]

$$(10) \qquad \int \sigma(E) \, \mathrm{d}E = \left(\frac{2\pi}{3} \right)^2 \frac{e^2}{\hbar c} \sum_n \hbar \omega_{0n} \mid \langle 0 \mid M_z \mid n \rangle \mid^2 =$$

$$= \frac{4\pi^2}{3} \frac{e^2}{\hbar c} \frac{\hbar^2}{M_P} \left\{ 1 + \frac{2 M_P}{3\hbar^2} (2m + \hbar) \langle 0 \mid r^2 U_{23} \mid 0 \rangle \right\} .$$

For a preliminary evaluation we have chosen for the ground state an ansatz of the form $(1/\pi)^{3/2} (x/\mu)^3 \exp[-r^2/2\mu^2 (r^2 - q^2)]$ and a Yukawa-shaped potential $U_{23} = s(\exp[-xr]/xr)$. The parameter μ is equal to 2,68 if one whishes to account for the binding energy difference of H^3 and He^3 which is due to the coulombian repulsion. The values obtained for (10) are for neutral symmetrical and even theories respectively:

3,96 MeV $\cdot 10^{-2}$ barns; 6,17 MeV $\cdot 10^{-2}$ barns; 4,87 MeV $\cdot 10^{-2}$ barns .

From the equation (5) it is now possible to deduce the corresponding expression for $\bar{E} = \int E \sigma(E) \, \mathrm{d}E \Big/ \int \sigma(E) \mathrm{d}E$.

One has

$$\bar{E} = \frac{\sum_n \hbar^2 \omega_{0n} \mid \langle 0 \mid M_z \mid n \rangle \mid^2}{\sum_n \hbar \omega_{0n} \mid \langle 0 \mid M_z \mid n \rangle \mid^2} = - \frac{\langle 0 \mid (P_z + S)^2 \mid 0 \rangle}{\langle 0 \mid (P_z + S) M_z \mid 0 \rangle} .$$

For the evaluation of $<0 \mid (P_z + S)^2 \mid 0>$ we observe that P_z is proportional to the kinetic energy in the ground state, as one can prove using the (8):

$$P_z^2 = -\frac{\hbar^2}{m_r^2}(p_{r_z}\tau_z' + p_{q_z}\tau_z'')^2 = -\frac{9}{2}\frac{\hbar^2}{M}(p_{r_z}^2 + p_{q_z}^2),$$

$<0 \mid P_z S + S P_z \mid 0>$ is a certain average of products of coordinates times first derivatives of the potentials, and S^2 – (cfr. (9)) – is an average of squares of coordinates times potentials squared.

For the case in which we are interested, namely of a totally symmetrical ground state, one has

$$(11)\quad \left(\frac{Mc}{\hbar}\right)^2\left(\int \sigma(E)\,\mathrm{d}E\right)\frac{E}{Mc^2} = 2<0 \mid T \mid 0> + \frac{3}{2}(2m + \hbar)<0 \mid 2U^s +$$

$$+ \left(r\frac{\partial}{\partial r} + q\frac{\partial}{\partial q}\right)U^s - \left[r\left(\frac{\partial U'}{\partial q} + \frac{\partial U''}{\partial r}\right) + q\left(\frac{\partial U'}{\partial r} - \frac{\partial U''}{\partial q}\right)\right] \mid 0> -$$

$$+ M\hbar^2\{[m^2 + (m+\hbar)^2]\cdot[<0 \mid (r^2+q^2)(U^{s2} + U'^2 + U''^2) -$$

$$- 2U^s(2rqU' + (r^2 - q^2)U'') \mid 0>] + 4\hbar^2 <0 \mid (rU'' - qU')^2 \mid 0>\}.$$

For the time being we have renounced to make a numerical evaluation of (11) because this would require a more accurate knowledge of the ground state which we do not have at present. An independent investigation of this latter point, taking into consideration the tensor force and the spin-orbit coupling, is now being carried out at this institute.

The fact that the symmetry classes of the potentials are put in evidence in (11) greatly simplifies the explicit evaluation of the integrals. The form of E corresponding to the quadrupole transition can be obtained following the same lines.

The measurements of $\int \sigma(E)\,\mathrm{d}E$ and of $\bar{E}$ are important clues to further information on the potentials which are responsible for the ground state of the triton.

These formulae could give the most direct means to obtain an answer to the question whether many-body forces play any non negligible part.

RIASSUNTO

Si deducono formule integrali per i due valori medi $\sigma = \int \sigma(E)\mathrm{d}E$ e $\bar{E} = \frac{\int E\sigma(E)\,\mathrm{d}E}{\int \sigma(E)\,\mathrm{d}E}$ per le transizioni di dipolo elettrico dei nuclei H^3 ed He^3. Si danno valori numerici per σ in corrrspondenza ad alcuni tipi di potenziali statici.

IL NUOVO CIMENTO Vol. VIII, N. 3 1 Marzo 1951

Mechanism of the Loss of Energy by Collisions in a Material Medium (I).

M. Schönberg

Centre de Physique Nucléaire, Université Libre - Bruxelles

(ricevuto il 4 Dicembre 1950)

Summary. — The theory of the loss of energy of a non accelerated charged particle in a material medium is investigated, using classical electrodynamics. Special attention is given to the mechanism of the loss. The results of Fermi, Halpern and Hall, Wick and A. Bohr are generalized and further extended. The points of view of action at a distance (Bohr) and field theory (Fermi) are discussed and compared. The mechanism of the emission of Cerenkov radiation is examined and the relations with the emission of acceleration radiation analysed.

---

1. – The theory of the loss of energy of a charged particle, moving in a material medium, due to its collisions with the electrons of the medium, was first developed by N. Bohr [1], using classical methods. Bohr's theory is based on the assumption that the modification of the electromagnetic field resulting from the polarization of the medium may be neglected, in the analysis of the energy loss by collisions. The quantum theory of ionization, developed mainly by Bethe [2], Bloch [3] and Williams [4], rests on a similar assumption. Later Swann [5] suggested that the dielectric constant of the medium might reduce the rate of loss by collisions. Fermi [6] investigated the influence of

---

[1] N. Bohr: *Phil. Mag.*, **25**, 10 (1913); **30**, 581 (1915).
[2] H. Bethe: *Zeits. f. Phys.*, **76**, 293 (1932).
[3] F. Bloch: *Ann. der Phys.*, **16**, 285 (1933); *Zeits. f. Phys.*, **81**, 363 (1933).
[4] E. J. Williams: *Proc. Roy. Soc.*, A **135**, 108 (1932); A **139**, 163 (1933).
[5] W. F. G. Swann: *Journ. Franklin Ist.*, **226**, 598 (1938).
[6] E. Fermi: *Phys. Rev.*, **57**, 485 (1940).

the polarization of the medium and found it to be considerable, in the case of particles with relativistic energies. FERMI used an extremely simplified model of the dispersive medium, in which the dielectric constant is considered to be due to a single electron per atom. HALPERN and HALL [7], WICK [8] and A. BOHR [9] have shown that some of the results of FERMI depend essentially on the simplified model of the dispersive medium. But they found that the polarization effects are still considerable, when more refined models than Fermi's one are used.

The treatments of the ionization loss of N. BOHR, BETHE, BLOCH and WILLIAMS describe the interaction between the ionizing particle and the electrons of the medium as electromagnetic actions at a distance, the forces acting on the electrons being computed with the Lorentz transformed Coulomb field of the ionizing particle. In Fermi's theory the energy loss is computed as the flux of the Poynting vector of the field created by the ionizing particle in the dispersive medium. The energy loss at distances larger than ρ from the path of the particle (ρ large with respect to atomic dimensions) is given by the flux of the Poynting vector through a cylindrical surface of radius ρ with its axis on the path. The loss in collisions, with impact parameters of the order of atomic dimensions, was assumed to be the same given by the Bethe-Bloch theory, the effects of the polarization of the medium being estimated as small, in close collisions.

In this paper we shall discuss in detail the theory of the loss of energy in collisions, in order to get a more complete picture of its mechanism, both in classical and quantum theory. In this first part we shall consider only the part of the loss that can be computed with the classical electromagnetic and dynamical theories. The quantum theory of the loss will be discussed in the second part of the paper, to be published later. The classical theory of the energy loss, given in this paper, follows the general lines of the Fermi treatment, but the solution of the Maxwell equations in dispersive media used is not taken in the form given by Fermi, which is not very convenient for the discussion of the case of a non absorbent medium. The form of the solution used is a generalization of the ordinary retarded potentials and is related to that derived originally by FRANK and TAMM [10], in the theory of the Cerenkov radiation. The relations between the methods of computation of the energy loss of N. BOHR and FERMI are systematically discussed and it is shown that

---

[7] O. HALPERN and H. HALL: *Phys. Rev.*, **57**, 459 (1940); **73**, 477 (1948).

[8] G. C. WICK: *Ric. Scient.*, **11**, 273 (1940); **12**, 858 (1941); *Nuovo Cimento*, **1**, 302 (1943).

[9] A. BOHR: *Det Kgl. Dans. Vid. Sels.*, **24**, n. 19 (1948).

[10] I. FRANK and IG. TAMM: *C. R. Ac. Sci. USSR*, **14**, 109 (1937); IG. TAMM: *Journ. of Phys. USSR*, **1**, 439 (1939).

Bohr's method can be generalized to the case of an absorbent dispersive medium, although it does not lead to correct results when the dispersive medium is assumed to be perfectly transparent. Thus an action at a distance theory of the loss does not seem to be possible when the medium is transparent, because of the existence of a flux of radiation at infinity.

N. BOHR [1] and WILLIAMS [4] have shown that the part of the ionization-excitation loss due to distant collisions increases with the energy, in the relativistic region, because of the increase of the radii of action (maximal impact parameters for ionization and excitation of the energy levels of the atoms of the medium) when the polarization effects are neglected. It was already shown by A. BOHR [9] that there is no such an increase of the radii of action in the Fermi theory and that the increase is actually due to emission of Cerenkov radiation. This result is established in a rigorous way in this paper, and it does not depend on the special form of the dielectric constant used, in the case of a non absorbent medium. In the case of an absorbent medium, it is not possible to get a clean cut separation of the primary ionization and excitation from the secondary ones resulting from the absorption of the Cerenkov radiation, so that the result regarding the effect of the Cerenkov radiation after the minimum can only be established in an approximate form. The saturation of the loss at high energies, found by FERMI, HALPERN and HALL and WICK, is established in a general way, largely independent of particular expressions of the dielectric constant.

The spatial distribution of the loss is discussed in detail. It is shown that the Cerenkov radiation is emitted in the immediate neighbourhood of the path of the ionizing particle. Although the accelerated motion of the electrons plays an important part in the emission of the Cerenkov radiation, it is more satisfactory to consider the Cerenkov radiation as emitted by the non accelerated ionizing particle, because its flux is the same through any cylindrical surface with axis on the path, in the case of a non absorbent medium.

In this part of the paper the experimental data are not discussed. Detailed computations have been made, using the results of this paper, by HUYBRECHTS and JANSSENS (unpublished). They have shown that it is possible to explain the observed variation of the number of grains with the energy of the particles in photographic plates. An analysis of the energy losses of ionizing particles in photographic plates has also been given recently by MESSEL and RITSON [11].

Some of the points treated in this paper are discussed, in a more detailed form, in a note of the author published in the *Bulletin du Centre de Physique Nucléaire de l'Université Libre de Bruxelles* (n. 20, August 1950).

---

[11] H. MESSEL and D. M. RITSON: *Phil. Mag.*, **41**, 1129 (1950).

2. – Solutions of Maxwell's equations for a homogeneous dispersive medium.

The electromagnetic behaviour of a dispersive medium is characterized by the existence of a density of polarization $\boldsymbol{P}$ dependent on the electric field. If the electric field $\boldsymbol{E}$ is such that the motions of the electrons can be assimilated to that of a system of harmonic oscillators acted by external forces, the relation between the density of polarization and the electric field can be described by a dielectric constant $\varepsilon(\omega)$

$$4\pi \boldsymbol{P}_\omega = (\varepsilon(\omega) - 1)\boldsymbol{E}_\omega \,, \tag{1}$$

$\boldsymbol{P}_\omega$ and $\boldsymbol{E}_\omega$ being respectively the Fourier components of $\boldsymbol{P}$ and $\boldsymbol{E}$ corresponding to the circular frequency ω

$$\boldsymbol{E}, \boldsymbol{P} = \int_{-\infty}^{+\infty} \boldsymbol{E}_\omega, \boldsymbol{P}_\omega \exp[-i\omega t]\, \mathrm{d}\omega \,. \tag{2}$$

It results from equations (1) and (2) that

$$4\pi \boldsymbol{P} = (\varepsilon_{0p} - 1)\boldsymbol{E} \,, \tag{3}$$

with

$$\varepsilon_{0p} = \varepsilon\left(i\frac{\partial}{\partial t}\right). \tag{4}$$

When the damping of the electronic oscillations is taken into account, $\varepsilon(\omega)$ is complex. Denoting by $c(\omega)$ the phase velocity of a wave of circular frequency ω and by $\varkappa(\omega)$ its amplitude absorption coefficient, we have the well known relation

$$\frac{\varepsilon(\omega)}{c^2} = \left[\frac{1}{c(\omega)} + i\frac{\varkappa(\omega)}{\omega}\right]^2 . \tag{5}$$

The Maxwell equations for a homogeneous dispersive and non magnetic medium are

$$\begin{cases} \operatorname{div} \varepsilon_{0p}\boldsymbol{E} = 4\pi j_0 \,, & \dfrac{1}{c}\dfrac{\partial}{\partial t}\varepsilon_{0p}\boldsymbol{E} = \operatorname{rot} \boldsymbol{H} - 4\pi \boldsymbol{j} \,, \\ \operatorname{div} \boldsymbol{H} = 0 \,, & \dfrac{1}{c}\dfrac{\partial \boldsymbol{H}}{\partial t} = -\operatorname{rot} \boldsymbol{E} \,, \end{cases} \tag{6}$$

j_0 and $\boldsymbol{j}$ being the densities of charge and current. The potentials are defined by the equations

$$\boldsymbol{H} = \operatorname{rot} \boldsymbol{A} \,, \qquad \boldsymbol{E} = -\operatorname{grad} A_0 - \frac{1}{c}\frac{\partial \boldsymbol{A}}{\partial t} \,, \tag{7}$$

and the generalized Lorentz condition

$$\frac{\varepsilon_{0p}}{c}\frac{\partial A_0}{\partial t} + \operatorname{div} \boldsymbol{A} = 0 . \tag{8}$$

The potentials are solutions of the generalized d'Alembert equations

$$\left(\frac{\varepsilon_{0p}}{c^2}\frac{\partial^2}{\partial t^2} - \Delta\right)\boldsymbol{A} , \quad \varepsilon_{0p} A_0 = 4\pi \boldsymbol{j},\ j_0 . \tag{9}$$

A solution of equations (9) can be obtained by a formal generalization of the ordinary retarded potentials

$$\boldsymbol{A}^{\mathrm{ret}},\ \varepsilon_{0p} A_0^{\mathrm{ret}} = \int_{-\infty}^{+\infty} \exp\left(-\frac{r}{c}\sqrt{\varepsilon_{0p}}\frac{\partial}{\partial t}\right)\boldsymbol{j},\ j_0 \frac{d_3 x'}{r} , \tag{10}$$

as well as by a formal generalization of the advanced potentials

$$\boldsymbol{A}^{\mathrm{adv}},\ \varepsilon_{0p} A_0^{\mathrm{adv}} = \int_{-\infty}^{+\infty} \exp\left(\frac{r}{c}\sqrt{\varepsilon_{0p}}\frac{\partial}{\partial t}\right)\boldsymbol{j},\ j_0 \frac{d_3 x'}{r} . \tag{11}$$

In equations (10) and (11), r denotes the distance between the point (x, y, z), where the potentials are computed, and the variable point (x', y', z') in the domain of integration. It is necessary to give a well defined meaning to the operator $\sqrt{\varepsilon_{0p}}$ in (10) and (11), in order to get true retarded or advanced potentials. Let us consider the Fourier expansion of $\boldsymbol{j}$

$$\boldsymbol{j} = \int_{-\infty}^{+\infty} \boldsymbol{j}_\omega \exp\left[-i\omega t\right] \mathrm{d}\omega . \tag{12}$$

We get from (10) and (12)

$$\boldsymbol{A}^{\mathrm{ret}} = \int_{-\infty}^{+\infty} \exp\left[-i\omega t\right] \mathrm{d}\omega \int_{-\infty}^{+\infty} \exp\left(i\frac{\omega}{c}\sqrt{\varepsilon(\omega)}\, r\right)\boldsymbol{j}_\omega \frac{d_3 x'}{r} . \tag{13}$$

In order to get a true retarded solution we must therefore take

$$0 \leqslant \arg\sqrt{\varepsilon(\omega)} < \pi \qquad \omega > 0 . \tag{14}$$

In the case of the advanced potential we get, in a similar way, the condition

$$-\pi < \arg\sqrt{\varepsilon(\omega)} \leqslant 0 \qquad \omega > 0 . \tag{15}$$

When ε is complex, $\sqrt{\varepsilon}$ must be taken with opposite signs in the two cases and $\boldsymbol{A}^{\mathrm{ret}} = \boldsymbol{A}^{\mathrm{adv}}$.

We are specially interested in the case of a point particle of charge e in uniform motion. Taking the x-axis along the path and choosing suitably the position of the origin of the coordinates, we have

$$j_0 = e\delta(x - vt)\,\delta(y)\,\delta(z)\,, \qquad \boldsymbol{j} = \frac{\boldsymbol{v}}{c}\, j_0\,, \tag{16}$$

$\boldsymbol{v}$ being the velocity of the particle. Now we get

$$\boldsymbol{j}_\omega(x') = \frac{e}{2\pi c}\,\frac{\boldsymbol{v}}{v}\,\delta(y')\,\delta(z')\,\exp\left[i\omega\,\frac{x'}{v}\right], \tag{17}$$

so that

$$\left.\begin{aligned} A_0^{\mathrm{ret}} &= \frac{e}{2\pi v}\int_{-\infty}^{+\infty} \varepsilon^{-1}\exp\left[-i\omega t\right]\mathrm{d}\omega\,\times \\ &\quad\times\int_{-\infty}^{+\infty}\exp\left(i\,\frac{\omega}{c}\,\sqrt{\varepsilon(\omega)}\,\sqrt{(x-x')^2+\rho^2}\right)\frac{\exp\left(i\omega\,\dfrac{x'}{v}\right)\mathrm{d}x'}{\sqrt{(x-x')^2+\rho^2}}\,, \\ \boldsymbol{A}^{\mathrm{ret}} &= \frac{\boldsymbol{v}}{c}\,\varepsilon_{0p}A_0^{\mathrm{ret}}\,, \end{aligned}\right\} \tag{18}$$

$$\left.\begin{aligned} A_0^{\mathrm{adv}} &= \frac{e}{2\pi v}\int_{-\infty}^{+\infty} \varepsilon^{-1}\exp\left[-i\omega t\right]\mathrm{d}\omega\,\times \\ &\quad\times\int_{-\infty}^{+\infty}\exp\left(-i\,\frac{\omega}{c}\,\sqrt{\varepsilon(\omega)}\,\sqrt{(x-x')^2+\rho^2}\right)\frac{\exp\left(i\omega\,\dfrac{x'}{v}\right)\mathrm{d}x'}{\sqrt{(x-x')^2+\rho^2}}\,, \\ \boldsymbol{A}^{\mathrm{adv}} &= \frac{\boldsymbol{v}}{c}\,\varepsilon_{0p}A_0^{\mathrm{adv}}\,, \end{aligned}\right\} \tag{19}$$

ρ denotes the distance from the point where the potentials are computed to the path

$$\rho = \sqrt{y^2+z^2}\,. \tag{20}$$

It is convenient to expand the spherical waves in (18) and (19) into cylindrical waves, by using the formulae of Weyrich

$$\frac{\exp\left(i\lambda\sqrt{x^2+\rho^2}\right)}{\sqrt{x^2+\rho^2}} = \frac{i}{2}\int_{-\infty}^{+\infty}\exp\left[iux\right]H_0^{(1)}(\rho\sqrt{\lambda^2-u^2})\,\mathrm{d}u\,, \tag{21}$$

$$(\rho,\, x \text{ real};\quad 0 \leqslant \arg\sqrt{\lambda^2-u^2} < \pi;\quad 0 \leqslant \arg\lambda < \pi)\,, \tag{21a}$$

$$\frac{\exp(-i\lambda\sqrt{x^2+\rho^2})}{\sqrt{x^2+\rho^2}} = -\frac{i}{2}\int_{-\infty}^{+\infty} \exp[-iux] H_0^{(2)}(\rho\sqrt{\lambda^2-u^2})\,du\,, \tag{22}$$

$$(\rho,\ x \text{ real};\ -\pi < \arg\sqrt{\lambda^2-u^2} \leqslant 0;\ -\pi < \arg\lambda \leqslant 0)\,, \tag{22a}$$

$$A_0^{\text{ret}} = \frac{ie}{2v}\int_{-\infty}^{+\infty} \varepsilon^{-1} H_0^{(1)}\left(\rho\sqrt{\frac{\omega^2}{v^2}(\beta^2\varepsilon-1)}\right)\exp\left[i\omega\left(\frac{x}{v}-t\right)\right]d\omega\,, \tag{23}$$

$$\left(0 \leqslant \arg\sqrt{\frac{\omega^2}{v^2}(\beta^2\varepsilon-1)} < \pi\right), \tag{23a}$$

$$-\frac{ie}{2v}\int_{-\infty}^{+\infty} \varepsilon^{-1} H_0^{(2)}\left(\rho\sqrt{\frac{\omega^2}{v^2}(\beta^2\varepsilon-1)}\right)\exp\left[i\omega\left(\frac{x}{v}-t\right)\right]d\omega, \tag{24}$$

$$\left(-\pi < \arg\sqrt{\frac{\omega^2}{v^2}(\beta^2\varepsilon-1)} \leqslant 0\right), \tag{24a}$$

β denotes as usually v/c. Let us put

$$k^2(\omega) = \frac{\omega^2}{v^2}(1-\beta^2\varepsilon) \qquad Rek \geqslant 0\,, \tag{25}$$

k is completely determined in the case of an absorbent medium (complex ε). In this case, both the advanced and retarded potentials coincide, as we have seen

$$\begin{cases} A_0^{\text{ret}} = A_0^{\text{adv}} = \dfrac{e}{\pi v}\displaystyle\int_{-\infty}^{+\infty} \varepsilon^{-1} K_0(k\rho)\exp\left[i\omega\left(\frac{x}{v}-t\right)\right]d\omega\,, \\ \boldsymbol{A}^{\text{ret}} = \boldsymbol{A}^{\text{adv}} = \dfrac{e}{\pi c}\dfrac{\boldsymbol{v}}{v}\displaystyle\int_{-\infty}^{+\infty} K_0(k\rho)\exp\left[i\omega\left(\frac{x}{v}-t\right)\right]d\omega\,, \end{cases} \tag{26}$$

The K are the modified Hankel functions

$$K_\nu(u) = \frac{i\pi}{2}\exp\left[\frac{i\nu\pi}{2}\right] H_\nu^{(1)}(u\exp[i\pi/2]) = \\ = -\frac{i\pi}{2}\exp[-i\nu\pi/2]\, H_\nu^{(2)}(u\exp[-i\pi/2])\,. \tag{27}$$

From (26) we get Fermi's formulae for the fields

$$E_x = -\frac{ie}{\pi v^2}\int_{-\infty}^{+\infty}\left(\frac{1}{\varepsilon}-\beta^2\right) K_0(k\rho)\exp\left[i\omega\left(\frac{x}{v}-t\right)\right]\omega\,d\omega\,, \tag{28}$$

$$E_{\mathrm{tr}} = \frac{e}{\pi v} \int_{-\infty}^{+\infty} \frac{1}{\varepsilon}\, kK_1(k\rho) \exp\left[i\omega\left(\frac{x}{v} - t\right)\right] \mathrm{d}\omega\,, \tag{29}$$

$$\boldsymbol{H} = \left[\frac{\boldsymbol{v}}{c} \times \varepsilon_{0p} \boldsymbol{E}\right]. \tag{30}$$

E_{tr} denotes the component of the electric field transversal to the path. When e is positive, the electric field has its transversal component directed from the path to the point (x, y, z).

When the damping of the electronic oscillations is neglected and ε is taken real, the retarded and advanced fields do not coincide any more. In this case we must distinguish the frequency ranges in which

$$\beta^2\varepsilon - 1 < 0 \qquad \text{(Bohr frequencies)} \tag{31}$$

from those in which

$$\beta^2\varepsilon - 1 \geqslant 0 \qquad \text{(Cerenkov frequencies).} \tag{32}$$

It results fron (23*a*) and (24*a*) that the Bohr frequencies give the same contributions to the retarded and advanced potentials, whereas the contributions of the Cerenkov frequencies are not the same. Therefore, in the case of a non absorbent dispersive medium, it is possible to define a pure wave field in terms of the retarded and advanced fields of a charged particle in uniform motion

$$\boldsymbol{E}^c = \frac{1}{2}\left(\boldsymbol{E}^{\mathrm{ret}} - \boldsymbol{E}^{\mathrm{adv}}\right), \qquad \boldsymbol{H}^c = \frac{1}{2}\left(\boldsymbol{H}^{\mathrm{ret}} - \boldsymbol{H}^{\mathrm{adv}}\right). \tag{33}$$

The field $(\boldsymbol{E}^c, \boldsymbol{H}^c)$ will be called the Cerenkov field, it contains only frequencies satisfying the condition (32), i.e. Cerenkov frequencies. $\boldsymbol{E}^c$ and $\boldsymbol{H}^c$ satisfy the homogeneous Maxwell equations

$$\begin{cases} \operatorname{div} \varepsilon_{0p} \boldsymbol{E}^c = 0\,, & \dfrac{1}{c}\dfrac{\partial}{\partial t} \varepsilon_{0p} \boldsymbol{E}^c = \operatorname{rot} \boldsymbol{H}^c\,, \\ \operatorname{div} \boldsymbol{H}^c = 0\,, & \dfrac{1}{c}\dfrac{\partial}{\partial t} \boldsymbol{H}^c = -\operatorname{rot} \boldsymbol{E}^c\,. \end{cases} \tag{34}$$

In the case of a non absorbent medium, the integration path in (28) and (29) can not be taken as the real ω-axis, because of the existence of poles of ε^{-1} on that axis. We shall prove later that the following assumptions are fulfilled:

a) The poles of ε^{-1} lie all below the real ω-axis and are all simple, when the damping is finite.

b) Those poles remain simple and move into the real axis, when the damping tends to zero.

Therefore the integration path can be taken as the real ω-axis indented by infinitesimal half-circles, centered at the poles ω of ε^{-1}, and lying on the upper part of the complex ω-plane. Denoting by $P.V.$ the Cauchy principal value, we have

$$(35a) \qquad E_x^{\mathrm{ret}} = -\frac{ie}{\pi v^2} P.V. \int_{-\infty}^{+\infty} \left(\frac{1}{\varepsilon} - \beta^2\right) K_0(k\rho) \exp\left[i\omega\left(\frac{x}{v} - t\right)\right] \omega \, d\omega - \\ - \frac{e}{v^2} \sum_{\bar{\omega}} a_{\bar{\omega}} \, \bar{\omega} \, K_0\left(\left|\frac{\bar{\omega}}{v}\right| \rho\right) \exp\left[i\bar{\omega}\left(\frac{x}{v} - t\right)\right],$$

$$(35b) \qquad E_{\mathrm{tr}}^{\mathrm{ret}} = \frac{e}{\pi v} P.V. \int_{-\infty}^{+\infty} \frac{k}{\varepsilon} K_1(k\rho) \exp\left[i\omega\left(\frac{x}{v} - t\right)\right] d\omega - \\ - \frac{ie}{v^2} \sum_{\bar{\omega}} a_{\bar{\omega}} \left|\bar{\omega}\right| K_1\left(\left|\frac{\bar{\omega}}{v}\right| \rho\right) \exp\left[i\bar{\omega}\left(\frac{x}{v} - t\right)\right].$$

$a_{\bar{\omega}}$ is the residue of ε^{-1} at the pole $\bar{\omega}$. Since the poles $\bar{\omega}$ are simple, we have

$$(36) \qquad a_{\bar{\omega}} = \lim_{\omega \to \bar{\omega}} (\omega - \bar{\omega}) \varepsilon^{-1}(\omega) = \left(\frac{d\varepsilon}{d\omega}\right)^{-}_{(\omega = \bar{\omega})}.$$

In equations (35) we must take

$$(37) \qquad \begin{cases} \arg k(\omega) = 0 & (\omega > 0, \ 1 - \beta^2\varepsilon > 0) \\ \arg k(\omega) = -\dfrac{i\pi}{2} & (\omega > 0, \ 1 - \beta^2\varepsilon < 0). \end{cases}$$

In the case of the advanced field, we would have to replace $-i\pi/2$ by $i\pi/2$, in the second equation (37).

It is important to notice that the ω are not Cerenkov frequencies, because they are zeros of $\varepsilon(\omega)$. The frequencies $\bar{\omega}$ play a very important part in the theory of the energy loss. We shall see that they account for the entire loss, when the energy of the ionizing particle is non relativistic, and for the whole of the direct ionization and excitation at relativistic energies.

3. – The well known Fourier expansion of the Lorentz transformed Coulomb field is a particular case of equations (28), (29), corresponding to

$$(38) \qquad \varepsilon = 1, \qquad k(\omega) = \frac{\omega}{v}\sqrt{1 - \beta^2},$$

In the vacuum all the frequencies are Bohr frequencies. It results from the asymptotic expression of the K functions

$$(39) \qquad K_\nu(u) \sim \sqrt{\frac{\pi}{2u}} \exp[-u],$$

that there is a range $R_{\text{vac}}(\omega)$

$$R_{\text{vac}}(\omega) = \frac{v}{|\omega|\sqrt{1-\beta^2}}, \tag{40}$$

for any Fourier component of a field. In the case of a dispersive non absorbent medium, only the Fourier components corresponding to Bohr frequencies do have finite ranges

$$R(\omega) = \frac{v}{|\omega|\sqrt{1-\beta^2\varepsilon}}. \tag{41}$$

The square of the absolute values of the Fourier components corresponding to Cerenkov frequencies tend to zero as ρ^{-1}, for large values of ρ. They give contributions to the flux of energy at infinity, in directions non parallel to the path, i.e. to the Cerenkov radiation.

In an absorbent medium there is a range for any frequency, because $k(\omega)$ is complex. Nevertheless, it is possible to distinguish approximately two types of frequencies, corresponding to the Bohr and Cerenkov frequencies, because of the smallness of the imaginary part of ε. Taking into account that the absorption coefficient $\varkappa(\omega)$ is small, we get from (5)

$$Im\varepsilon \cong \frac{2c^2}{c(\omega)}\frac{\varkappa(\omega)}{\omega}, \qquad Re\varepsilon \cong \frac{c^2}{c^2(\omega)}, \tag{42}$$

therefore

$$R(\omega) = \frac{1}{Rek} \cong \begin{cases} \dfrac{v}{|\omega|\sqrt{1-\beta^2 Re\varepsilon}} & \text{for } c(\omega) > v \\ \dfrac{1}{\varkappa(\omega)}\sqrt{1-\dfrac{c^2(\omega)}{v^2}} & \text{for } c(\omega) < v\,. \end{cases} \tag{43}$$

The frequencies, whose velocities of propagation are less than v, have long ranges. They correspond to the Cerenkov frequencies of a non absorbent medium.

4. – The increase and saturation of the energy loss in the relativistic region.

The energy transmitted to the medium at distances larger than ρ, per unit time, is given by the flux of the Poynting vector $(c/4\pi)[\boldsymbol{E}\times\boldsymbol{H}]$ through a cylindrical surface of radius ρ, having its axis on the path. Denoting by n the direction of the normal to that surface S_ϱ, we have

$$-\frac{\mathrm{d}W_\varrho}{\mathrm{d}x} = \frac{c}{4\pi v}\int_{S_\varrho}[\boldsymbol{E}\times\boldsymbol{H}]_n\,\mathrm{d}S = -\frac{e\rho}{2v}\int_{-\infty}^{+\infty} HE_x\,\mathrm{d}x\,. \tag{44}$$

In the case of an absorbent medium (44) leads to the Fermi formula

$$(45)\quad -\frac{\mathrm{d}W_\varrho}{\mathrm{d}x} = \frac{e^2\rho}{\pi v^2}\int_{-\infty}^{+\infty}\left(\frac{1}{\varepsilon}-\beta^2\right)k(-\omega)K_1(k(-\omega)\rho)K_0(k(\omega)\rho)i\omega\,\mathrm{d}\omega = $$

$$= \frac{2e^2\rho}{\pi v^2}\,Re\int_0^{\infty}\left(\frac{1}{\varepsilon}-\beta^2\right)k^*(\omega)K_1(k^*(\omega)\rho)K_0(k(\omega)\rho)\,i\omega\,\mathrm{d}\omega\,,$$

taking into account that

$$(46)\qquad k(-\omega) = k^*(\omega)\,.$$

In the case of a non absorbent medium, the real ω-axis must be indented, as we did in the derivation of equations (35). Instead of (45) we have

$$(47)\quad -\frac{\mathrm{d}W_\varrho}{\mathrm{d}x} = \frac{2e^2\rho}{\pi v^2}\,Re\left[P.V.\int_0^{\infty}\left(\frac{1}{\varepsilon}-\beta^2\right)k^*K_1(k^*\rho)K_0(k\rho)\,i\omega\,\mathrm{d}\omega\right] +$$

$$+\frac{e^2\rho}{v^2}\sum_{\omega}\alpha_{\omega}\,\bar{\omega}\,\frac{|\bar{\omega}|}{v}\,K_1\left(\frac{|\bar{\omega}|\rho}{v}\right)K_0\left(\frac{|\bar{\omega}|\rho}{v}\right).$$

The flux of the Poynting vector gives the total rate of flow of energy through S_ϱ, but this rate of flow does not coincide with the energy lost at distances larger than ρ, because it includes the radiation emitted at distances less than ρ and not absorbed inside S_ϱ.

Introducing the asymptotic expression of the K functions (39) into (45) we get

$$(48)\quad -\frac{\mathrm{d}W_\varrho}{\mathrm{d}x} \sim \frac{e^2}{v^2}\,Re\int_0^{\infty}\left(\frac{1}{\varepsilon}-\beta^2\right)\sqrt{\frac{k^*}{k}}\,\exp\left[-(k+k^*)\rho\right]i\omega\,\mathrm{d}\omega \cong$$

$$\cong -\frac{e^2}{v^2}\int_{c(\omega)<v}\left(\frac{1}{\varepsilon}-\beta^2\right)\exp\left[-2Rek\rho\right]\omega\,\mathrm{d}\omega \qquad (\omega>0)\,,$$

because, when $c(\omega) > v$, k is nearly real so that the real part of the integral taken over the corresponding ranges is negligible. Thus, at large distances, the flux of energy is only due to the frequencies whose $c(\omega)$ are less than v. It is interesting to notice that the frequencies whose $c(\omega)$ are larger than v do not give sizable contributions to the loss, already at distances for which the corresponding Fourier components of the fields are still sizable. Since k is nearly imaginary when $c(\omega) < v$, (48) shows that, at large distances, the energy loss is due to a radiation which is slowly absorbed. This is the Cerenkov radiation.

For small values of $|u|$ we have

$$K_0(u) \backsimeq \log \frac{2}{\gamma u}, \qquad K_1(u) \backsimeq \frac{1}{u} \qquad (\log \gamma = 0.577...) . \tag{49}$$

Therefore, for small values of ρ

$$-\frac{dW_e}{dx} \backsimeq \frac{2e^2}{\pi v^2} Re \int_0^\infty \left(\frac{1}{\varepsilon} - \beta^2\right) \log \frac{2}{\gamma k \rho} i\omega \, d\omega , \tag{50}$$

hence

$$\frac{d}{d\rho}\left(-\frac{dW_e}{dx}\right) \backsimeq -\frac{2e^2}{\pi v^2 \rho} Re \int_0^\infty \left(\frac{1}{\varepsilon} - \beta^2\right) i\omega \, d\omega . \tag{51}$$

The rate of loss of energy in the cylindrical layer $\rho - \rho + d\rho$, per unit path, is nearly independent of ρ, for small values of ρ. It is also nearly independent of the energy, in the relativistic region. The increase in loss after the minimum is, therefore, contained in the energy transmitted to the medium at large distances from the path, i.e. in the Cerenkov radiation. Neglecting the absorption of radiation in (48) and comparing with (50), we see that the Cerenkov radiation is emitted in the immediate neighbourhood of the path, because the contribution of the frequencies whose $\varepsilon(\omega)$ are less than v becomes the same in (48) and (50).

5. – The results of the last section can be given in a more precise mathematical form, in the case of a non absorbent medium. We shall prove that the integral in (47) is proportional to ρ^{-1}, so that the contribution of the corresponding term to the loss is independent of ρ. The transformations we shall use are equivalent to those used by TAMM [11], who overlooked the contribution of the residues in (47) and did not take into account that the integral is actually a principal value. We shall see that only the Cerenkov frequencies contribute to the first term in (47), which represents the flux of Cerenkov radiation. We have

$$2Re\left[P.V. \int_0^\infty \left(\frac{1}{\varepsilon} - \beta^2\right) k^* K_1(k^*\rho) K_0(k\rho) i\omega \, d\omega\right] = \tag{52}$$

$$= P.V. \int_0^\infty \left(\frac{1}{\varepsilon} - \beta^2\right) \{ k^* K_1(k^*\rho) K_0(k\rho) - \text{comp. conj.} \} \, i\omega \, d\omega .$$

k is either real or imaginary. When it is real, the right hand side of (52)

vanishes. When k is imaginary, its argument is $-i\pi/2$, hence

$$(53)\qquad \begin{aligned} k^*K_1(k^*\rho)K_0(k\rho) - kK_1(k\rho)K_0(k^*\rho) &= \\ = -k\left[K_0(k\rho)K_1(\exp[i\pi]\,k\rho) + K_0(\exp[i\pi]\,k\rho)K_1(k\rho)\right] &= \\ = i\pi k\left[K_0(k\rho)I_1(k\rho) + I_0(k\rho)K_1(k\rho)\right] &= \frac{i\pi}{\rho}\,. \end{aligned}$$

In the derivation of (53) we used the following properties of the K functions

$$(54)\qquad \begin{cases} K_\nu(\exp[mi\pi]\,u) = \exp[-m\nu i\pi]\,K_\nu(u) - i\pi\,\dfrac{\sin m\nu\pi}{\sin \nu\pi}\,I_\nu(u)\,, \\ K_0(u)I_1(u) + I_0(u)K_1(u) = \dfrac{1}{u}\,. \end{cases}$$

It results from the preceding considerations that

$$(55)\qquad -\frac{dW_\varrho}{dx} = -\frac{e^2}{v^2}\int_{\substack{c(\omega)<v \\ \omega\geqslant 0}}\left(\frac{1}{\varepsilon}-\beta^2\right)\omega\,d\omega + \frac{e^2\rho}{v^2}\sum_{\bar\omega} a_{\bar\omega}\,\bar\omega\,\left|\frac{\bar\omega}{v}\right|\,K_1\left(\frac{|\bar\omega|\rho}{v}\right)K_0\left(\frac{|\bar\omega|\rho}{v}\right);$$

hence we get the formula of FRANK and TAMM [10] for the Cerenkov loss

$$(56)\qquad -\frac{dW_\infty}{dx} = -\frac{e^2}{v^2}\int_{c(\omega)<v}\left(\frac{1}{\varepsilon}-\beta^2\right)\omega\,d\omega \qquad (\omega\geqslant 0)\,.$$

It results from (55) and (56) that, in a dispersive non absorbent medium:

a) $-dW_\varrho/dx$ tends asymptotically to a constant value, the rate of emission of Cerenkov radiation per unit path.

b) The variation of the rate of loss, in the relativistic range of energies, is determined entirely by the emission of Cerenkov radiation.

c) The radii of action for primary ionization or excitation are practically constant in the relativistic range of energies.

d) There is a saturation of the loss at distances larger than the atomic dimensions for high energies.

e) The flux of the Cerenkov radiation is the same through all the cylinders around the path, so that the radiation must be emitted in the immediate neighbourhoud of the path.

For small values of ρ we may use the expressions (49)

$$(57)\qquad -\frac{dW_\varrho}{dx} = \frac{dW_\infty}{dx} + \frac{e^2}{v^2}\sum_{\bar\omega} a_{\bar\omega}\,\bar\omega\log\frac{2v}{\gamma\,|\bar\omega|\,\rho}\,.$$

The saturation value of the part of the loss due to interactions at distances larger than the atomic dimensions is

$$(58)\qquad \left(-\frac{dW_{\varrho_0}}{dx}\right)_{(v=c)} = \frac{e^2}{c^2}\int_{\varepsilon>1}\left(1-\frac{1}{\varepsilon}\right)\omega\,d\omega + \frac{e^2}{c^2}\sum_{\bar\omega} a_{\bar\omega}\,\bar\omega\log\frac{2c}{\gamma\,|\bar\omega|\,\rho_0}\,,$$

ρ_0 being of the order of 10^{-8} cm.

It is interesting to notice that we would have an inflow of Cerenkov radiaton using the advanced solution of the Maxwell equations, because, in this case, in (52) the sign of arg k would be changed.

6. – The results of the preceding sections were obtained in a very general way, assuming only some properties of the dielectric constant. We shall now make use of the Lorentz expression of $\varepsilon(\omega)$

$$(59)\quad \varepsilon(\omega) = 1 + \left(\frac{f_0}{-\nu^2 - ig_0\nu} + \sum_{j=1}^{r} \frac{f_j}{\nu_j^2 - \nu^2 - ig_j\nu}\right) \Big/ \left(1 - \frac{1}{3}\sum_{j=1}^{r} \frac{f_j}{\nu_j^2 - \nu^2 - ig_j\nu}\right).$$

The frequencies ν and damping constants g, in (59), are measured in units α

$$\alpha = \sqrt{\frac{Ne^2}{\pi m}}, \qquad \omega = 2\pi\alpha\nu,$$

N being the number of electrons per unit volume and m the mass of the electron. The ν_j are the frequencies of the atomic electrons and the f_j the corresponding fractions of the total number of electrons. f_0 is the fraction of the conduction electrons. We shall consider only cases in which f_0 is negligible, so that

$$f_0 = 0, \qquad \sum_{j=1}^{r} f_j = 1.$$

We shall assume that

$$\nu_1 < \nu_2 < \nu_3 < \ldots < \nu_r.$$

The Lorentz expression of the dielectric constant (59) was derived assuming that the force acting on the electrons is

$$(60)\qquad e\,\boldsymbol{E}_{\text{act}} = e\left(\boldsymbol{E} + \frac{4\pi}{3}\boldsymbol{P}\right).$$

In the case of a gas, the Lorentz correction to the force acting on the electrons may be neglected and $\boldsymbol{E}_{\text{act}}$ can be taken simply as $\boldsymbol{E}$. The dielectric constant ε_S is then given by the Sellmayer formula

$$(61)\qquad \varepsilon_S(\omega) = 1 + \sum_{j=1}^{r} \frac{f_j}{\nu_j^2 - \nu^2 - ig_j\nu},$$

which was used by FERMI, WICK and AAGE BOHR.

In the discussion of the behaviour of $\varepsilon(\omega)$ it is convenient to consider the function L

$$(62)\qquad L(\omega) = \frac{\varepsilon(\omega) - 1}{\varepsilon(\omega) + 2} = \frac{1}{3}\sum_{j=1}^{r} \frac{f_j}{\nu_j^2 - \nu^2 - ig_j\nu}.$$

We shall neglect the damping constant g, unless the contrary is specified.

L varies from $-\infty$ to $+\infty$ and is a crescent function in each of the intervals $\omega_j - \omega_{j+1}$. Therefore, there is a single zero $\bar{\omega}_j$ and a single pole $\bar{\omega}_{j+1}$ of ε in that interval, corresponding respectively to the values $-1/2$ and 1 of L. There is also a zero $\bar{\omega}_r > \omega_r$, and a pole $\bar{\omega}_1$ in the interval $0 - \omega_1$, because $\varepsilon(0) > 1$ and $L(0) < 1$.

In the case of finite damping (absorbent medium)

$$ImL(\omega) = \frac{1}{3}(Re\,\nu)\sum_{j=1}^{r} f_j \frac{2Im\nu + g_j}{|\nu_j^2 - \nu^2 - ig_j\nu|^2}, \tag{63}$$

therefore, ImL can not vanish when $Im\omega \geqslant 0$ and the zeros and poles of ε must have negative imaginary parts.

It is easily seen that

$$a_j = a_{\bar{\omega}_j} = -a_{-\bar{\omega}_j} = \left(\frac{4}{3}\frac{dL}{d\omega}\right)^{-1}_{(\omega=\bar{\omega}_j)}. \tag{64}$$

The frequencies $\bar{\omega}_j$ and the a_j can be computed approximately

$$\bar{\nu}_j \backsimeq \nu_j + \frac{1}{3}\frac{f_j}{\nu_j}, \qquad a_j \backsimeq \pi\alpha\frac{f_j}{\nu_j}, \tag{65}$$

and using (65) we get

$$\left.\begin{aligned} &\frac{e^2\rho}{v^2}\sum_{\omega} a_{\omega}\,\bar{\omega}\,\frac{|\bar{\omega}|}{v}\,K_1\left(\frac{|\bar{\omega}|\rho}{v}\right)K_0\left(\frac{|\bar{\omega}|\rho}{v}\right) \backsimeq \\ &\qquad \backsimeq \frac{4\pi Ne^4}{mv^2}\sum_{j=1}^{r} f_j\,\frac{\bar{\omega}_j\rho}{v}\,K_1\left(\frac{\bar{\omega}_j\rho}{v}\right)K_0\left(\frac{\bar{\omega}_j\rho}{v}\right). \end{aligned}\right\} \tag{66}$$

For small values of ρ

$$\frac{e^2\rho}{v^2}\sum_{\omega} a_{\omega}\,\bar{\omega}\,\frac{|\bar{\omega}|}{v}\,K_1\left(\frac{|\bar{\omega}|\rho}{v}\right)K_0\left(\frac{|\bar{\omega}|\rho}{v}\right) \backsimeq \frac{4\pi Ne^4}{mv^2}\log\frac{v}{\pi\gamma\alpha\rho\bar{\nu}_m}, \tag{67}$$

with

$$\bar{\nu}_m = \bar{\nu}_1^{f_1}\bar{\nu}_2^{f_2}\ldots\bar{\nu}_r^{f_r}. \tag{68}$$

When $v \ll c$ (67) coincides approximately with Bohr's non relativistic formula for the loss, with $\bar{\nu}_m$ replacing Bohr's mean frequency ν_m

$$\nu_m = \nu_1^{f_1}\nu_2^{f_2}\ldots\nu_r^{f_r}. \tag{69}$$

In each interval $\omega_j - \omega_{j+1}$ there is a root ω'_{j+1} of the equation $1 - \beta^2\varepsilon = 0$. ω'_{j+1} is the lower limit of the Cerenkov band in that interval, the upper limit being the pole ω_{j+1} of ε. There is also a Cerenkov band in the interval $0 - \omega_1$, whose lower limit is 0 when $\beta^2 \geqslant \varepsilon^{-1}(0)$ and ω'_1 when $\beta^2 < \varepsilon^{-1}(0)$. The intensities of the Cerenkov bands can be easily computed by using the formula

$$\frac{1}{\varepsilon} - 1 = \sum_{j=1}^{r} a_j\left(\frac{1}{\omega - \omega_j} - \frac{1}{\omega + \bar{\omega}_j}\right) = 2\sum_{j=1}^{r}\frac{a_j\bar{\omega}_j}{\omega^2 - \bar{\omega}_j^2}. \tag{70}$$

Thus we get

$$\int \left(\frac{1}{\varepsilon} - \beta^2\right) \omega \, d\omega = \frac{1}{2}(1-\beta^2)\omega^2 + \sum_{j=1}^{r} a_j \bar{\omega}_j \log(\omega^2 - \bar{\omega}_j^2) \,. \tag{71}$$

7. – Generalization of the formula of Halpern and Hall.

We have seen in section 5 that the first term in the right hand side of (47) gives the Cerenkov loss. Moreover we have seen that the quantity under the integral in (47) has as real part $\omega\rho^{-1} \arg k\,(1/\varepsilon - \beta^2) = -(\omega/2\rho)[(1/\varepsilon - \beta^2)] \times$ $\times Re(i \log k^2)$, hence

$$-\frac{dW_\infty}{dx} = -\frac{e^2}{\pi v^2} Re\left[P.V. \int_0^\infty \left(\frac{1}{\varepsilon} - \beta^2\right) \log k^2 i\omega \, d\omega\right] = \tag{72}$$

$$= -\frac{e^2}{\pi v^2} Re \int_{0+i\eta}^{\infty+i\eta} \left(\frac{1}{\varepsilon} - \beta^2\right) \log \bar{k}^2 i\omega \, d\omega + \frac{e^2}{v^2} \sum_{j=1}^{r} a_j \bar{\omega}_j \log \bar{\nu}_j^2 \,,$$

$$\bar{k}^2 = \nu^2(1 - \beta^2\varepsilon) \tag{72a}$$

η being positive and infinitesimal. We shall now deform the integration path and replace it by the positive imaginary axis and a quarter of circle with infinite radius, centered at the origin. On the imaginary axis $\nu = iy$, and $\nu = b \exp[i\varphi]$ on the circle, so that

$$-\frac{dW_\infty}{dx} = \frac{e^2}{v^2} \sum_{j=1}^{r} a_j \bar{\omega}_j \log \bar{\nu}_j^2 - \frac{4Ne^4}{mv^2} \lim_{b\to\infty} \left[\pi \int_{a'}^{b} \left(\frac{1}{\varepsilon} - \beta^2\right) y \, dy + \right. \tag{73}$$

$$\left. + Re \int_0^{\pi/2} \left(\frac{1}{\varepsilon} - \beta^2\right) \log(\exp[2i\varphi]\, b^2(1 - \beta^2\varepsilon)) b^2 \exp[2i\varphi] \, d\varphi\right] ,$$

$$a' = \begin{cases} 0 & v \leqslant c(0) \\ \dfrac{u}{2\pi\alpha} & v > c(0) \,, \end{cases} \tag{74}$$

u being the absolute value of the complex roots of $1 - \beta^2\varepsilon = 0$ for $v > c(0)$. The integrals in (73) are easily evaluated using (70) and (71)

$$\int_{a'}^{b} \left(\frac{1}{\varepsilon} - \beta^2\right) y \, dy = \frac{1}{2}(1-\beta^2)(b^2 - a'^2) - \sum_{j=1}^{r} \frac{a_j \bar{\omega}_j}{4\pi^2\alpha^2} \log \frac{b^2 - \bar{\nu}_j^2}{a'^2 + \bar{\nu}_j^2} \,, \tag{75}$$

$$Re \int_0^{\pi/2} \left(\frac{1}{\varepsilon} - \beta^2\right) \log(b^2 \exp[2i\varphi](1 - \beta^2\varepsilon)) b^2 \exp[2i\varphi] \, d\varphi \sim \tag{76}$$

$$\sim -\frac{\pi}{2}\left[b^2(1-\beta^2) - \beta^2 - \log(b^2(1-\beta^2))\right] .$$

The divergences in (73) must cancel, hence

$$\sum_{j=1}^{r} a_j \bar{\omega}_j = 2\pi^2\alpha^2 . \tag{77}$$

We shall later give a direct proof of (77). Finally we get

$$-\frac{dW_\infty}{dx} = \frac{e^2}{v^2}\sum_{j=1}^{r} a_j\bar{\omega}_j \log \bar{\nu}_j^2 - \frac{2\pi Ne^4}{mv^2}\left[\log \tilde{\nu}_M^2 + \log(1-\beta^2) + \beta^2 - a'^2(1-\beta^2)\right], \tag{78}$$

with

$$\tilde{\nu}_M^2 = \prod_{j=1}^{r} (\bar{\nu}_j^2 + a'^2)^{f'_j}, \qquad f'_j = \frac{a_j\bar{\omega}_j}{2\pi^2\alpha^2}, \tag{79}$$

and

$$-\frac{dW_\infty}{dx} = \frac{2\pi Ne^4}{mv^2}\left[\log \frac{\bar{\nu}_M^2}{\tilde{\nu}_M^2(1-\beta^2)} - \beta^2 + a'^2(1-\beta^2)\right] \tag{80}$$

$$\bar{\nu}_M = \prod_{j=1}^{r} \bar{\nu}_j^{f'_j}, \tag{81}$$

$$-\frac{dW_\varrho}{dx} = \frac{4\pi Ne^4}{mv^2}\sum_{j=1}^{r} f'_j \frac{\omega_j\rho}{v} K_1\left(\frac{\bar{\omega}_j\rho}{v}\right) K_0\left(\frac{\bar{\omega}_j\rho}{v}\right) + \frac{2\pi Ne^4}{mv^2} \times \times \left[\log \frac{\bar{\nu}_M^2}{\tilde{\nu}_M^2(1-\beta^2)} - \beta^2 + a'^2(1-\beta^2)\right]. \tag{82}$$

It is interesting to remark that equations (80) and (82) are exact, provided the absorption coefficient be taken as zero. Equation (82) gives a generalization of the formula of Halpern and Hall. For small values of ρ

$$-\frac{dW_\varrho}{dx} = \frac{2\pi Ne^2}{mv^2}\log\left[\frac{(v/\pi\gamma\alpha\rho)^2}{\tilde{\nu}_M^2(1-\beta^2)} - \beta^2 + a'^2(1-\beta^2)\right]. \tag{83}$$

In order to obtain the formula of Halpern and Hall we replace the $\bar{\nu}_j$ by the ν_j and the f'_j by the f_j in the definition of $\tilde{\nu}_M$.

When $\beta^2/(1-\beta^2) > \bar{\nu}_r^2$ we have

$$a'^2 \backsimeq \frac{\beta^2}{1-\beta^2}, \qquad \tilde{\nu}_M \backsimeq a', \tag{84}$$

so that for small values of ρ

$$-\frac{dW_\varrho}{dx} \backsimeq \frac{4\pi Ne^4}{mc^2}\log\frac{c}{\pi\gamma\alpha\rho} \tag{85}$$

and the loss of energy at distances larger than the atomic dimensions becomes saturated and independent of the atomic frequencies.

Equation (77) can be obtained directly by computing $\int_I [(1/\varepsilon)-1]\omega\, d\omega$

along a circle of infinite radius with the Lorentz expression of ε and expressing the same integral in terms of the residues a_j. We get from (59), for zero damping

$$\frac{1}{\varepsilon} - 1 \sim - \sum_{j=1}^{r} \frac{f_j}{\nu_j^2 - \nu^2} , \tag{86}$$

so that

$$\lim_{\Gamma \to \infty} \int_{\Gamma} \left(\frac{1}{\varepsilon} - 1 \right) \omega \, \mathrm{d}\omega = 2\pi i \cdot 4\pi^2 \alpha^2 = 2\pi i \cdot 2 \sum_{j=1}^{r} a_j \bar{\omega}_j . \tag{87}$$

The methods of this section could be applied to any form of a real ε depending only on ω^2 and having only real simple zeros.

8. – The action at a distance and the field treatments of the loss of energy.

The force acting on the electrons $e\boldsymbol{E}_{\mathrm{act}}$, in the Lorentz theory of the dispersion, is given by (60). The work done per unit time on the electrons contained in a volume V is

$$\int_V \left(\boldsymbol{E}_{\mathrm{act}} \cdot \frac{\partial \boldsymbol{P}}{\partial t} \right) \mathrm{d}_3 x = \int_V \left(\boldsymbol{E} \cdot \frac{\partial \boldsymbol{P}}{\partial t} \right) \mathrm{d}_3 x + \frac{2\pi}{3} \frac{\partial}{\partial t} \int_V \boldsymbol{P}^2 \mathrm{d}_3 x . \tag{88}$$

We get from the Maxwell equations, when V is not traversed by the path

$$\int_V \left(\boldsymbol{E} \cdot \frac{\partial \boldsymbol{P}}{\partial t} \right) \mathrm{d}_3 x = - \frac{1}{8\pi} \frac{\partial}{\partial t} \int_V (\boldsymbol{E}^2 + \boldsymbol{H}^2) \, \mathrm{d}_3 x - \frac{c}{4\pi} \int_S \boldsymbol{E} \times \boldsymbol{H}_n \, \mathrm{d}S , \tag{89}$$

S being the surface enclosing V. n denotes the outer normal of S. It results from (88) and (89) that

$$\int_V \left(\boldsymbol{E}_{\mathrm{act}} \cdot \frac{\partial \boldsymbol{P}}{\partial t} \right) \mathrm{d}_3 x = - \frac{\partial}{\partial t} \int_V \left(\frac{\boldsymbol{E}^2 + \boldsymbol{H}^2}{8\pi} - \frac{2\pi}{3} \boldsymbol{P}^2 \right) \mathrm{d}_3 x - \frac{c}{4\pi} \int_S [\boldsymbol{E} \times \boldsymbol{H}]_n \, \mathrm{d}S . \tag{90}$$

Let V_ϱ be the region outside the cylindrical surface S_ϱ of radius ϱ with axis on the path. In this case, the first term in the right hand side of (90) vanishes, because $\boldsymbol{E}$, $\boldsymbol{H}$ and $\boldsymbol{P}$ depend on x and t, only through the combination $x - vt$. Hence, the rate of work done by $\boldsymbol{E}_{\mathrm{act}}$ and $\boldsymbol{E}$ on the electrons of V_ϱ is the same and

$$\int_{V_\varrho} \left(\boldsymbol{E}_{\mathrm{act}} \cdot \frac{\partial \boldsymbol{P}}{\partial t} \right) \mathrm{d}_3 x = \frac{c}{4\pi} \left\{ \int_{S_\varrho} - \int_{S_\infty} \right\} [\boldsymbol{E} \times \boldsymbol{H}]_n \, \mathrm{d}S , \tag{91}$$

therefore

$$-\frac{\mathrm{d}W_\varrho}{\mathrm{d}x}=-\frac{\mathrm{d}W_\infty}{\mathrm{d}x}+\frac{1}{v}\int_{V_\varrho}\left(\boldsymbol{E}_{\mathrm{act}}\cdot\frac{\partial\boldsymbol{P}}{\partial t}\right)\mathrm{d}_3x\,. \tag{92}$$

In the case of an absorbent medium, the first term in the right hand side of (92) vanishes, because the K functions in (45) vanish on S_∞. In this case $-\mathrm{d}W_\varrho/\mathrm{d}x$ coincides with the energy transmitted to the electrons, per unit length of path, at distances larger than ϱ. In a non absorbent medium, the same is not true and we get from (82) and (80)

$$\frac{1}{v}\int_{V_\varrho}\left(\boldsymbol{E}_{\mathrm{act}}\cdot\frac{\partial\boldsymbol{P}}{\partial t}\right)\mathrm{d}_3x\quad\frac{4\pi Ne^4}{mv^2}\sum_{j=1}^{r}f_j\frac{\bar\omega_j\varrho}{v}K_1\left(\frac{\bar\omega_j\varrho}{v}\right)K_0\left(\frac{\bar\omega_j\varrho}{v}\right). \tag{93}$$

We shall now compute directly the rate of work done on the electrons. The polarization $\boldsymbol{P}$ can be divided into the parts $\boldsymbol{P}_j$ corresponding to the various electronic frequencies ν_j

$$\boldsymbol{P}=\sum_{j=1}^{r}\boldsymbol{P}_j\,. \tag{94}$$

Taking into account (60), we get

$$\frac{\partial^2\boldsymbol{P}_j}{\partial t^2}+2\pi\alpha g_j\frac{\partial\boldsymbol{P}_j}{\partial t}+\omega_j^2\boldsymbol{P}_j=\frac{Ne^2}{m}f_j\boldsymbol{E}+\frac{4\pi Ne^2}{3m}f_j\sum_{l=1}^{r}\boldsymbol{P}_l\,. \tag{95}$$

In the dispersion theory, equation (95) is solved by Fourier expansion, taking

$$\boldsymbol{P}_{j,\omega}=\frac{Ne^2f_j}{m}\frac{\boldsymbol{E}_\omega+\frac{4\pi}{3}\sum_{l=1}^{r}\boldsymbol{P}_{l,\omega}}{\omega_j^2-\omega^2-2\pi i\alpha g_j\omega}\,, \tag{96}$$

so, that

$$\boldsymbol{P}=\frac{1}{4\pi}\int(\varepsilon-1)\,\boldsymbol{E}_\omega\exp\left[-i\omega t\right]\mathrm{d}\omega\,, \tag{97}$$

with

$$\varepsilon=1+\sum_{j=1}^{r}{}'\frac{f_j}{\nu_j^2-\nu^2-ig_j\nu}\Big/\left(1-\frac{1}{3}\sum_{j=1}^{r}\frac{f_j}{\nu_j^2-\nu^2-ig_j\nu}\right). \tag{98}$$

In the approximation in which the Lorentz correction to the force acting on the electrons is neglected, (95) is replaced by

$$\frac{\partial^2\boldsymbol{P}_{B,j}}{\partial t^2}+2\pi\alpha g_j\frac{\partial\boldsymbol{P}_{B,j}}{\partial t}+\omega_j^2\boldsymbol{P}_{B,j}=\frac{Ne^2}{m}f_j\boldsymbol{E}\,, \tag{99}$$

and instead of (97) we get

$$\boldsymbol{P}_{ll} = \frac{1}{4\pi}\int_{-\infty}^{+\infty} (\varepsilon_S - 1)\boldsymbol{E}_\omega \exp[-i\omega t]\,\mathrm{d}\omega. \tag{100}$$

ε_S being the Sellmayer form of the dielectric constant (61). We denote the polarization derived from (99) by $\boldsymbol{P}_{ll}$ because it comes in in the expression of the loss in the Bohr approximation, $\boldsymbol{E}$ being replaced by $\boldsymbol{E}_{\mathrm{vac}}$ in (100)

$$\frac{1}{r}\int_{V_\varrho}\left(\boldsymbol{E}_{\mathrm{vac}}\cdot\frac{\partial \boldsymbol{P}_{ll}}{\partial t}\right)\mathrm{d}_3 r = -\frac{i}{4\pi e}\int_{V_\varrho}\mathrm{d}_3 x\int_{-\infty}^{+\infty}(\varepsilon_S - 1)(\boldsymbol{E}_{\mathrm{vac}}\cdot\boldsymbol{E}_{\mathrm{vac},\omega})\exp[-i\omega t]\omega\,\mathrm{d}\omega \tag{101}$$

$$= \frac{i}{2v}\int_{\varrho}^{\infty}\rho'\,\mathrm{d}\rho'\int_{-\infty}^{+\infty}\mathrm{d}x\int_{-\infty}^{+\infty}(1-\varepsilon_S)(\boldsymbol{E}_{\mathrm{vac},\omega}\cdot\boldsymbol{E}_{\mathrm{vac},\omega'})\exp[-i(\omega+\omega')t]\omega\,\mathrm{d}\omega\,\mathrm{d}\omega'.$$

The Fourier components of the field in the vacuum are of the form

$$\boldsymbol{E}_{\mathrm{vac},\omega} = \boldsymbol{B}_{\mathrm{vac},\omega}\exp[i\omega x/v], \tag{102}$$

the $\boldsymbol{B}_{\mathrm{vac},\omega}$ being independent of x, therefore

$$\frac{1}{r}\int_{V_\varrho}\left(\boldsymbol{E}_{\mathrm{vac}}\cdot\frac{\partial \boldsymbol{P}_{ll}}{\partial t}\right)\mathrm{d}_3 r = 2\pi\int_{\varrho}^{\infty}\rho'\,\mathrm{d}\rho'\,Re\int_0^{\infty}(1-\varepsilon_S)\,|\,\boldsymbol{B}_{\mathrm{vac},\omega}\,|^2\,i\omega\,\mathrm{d}\omega. \tag{103}$$

We get from (28) and (29), putting $\varepsilon = 1$

$$|\,\boldsymbol{B}_{\mathrm{vac}}(\omega)\,|^2 = \frac{e^2\omega^2}{\pi^2 v^4}(1-\beta^2)\left|K_1^2\left(\frac{\omega\varrho}{v}\sqrt{1-\beta^2}\right) + (1-\beta^2)K_0^2\left(\frac{\omega\varrho}{v}\sqrt{1-\beta^2}\right)\right|. \tag{104}$$

We shall now neglect the damping constants g and deform the integration path in the ω-plane, in (101), to avoid the poles of ε_S. When $g \neq 0$ those poles lie below the real ω-axis and they tend to $\pm\omega_j$, when the g tend to zero. The residue at ω_j is $-\pi\alpha(f_j/\nu_j)$. Indenting the positive real axis with half-circles in the upper part of the plane, we get in the usual way

$$\frac{1}{r}\int_{V_\varrho}\left(\boldsymbol{E}_{\mathrm{vac}}\cdot\frac{\partial \boldsymbol{P}}{\partial t}\right)\mathrm{d}_3 r = 2\pi\int_{\varrho}^{\infty}\rho'\,\mathrm{d}\rho'\,Re\left\{P.V.\int_0^{\infty}(1-\varepsilon_S)\,|\,\boldsymbol{B}_{\mathrm{vac},\omega}\,|^2\,i\omega\,\mathrm{d}\omega\right\} + \tag{105}$$

$$+\frac{4\pi N e^4}{mv^4}(1-\beta^2)\int_{\varrho}^{\infty}\sum_{j=1}^{r} f_j\omega_j^2\left[K_1^2\left(\frac{\omega_j\rho'}{v}\sqrt{1-\beta^2}\right) + (1-\beta^2)K_0^2\left(\frac{\omega_j\rho'}{v}\sqrt{1-\beta^2}\right)\right]\rho'\mathrm{d}\rho'.$$

The principal value term in (105) vanishes, because ε_S is real. The integrals

arising from the residues can be evaluated using the Lommel formula

$$\int K_\mu^2(lu)u\,\mathrm{d}u = \frac{u^2}{2}\left[K_\mu^2(lu) - K_{\mu-1}(lu)K_{\mu+1}(lu)\right]. \tag{106}$$

Finally we get

$$\frac{1}{v}\int_{V_\varrho}\left(\boldsymbol{E}_{\mathrm{vac}}\cdot\frac{\partial\,\boldsymbol{P}}{\partial t}\right)\mathrm{d}_3x = \frac{2\pi Ne^4\rho^2}{mv^4}(1-\beta^2)\sum_{j-1}^{r} f_j\omega_j^2\left[\beta^2\,K_0^2\left(\frac{\omega_j\rho}{v}\sqrt{1-\beta^2}\right)-\right. \tag{107}$$

$$\left.-\beta^2K_1^2\left(\frac{\omega_j\rho}{v}\sqrt{1-\beta^2}\right)+\frac{2v}{\omega_j\rho\sqrt{1-\beta^2}}\,K_0\left(\frac{\omega_j\rho}{v}\sqrt{1-\beta^2}\right)K_1\left(\frac{\omega_j\rho}{v}\sqrt{1-\beta^2}\right)\right].$$

For non relativistic velocities (107) and (93) coincide approximately, therefore the spatial distribution of the excitation and the ionization obtained from the Bohr treatment coincides approximately with that of the field treatment. Equation (107) shows clearly the increase of the radii of action in the relativistic region, due to the $\sqrt{1-\beta^2}$ in the K functions. For small values of ρ we can simplify (107)

$$\frac{1}{v}\int_{V_\varrho}\left(\boldsymbol{E}_{\mathrm{vac}}\cdot\frac{\partial\boldsymbol{P}_B}{\partial t}\right)\mathrm{d}_3x = \frac{2\pi Ne^4}{mv^2}\left[\sum_{j=1}^{r}2f_j\log\frac{2v}{\gamma\omega_j\rho\sqrt{1-\beta^2}}-\beta^2\right]. \tag{108}$$

Equation (108) shows that the logarithmic increase of the loss in collisions with impact parameters larger than the atomic dimensions is due to a $\sqrt{1-\beta^2}$ coming from a K function. Thus we obtain the well known result that the increase of the loss, in the Bohr treatment for relativistic energies, is due to an increase of the radii of action.

The preceding computation can be easily extended to the case of a dispersive non absorbent medium, taking into account the polarization effects. We have

$$\frac{1}{v}\int_{V_\varrho}\left(\boldsymbol{E}_{\mathrm{act}}\cdot\frac{\partial\boldsymbol{P}}{\partial t}\right)\mathrm{d}_3x = 2\pi\int_{\varrho}^{\infty}\rho'\,\mathrm{d}\rho'\,Re\int_0^{\infty}(1-\varepsilon)\,|\,\boldsymbol{B}_\omega\,|^2 i\omega\,\mathrm{d}\omega\,, \tag{109}$$

with

$$\boldsymbol{B}_\omega = \boldsymbol{E}_\omega\exp\left[-i\omega x/v\right]. \tag{110}$$

It follows from (28) and (29) that

$$|\,\boldsymbol{B}_\omega\,|^2 = \frac{e^2}{\pi^2v^2}\left|\frac{k}{\varepsilon}\right|^2\left[|\,K_1(k\rho')\,|^2+|\,1-\beta^2\varepsilon\,|\,|\,K_0(k\rho')\,|^2\right], \tag{111}$$

$$Re\left\{(1-\varepsilon)\,|\,\boldsymbol{B}_\omega\,|^2\,i\omega\right\} = \tag{112}$$

$$= \frac{e^2\omega^2}{\pi^2v^4}\,Re\left[\frac{i\omega}{\varepsilon}\,|\,1-\beta^2\varepsilon\,|\left\{|\,K_1(k\rho')\,|^2+|\,1-\beta^2\varepsilon\,|\,|\,K_0(k\rho')\,|^2\right\}\right].$$

In the case of zero damping, it is possible to deform suitably the integration path in (109), as it was done with (103), and we get

$$(113)\quad \frac{1}{r}\int_{V_\varrho}\left(\boldsymbol{E}\cdot\frac{\partial \boldsymbol{P}}{\partial t}\right)\mathrm{d}_3 r = -\frac{2e^2}{v^2}\int_{\varrho}^{\infty}\sum_{j=1}^{r} a_j\left[\frac{\overline{\omega}_j^3}{v^2}\right\} K_1^2\left(\frac{\overline{\omega}_j\rho'}{v}\right) + K_0^2\left(\frac{\overline{\omega}_j\rho'}{v}\right)\Bigg\}\Bigg]\rho'\,\mathrm{d}\rho' .$$

The integrals in (113) can be evaluated with the Lommel formula (106) and thus we obtain in a different way equation (93). $\sqrt{1-\beta^2}$ does not appear any more in (113). The difference between the present case and Bohr's one results from the fact that $\sqrt{1-\beta^2}$ is replaced by $\sqrt{1-\beta^2\varepsilon}$ and the contribution to (113) comes from residues at the zeros of ε. It is interesting to remark that, even when the Lorentz correction to the force acting on the electrons can be neglected and ε replaced by ε_S – as it happens in the case of gases – $\sqrt{1-\beta^2}$ will still not appear in (113).

In the case of an absorbent medium, we get from (109) and (112)

$$(114)\quad \frac{1}{r}\int_{V_\varrho}\left(\boldsymbol{E}\cdot\frac{\partial \boldsymbol{P}}{\partial t}\right)\mathrm{d}_3 r$$

$$= -\frac{2e^2}{\pi r^4}\int_{\varrho}^{\infty}\rho'\,\mathrm{d}\rho' R\cdot\int_0^{\infty}\left[\frac{i\omega^3}{\varepsilon}\,|\,1-\beta^2\varepsilon\,|\left\{|\,K_1(k\rho')\,|^2 + |\,1-\beta^2\varepsilon\,|\,|\,K_0(k\rho')\,|^2\right\}\right]\mathrm{d}\omega .$$

This equation is equivalent to (45), as it can be seen by differentiating (45)

$$(115)\quad \frac{\mathrm{d}}{\mathrm{d}\rho}\left(-\frac{\mathrm{d}W_\varrho}{\mathrm{d}x}\right) =$$

$$-\frac{2e^2\rho}{\pi r^4}\,R\int_0^{\infty}\left[\frac{i\omega^3}{\varepsilon}\,|\,1-\beta^2\varepsilon\,|\left\{|\,K_1(k\rho)\,|^2 + |\,1-\beta^2\varepsilon\,|\,|\,K_0(k\rho)\,|^2\right\}\right]\mathrm{d}\omega .$$

It results from the preceding considerations that an improved form of Bohr's treatment, in which the field in the dispersive medium is used instead of the field in the vacuum, leads to a satisfactory result in the case of an absorbent medium – although it does not give the total loss of energy in the case of a non absorbent medium – provided the rate of work on the electrons be computed with the solutions of the equations of motion of the electrons including the damping terms. Equation (115) gives the spatial distribution of the excitation and ionization of the medium. For large values of ρ (115) can be simplified, using the asymptotic expression of the K functions. It can be seen that, for large ρ

$$(116)\quad \frac{\mathrm{d}}{\mathrm{d}\rho}\left(-\frac{\mathrm{d}W_\varrho}{\mathrm{d}x}\right) \backsimeq -\frac{2e^2}{c^2 v}\int_{\substack{c(\omega)<v\\ \omega\geqslant 0}}\varkappa(\omega)c(\omega)\sqrt{|\,1-\beta^2\varepsilon\,|}\exp\left[\frac{-2\varkappa(\omega)\rho}{\sqrt{1-c^2(\omega)/v^2}}\right]\omega\,\mathrm{d}\omega .$$

The corresponding equation in the Bohr theory is obtained easily from (105)

$$(117)\quad \frac{\mathrm{d}}{\mathrm{d}\rho}\left(-\frac{\mathrm{d}W_e}{\mathrm{d}x}\right)_B \cong \frac{2\pi^2 N e^4}{mv^3}\sqrt{1-\beta^2}\sum_{j=1}^{r} f_j\omega_j\,(2-\beta^2)\exp\left(-\frac{2\omega_j\rho}{v}\sqrt{1-\beta^2}\right).$$

Both (116) and (117) give exponential decays of the rate of variation of the ionization and excitation, at large distances from the path. But the ranges in the Bohr theory are determined by the energy of the ionizing particle and the atomic frequencies, whereas in (116) the ranges of the excitation and ionization are determined (for relativistic energies) by the absorption coefficients of the frequencies of the Cerenkov spectrum and do not increase indefinitely with the energy of the particle. Nevertheless, for energies of the particle which are not exceedingly high with respect to its rest mass, the range of excitation and ionization (secondary) may be higher than in the Bohr theory, because of the smallness of the absorption coefficients.

9. – The mechanism of emission of the Cerenkov radiation.

We have already seen in section 5 that the flux of the Cerenkov radiation is the same through all the cylindrical surfaces with axis on the path of the ionizing particles, in the case of a non absorbent medium. Since there is no absorption, the whole Cerenkov radiation must come from the immediate neighbourhood of the path. Therefore the Cerenkov radiation may be considered as emitted by the ionizing particle, rather than by the electrons of the medium (as it was assumed by TAMM [10] and A. BOHR [9]). These authors assumed that the Cerenkov radiation represents a part of the energy given to the electrons of the medium, which is later reemitted. Equation (93) shows that the rate of work done on the electrons does not include the Cerenkov loss, in the case of a non absorbent medium. Strictly speaking, the Cerenkov radiation represents a part of the electromagnetic field of the system ionizing particle plus electrons, which gets loose and travels in the dispersive medium, starting from the immediate neighbourhood of the path.

The Cerenkov radiation is closely related to the Cerenkov field defined by equations (33). It results from the analysis of section 2 that

$$(118)\quad E_x^c = \frac{e}{v^2}\int_{c(\omega)<v}\left(\frac{1}{\varepsilon}-\beta^2\right)J_0\left(\frac{\omega\rho}{v}\sqrt{\beta^2\varepsilon-1}\right)\cos\left(\omega\left(\frac{x}{v}-t\right)\right)\omega\,\mathrm{d}\omega \qquad (\omega>0).$$

At the position of the particle $x = vt$ and $\rho = 0$, so that

$$(119)\quad (E_x^c)_{\mathrm{part}} = \frac{e}{v^2}\int_{c(\omega)<v}\left(\frac{1}{\varepsilon}-\beta^2\right)\omega\,\mathrm{d}\omega = \frac{1}{e}\frac{\mathrm{d}W_\infty}{\mathrm{d}x}.$$

The rate of work done on the particle by the Cerenkov field is, therefore, equal to minus the rate of emission of Cerenkov radiation. All the components of the Cerenkov field are finite on the path

$$(120)\quad E^c_{tr} = -\frac{e}{v^2}\int_{c(\omega)<v} \frac{1}{\varepsilon}\sqrt{\beta^2\varepsilon - 1}\; J_1\left(\frac{\omega\rho}{v}\sqrt{\beta^2\varepsilon - 1}\right)\sin\left(\omega\left(\frac{x}{v} - t\right)\right)\omega\,\mathrm{d}\omega \quad (\omega > 0)\,,$$

$$(121)\quad H^c = -\frac{e}{vc}\int_{c(\omega)<v} \sqrt{\beta^2\varepsilon - 1}\; J_1\left(\frac{\omega\rho}{c}\sqrt{\beta^2\varepsilon - 1}\right)\sin\left(\omega\left(\frac{x}{v} - t\right)\right)\omega\,\mathrm{d}\omega \quad (\omega > 0)\,.$$

The Cerenkov field may be considered as the part of the total field, created by the moving particle and the electrons, that gets loose and gives rise to a damping force. The rate of work of that damping force, acting on the ionizing particle, corresponds to the Cerenkov loss. We shall see later that this is the only loss due to the Cerenkov field. The expression of the total field on the path is not satisfactory, because, for strong fields, equation (1) is not valid. On the other hand the Cerenkov field is a solution of the homogeneous Maxwell equations (34), which may be assumed to hold, even on the path, since the field intensities are everywhere moderate.

It is worthwhile to notice that there is a part of the contribution of the Cerenkov frequencies to the retarded field which is not included in the Cerenkov field. Let us call Bohr field the difference between the retarded and the Cerenkov fields and denote its electric and magnetic parts by $\boldsymbol{E}^B$ and $\boldsymbol{H}^B$

$$(122)\qquad \boldsymbol{E}^B = \frac{1}{2}(\boldsymbol{E}^{\mathrm{ret}} + \boldsymbol{E}^{\mathrm{adv}})\,, \qquad \boldsymbol{H}^B = \frac{1}{2}(\boldsymbol{H}^{\mathrm{ret}} + \boldsymbol{H}^{\mathrm{adv}})\,.$$

We have

$$(123)\quad E^B_\omega = -\frac{ie}{2\pi v^2}\int_{-\infty+i\eta}^{+\infty+i\eta}\left(\frac{1}{\varepsilon} - \beta^2\right)K_0(k\rho)\left(1 + \frac{k^2}{|k|^2}\right)\exp\left[i\omega\left(\frac{x}{v} - t\right)\right]\omega\,\mathrm{d}\omega -$$

$$-\frac{e}{v^2}\sum_{\text{bands}}\int\left(\frac{1}{\varepsilon} - \beta^2\right)N_0\left(\frac{\omega\rho}{v}\sqrt{\beta^2\varepsilon - 1}\right)\sin\left(\omega\left(\frac{x}{v} - t\right)\right)\omega\,\mathrm{d}\omega\,.$$

The second group of terms in the right hand side of (123) is due to the Cerenkov frequencies. The Bohr field satisfies the inhomogeneous Maxwell equations (6). It diverges on the path in an insatisfactory way, because, even subtracting the Lorentz transformed Coulomb field, we still do not get rid of the divergences, although the motion of the particle is non accelerated. Denoting by $\boldsymbol{P}^B$ the polarization corresponding to $\boldsymbol{E}^B$, we have

$$(124)\qquad \int_{V_e}\left(\boldsymbol{E}^{\mathrm{ret}}\cdot\frac{\partial\boldsymbol{P}^{\mathrm{ret}}}{\partial t}\right)\mathrm{d}_3x = \int_{V_e}\left(\boldsymbol{E}^B\cdot\frac{\partial\boldsymbol{P}^B}{\partial t}\right)\mathrm{d}_3x\,.$$

This results from the fact that the resonance frequencies ω do not belong to the Cerenkov bands and that the contributions of the Bohr frequencies to both the retarded and Bohr fields are the same. We get from (124)

$$(125) \qquad \int_{\tau_\varrho} \left(\boldsymbol{E}^c \cdot \frac{\partial \boldsymbol{P}^{\mathrm{ret}}}{\partial t} \right) \mathrm{d}_3 x + \int_{V_\varrho} \left(\boldsymbol{E}^B \cdot \frac{\partial \boldsymbol{P}^c}{\partial t} \right) \mathrm{d}_3 x = 0 \, .$$

This equation shows that the Cerenkov field does not transmit energy to the electrons of the medium because it induces a polarization $\boldsymbol{P}^C$, that modifies the rate of work of the Bohr field by an amount which compensates exactly its rate of work.

The considerations developed in this section are remarkably similar to those of the theory of point charges interacting with an electromagnetic field. The Cerenkov field corresponds to the radiation field of point particles defined by LEITE LOPES and SCHÖNBERG [12] and by WHEELER and FEYNMAN [13]. It is possible to define a density of energy w^c and a Poynting vector $\boldsymbol{U}^c$ of the Cerenkov field

$$(126) \qquad w^c = \frac{1}{16\pi} \left[\{ (\boldsymbol{E}^{\mathrm{ret}})^2 + (\boldsymbol{H}^{\mathrm{ret}})^2 \} - \{ (\boldsymbol{E}^{\mathrm{adv}})^2 + (\boldsymbol{H}^{\mathrm{adv}})^2 \} \right] ,$$

$$(127) \qquad \boldsymbol{U}^c = \frac{c}{8\pi} \{ [\boldsymbol{E}^{\mathrm{ret}} \times \boldsymbol{H}^{\mathrm{ret}}] - [\boldsymbol{E}^{\mathrm{adv}} \times \boldsymbol{H}^{\mathrm{adv}}] \} ,$$

as it was done by SCHÖNBERG [14] for the radiation field of a system of point particles. It is easily seen that

$$(128) \qquad - \frac{\mathrm{d}W_\infty}{\mathrm{d}x} = \frac{1}{v} \int_{S_\varrho} U_n^c \, \mathrm{d}S \, .$$

In the general case of an accelerated ionizing particle, one half the difference between the retarded and advanced solutions of the Maxwell equations in the dispersive non absorbent medium would give the radiation field, that accounts for the emission of both the Cerenkov and the acceleration radiation. The Cerenkov field considered in this paper is therefore a particular case of the radiation field of the theory of point particles. The emission of Cerenkov radiation is ultimately due to the fact that there are accelerated electrons in the medium, even when the ionizing particle is non accelerated. But, as a consequence of complicated interference effects, the flux of radiation comes from the path of the ionizing particle.

---

[12] J. LEITE LOPES and M. SCHÖNBERG: *Phys. Rev.*, **67**, 122 (1945).
[13] J. A. WHEELER and R. P. FEYNMAN: *Rev. Mod. Phys.*, **17**, 157 (1945).
[14] M. SCHÖNBERG: *Phys. Rev.*, **69**, 211 (1946).

The Bohr field plays, in the present theory, a part analogous to that of one half the sum of the retarded and advanced fields in the theory of charged point particles. In that theory, the half-retarded half-advanced solution of the inhomogeneous field equations gives rise to relativistic actions at a distance. In our case, the Bohr field accounts for the primary excitation and ionization of the atoms, which are due tó the Coulomb field at low velocities (non relativistic action at a distance). When the damping is taken into account, the total field coincides wth the Bohr field, so that the entire loss can be ascribed to relativistic actions at a distance (emission and absorption of virtual quanta in quantum electrodynamics).

From a purely mathematical point of view, it is interesting to consider the case of a medium with a dielectric constant ε independent of the frequency and real, but larger than unity. In such an ideal case all the frequencies would be Bohr frequencies for $v < c/\sqrt{\varepsilon}$ and would become Cerenkov frequencies for $v > c/\sqrt{\varepsilon}$. When $v < c/\sqrt{\varepsilon}$ the retarded and advanced solutions do coincide, as it happens in the vacuum, but they would be distinct for $v > c/\sqrt{\varepsilon}$ and this would lead to the emission of radiation. In the case of a non absorbent dispersive medium, a frequency belongs to the Cerenkov spectrum when its contributions to the retarded and advanced fields are distinct.

RIASSUNTO (*)

Si esamina la teoria della perdita d'energia di una particella carica non accelerata in un mezzo materiale nell'ambito dell'elettrodinamica classica, dando speciale rilievo al meccanismo della perdita. Si generalizzano e si estendono ulteriormente i risultati di Fermi, Halpern e Hall e di Wick e A. Bohr. Si discutono e si confrontano i punti di vista dell'azione a distanza (Bohr) e della teoria del campo (Fermi). Si discute, infine, il meccanismo dell'emissione della radiazione di Cerenkov e se ne analizzano le relazioni con l'emissione della radiazione d'accelerazione.

(*) *Traduzione a cura della Redazione.*

Scattering of Neutrons By Deuterons.

E. Clementel

University of Manchester (England) (*)

(ricevuto il 9 Dicembre 1950)

Summary. — The scattering of thermal neutrons by deuterons has been treated by solving by a variational method the equation of motion for S waves. A trial function with three variational parameters and a Gaussian potential with a depth of 45 MeV and a range of $2 \cdot 10^{-13}$ cm have been used. The value of the cross section does not depend sensibly on the types of forces which have been considered (neutral, symmetrical and a combination of Heisenberg and Majorana forces), and the contribution both of the states of quartet and doublet are of the same order. The ratio between the experimental and the theoretical cross section is about two; a better agreement would be obtained by increasing the range of the potential. A formula for the calculation of the phases for the higher order waves has also been given.

1. – Introduction.

The scattering of neutrons by deuterons has been treated by various authors using mainly a potential of Gaussian type. However, the mathematical difficulties of the problem have made it necessary to adopt approximations which do not always seem to be permitted. The results of the various authors are in any case discordant, and it is not easy to establish whether the disagreement is due to the different methods used for the solution of the equation of motion, or whether it is due to the choice of the constants in the general expression of the potential. Buckingam and Massey [1] treated the problem by using a potential of exponential type, for which a laborious numerical

(*) Now at Istituto di Fisica, Università di Padova (Italy).

(1) R. A. Buckingam and H. S. W. Massey: *Proc. Roy. Soc.*, **179**, 123 (1941).

integration of the equation of motion is unavoidable. The result obtained by these authors is in good agreement with the experimental data up to an energy of about 10 MeV. The object of this note is to see whether or not the Gauss potential, with which the problem can be treated analytically, gives the same results as the exponential potential. For this purpose the equation of motion has been solved by a variational method. As usual, the polarization effect has been neglected. Apart from that, no other approximation has been made. The method has been applied in particular to the case of thermal neutrons.

2. – Equation of motion.

The general form of the wave equation for a system of three particles of the same mass M, is

$$(1) \qquad \left\{ -\frac{\hbar^2}{2M}(\Delta_1 + \Delta_2 + \Delta_3) + V_{12} + V_{13} + V_{23} \right\} \Psi(1, 2, 3) = (E_0 + \varepsilon)\Psi(1, 2, 3) .$$

Here the index 1 denotes the incident neutron and 2 and 3 respectively the neutron and proton forming the deuteron; ε indicates the binding energy of the ground state of the deuteron, E_0 the energy of the incident neutron in the laboratory system, V_{ij} the interaction energies, for which we shall assume the most general form

$$(2) \qquad V_{ij} = -[mP_{ij} + hP_{ij}Q_{ij} + bQ_{ij} + w]J(r_{ij}) .$$

$J(r_{ij})$ is a function only of the distance $r_{ij} = |\boldsymbol{r}_i - \boldsymbol{r}_j|$, P_{ij} and Q_{ij} are respectively the operators which interchange the coordinates and the spins of the particles i, j. Introducing the Pauli matrices $\boldsymbol{\sigma}_i$, $\boldsymbol{\sigma}_j$ we can write

$$(3) \qquad Q_{ij} = \frac{1}{2}(1 + \boldsymbol{\sigma}_i\boldsymbol{\sigma}_j) .$$

The quantities m, h, b and w are pure numbers satisfying the condition $m - h + b + w = 1$. As we neglect the polarization of the deuteron by the field of the incident neutron and we limit ourselves to elastic scattering, the wave function of the system, apart from the factor representing the motion of the centre of mass, is given by the function

$$(4) \qquad \Psi(1, 2, 3) = (1 - P_{12}Q_{12})F(\boldsymbol{r})\psi(\boldsymbol{\rho})\chi(123) ,$$

antisymmetric in the two identical particles, where

$$(5) \qquad \boldsymbol{r} = \boldsymbol{r}_1 - \frac{1}{2}(\boldsymbol{r}_2 + \boldsymbol{r}_3) , \quad \boldsymbol{\rho} = \boldsymbol{r}_3 - \boldsymbol{r}_2 .$$

$\psi(\boldsymbol{\rho})$ is the unperturbed function of the ground state of the deuteron (2, 3), $F(\boldsymbol{r})$ the position function of the neutron 1 relative to the centre of mass of the deuteron, $\chi(123)$ the spin function for a definite value S of the total spin of the system, with the possible values 3/2 (quartet) and 1/2 (doublet), according as the sign of the incident neutron is parallel or antiparallel to that of the deuteron. The function $\psi(\rho)$ satisfies the wave equation

$$\left\{\frac{\hbar^2}{M}\Delta + J(\rho)\right\}\psi(\rho) = -\varepsilon\psi(\rho)\,. \tag{6}$$

Substituting the form (4) for $\Psi(123)$ in (1), multiplying both sides by $\psi^*(\boldsymbol{\rho})\chi^*(123)$, integrating over $\boldsymbol{\rho}$ and summing over the spins, we obtain the equation

$$\begin{aligned}\frac{3\hbar^2}{4M}(\Delta + E)F(\boldsymbol{r}) = {} & \Sigma\int \psi^*(\boldsymbol{\rho})\chi^*(123)[V_{12} + V_{13}][1 - P_{12}Q_{12}]F(\boldsymbol{r})\psi(\boldsymbol{\rho})\chi(123)\,\mathrm{d}\boldsymbol{\rho} - \\ & - \Sigma\int \psi^*(\boldsymbol{\rho})\chi^*(123)V_{23}P_{12}Q_{12}F(\boldsymbol{r})\psi(\boldsymbol{\rho})\chi(123)\,\mathrm{d}\boldsymbol{\rho} + \\ & + \Sigma\int \psi^*(\boldsymbol{\rho})\chi^*(123)P_{12}Q_{12}\left\{\frac{\hbar^2}{2M}\left(2\Delta_\varrho + \frac{2}{3}\Delta_r\right) + E + \varepsilon\right\}F(\boldsymbol{r})\psi(\boldsymbol{\rho})\chi(123)\,\mathrm{d}\boldsymbol{\rho}\,.\end{aligned} \tag{7}$$

Use has been made of (6) and $E = (2/3)E_0$ denotes the energy of the incident neutron in the centre of mass system.

Taking into account that the spins of neutrons and proton in the deuteron are parallel, it is easy to derive [2] from (3) the following relations

$$\begin{cases} Q_{12} = Q_{13} = Q_{13}Q_{12} = Q_{23}Q_{12}\,, \\ \Sigma\chi^*Q_{12}\chi = \dfrac{1}{2}\left[S(S+1) - \dfrac{7}{4}\right] \equiv \gamma\,, \end{cases} \tag{8}$$

and therefore it is $\gamma = -1/2$ for the doublet, $\gamma = 1$ for the quartet state. For the operator P_{ij} we have relations of the type

$$\begin{cases} P_{12}\boldsymbol{r} = \boldsymbol{r}_2 - \dfrac{1}{2}(\boldsymbol{r}_1 + \boldsymbol{r}_3) = -\dfrac{1}{2}\boldsymbol{r} - \dfrac{3}{4}\boldsymbol{\rho}\,, \\ P_{12}\boldsymbol{\rho} = \boldsymbol{r}_3 - \boldsymbol{r}_1 = -\dfrac{1}{2}\boldsymbol{\rho} - \boldsymbol{r}\,, \qquad \text{etc.}\,. \end{cases} \tag{9}$$

With these rules the operations indicated on the right hand side of (7) do not present any difficulty, except for the term involving Δ_r, which has been evaluated extensively by BUCKINGAM and MASSEY.

Putting

$$\alpha = 2w + 2\gamma b - \gamma m - h\,, \qquad \beta = 2m + 2\gamma h - \gamma w + b\,, \tag{10}$$

---

[2] L. MOTZ and J. SCHWINGER: *Phys. Rev.*, **58**, 26 (1940).

and using the new coordinate

$$P_{12}\boldsymbol{r} = \boldsymbol{r}' = -\frac{3}{4}\boldsymbol{\rho} - \frac{1}{2}\boldsymbol{r}\,, \tag{11}$$

the equation of the problem can be written as follows

$$\begin{aligned}(12)\quad \frac{3\hbar^2}{4M}(\Delta + E)F(\boldsymbol{r}) = {} & \alpha F(\boldsymbol{r}) \int \psi(\boldsymbol{\rho}) J\left(\left|\frac{1}{2}\boldsymbol{\rho} + \boldsymbol{r}\right|\right) \psi(\boldsymbol{\rho})\,\mathrm{d}\boldsymbol{\rho} + \\ & + \beta\left(\frac{4}{3}\right)^3 \int \psi\left(\frac{2}{3}\,|\,2\boldsymbol{r}' + \boldsymbol{r}\,|\right) J\left(\frac{2}{3}\,|\,\boldsymbol{r}' + \boldsymbol{r}\,|\right) \psi\left(\frac{2}{3}\,|\,\boldsymbol{r}' + 2\boldsymbol{r}\,|\right) F(\boldsymbol{r}')\,\mathrm{d}\boldsymbol{r}' + \\ & + \tfrac{1}{3}\beta\left(\frac{4}{3}\right)^3 \int \psi\left(\frac{2}{3}\,|\,2\boldsymbol{r}' + \boldsymbol{r}\,|\right) \times \\ & \times \left[J\left(\frac{2}{3}\,|\,\boldsymbol{r}' + 2\boldsymbol{r}\,|\right) + J\left(\frac{2}{3}\,|\,2\boldsymbol{r}' + \boldsymbol{r}\,|\right)\right] \psi\left(\frac{2}{3}\,|\,\boldsymbol{r}' + 2\boldsymbol{r}\,|\right) F(\boldsymbol{r}')\,\mathrm{d}\boldsymbol{r}' + \\ & - \gamma\left(E - \frac{5}{3}\varepsilon\right)\left(\frac{4}{3}\right)^3 \int \psi\left(\frac{2}{3}\,|\,2\boldsymbol{r}' + \boldsymbol{r}\,|\right) \psi\left(\frac{2}{3}\,|\,\boldsymbol{r}' - 2\boldsymbol{r}\,|\right) F(\boldsymbol{r}')\,\mathrm{d}\boldsymbol{r}' + \\ & + \gamma\,\frac{3\hbar^2}{4M}\left(\frac{4}{3}\right)^5 \int \psi'(u)\,\frac{\boldsymbol{u}\cdot\boldsymbol{v}}{uv}\,\psi'(v) F(\boldsymbol{r}')\,\mathrm{d}\boldsymbol{r}',\end{aligned}$$

where in the last term we have

$$u = \frac{2}{3}\,|\,2\boldsymbol{r}' + \boldsymbol{r}\,|\,, \qquad v = \frac{2}{3}\,|\,\boldsymbol{r}' + 2\boldsymbol{r}\,|\,, \tag{13}$$

and it has also been taken into account that the functions which appear in (7) depend only on the absolute value of their arguments.

3. – Calculation of the phase $\delta_0(l = 0)$.

The potential J and the function ψ are assumed to be of the Gaussian type, i.e. of the form

$$\begin{cases} J(|\,\boldsymbol{r}_1 - \boldsymbol{r}_2\,|) = V_0 \exp\left[-\varkappa^2\,|\,\boldsymbol{r}_1 - \boldsymbol{r}_2\,|^2\right], \\ \psi(|\,\boldsymbol{r}_1 - \boldsymbol{r}_2\,|) = \left(\dfrac{2a^2}{\pi}\right)^{3/4} \exp\left(-a^2\,|\,\boldsymbol{r}_1 - \boldsymbol{r}_2\,|^2\right). \end{cases} \tag{14}$$

Let us put

$$\begin{cases} k^2 = \dfrac{4M}{3\hbar^2}E\,, \qquad \nu = \dfrac{8a^2\varkappa^2}{8a^2 + \varkappa^2}\,, \qquad \omega = \left(\dfrac{4}{3}\right)^3\left(\dfrac{2a^2}{\pi}\right)^{3/2}, \\ u = k_0^2\left(\dfrac{\nu}{\varkappa^2}\right)^{3/2}, \quad q = k_0^2\omega, \quad p = \dfrac{1}{3}\,q\,, \quad m = \left(\dfrac{4a}{3}\right)^4\omega\,, \quad n(k) = \left(k^2 - \dfrac{5}{3}\,k_a^2\right)\omega, \end{cases} \tag{15}$$

where k_0^2 and k_a^2 are the value of k^2 calculated for $E = V_0$ and $E = \varepsilon$ respectively. After elementary transformations the equation (12) reads

$$
\begin{aligned}
(16)\quad (\Delta + k^2)F(\boldsymbol{r}) = &- \alpha u \exp[-\nu r^2] F(\boldsymbol{r}) - \\
&- \beta q \int \exp[-\lambda_1(r^2 + r'^2) - 2\mu_1 \boldsymbol{r}\cdot\boldsymbol{r}'] F(\boldsymbol{r}')\,\mathrm{d}\boldsymbol{r}' - \\
&- \gamma p \int \exp[-\lambda_2 r^2 - \lambda_1 r'^2 - 2\mu_2 \boldsymbol{r}\cdot\boldsymbol{r}'] F(\boldsymbol{r}')\,\mathrm{d}\boldsymbol{r}' - \\
&- \gamma p \int \exp[-\lambda_1 r^2 - \lambda_2 r'^2 - 2\mu_2 \boldsymbol{r}\cdot\boldsymbol{r}'] F(\boldsymbol{r}')\,\mathrm{d}\boldsymbol{r}' + \\
&+ \gamma n(k) \int \exp[-\lambda_3(r^2 + r'^2) - 2\mu_3 \boldsymbol{r}\cdot\boldsymbol{r}'] F(\boldsymbol{r}')\,\mathrm{d}\boldsymbol{r}' + \\
&+ \gamma m \int \exp[-\lambda_3(r^2 + r'^2) - 2\mu_3 \boldsymbol{r}\cdot\boldsymbol{r}'](2\boldsymbol{r}' + \boldsymbol{r})\cdot(\boldsymbol{r}' + 2\boldsymbol{r}) F(\boldsymbol{r}')\,\mathrm{d}\boldsymbol{r}',
\end{aligned}
$$

with the following meaning for the new constants

$$
(17)\quad \begin{cases} \lambda_1 = (4/9)(5a^2 + \varkappa^2), & \lambda_2 = (4/9)(5a^2 + 4\varkappa^2), \qquad \lambda_3 \quad (4/9)5a^2, \\ \mu_1 = (4/9)(4a_2 - \varkappa^2), & \mu_2 = (4/9)(4a^2 + 2\varkappa^2), \qquad \mu_3 = (4/9)4a^2. \end{cases}
$$

It is well known from Collision theory that the most general solution of equation (16) is given by the expansion

$$
(18)\qquad F(\boldsymbol{r}) = \sum_l F_l(\boldsymbol{r}) = \sum_l \frac{f_l(r)}{r} P_l(\cos\vartheta).
$$

If in the scattering process only S waves are involved, the expansion (18) reduces to the radial term $f_0(r)/r$, and therefore from (16) one gets an equation in $f_0(r)$. The integrations over the angular variables are quite elementary, and we shall write the resulting equation in the simple form

$$
(19)\qquad \left(\frac{\mathrm{d}^2}{\mathrm{d}r^2} + k^2\right) f_0(r) = U(r) f_0(r) + \int_0^\infty \ldots f_0(r')\,\mathrm{d}r'.
$$

The equation (19) can be solved by a variational method [3]. For $f_0(r)$ we must require the asymptotic behaviour

$$
(20)\qquad f_0(r) \cong \frac{\operatorname{sen} kr}{k} + \frac{\operatorname{tg}\delta_0}{k}\cos kr.
$$

Defining now

$$
(21)\qquad I = \int_0^\infty f_0(r)\,\mathrm{d}r \left\{ \left(\frac{\mathrm{d}^2}{\mathrm{d}r^2} + k^2\right) f_0(r) - \left[U(r) f_0(r) - \int_0^\infty \ldots f_0(r')\,\mathrm{d}r' \right] \right\},
$$

---

[3] N. F. MOTT and H. S. W. MASSEY: *Theory of Atomic Collisions* (Oxford, 1949), p. 128; S. S. HUANG: *Phys. Rev.*, **76**, 1878 (1949).

the first variation of I, because of the symmetry in the integrations over r and r', gives the condition

$$\delta\left(I + \frac{\operatorname{tg}\delta_0}{k}\right) = 0\,. \tag{22}$$

It is to be noted that the integral (21) vanishes if $f_0(r)$ is a solution of equation (19). In the integral I we now replace $f_0(r)$ by a trial function of the type

$$f_0(r) = \frac{\operatorname{sen} kr}{k}\,(1 + \zeta \exp[-\varepsilon r^2]) + \tag{23}$$
$$+ \cos kr(1 - \exp[-\varepsilon r^2])(\xi + \eta \exp[-\varepsilon r^2])\,,$$

where $\xi = \operatorname{tg}\delta_0/k$. Such a function satisfies the condition $f_0(0) = 0$ and presents the asymptotic behaviour (20). The stationary property with respect to the variational parameters, expressed by (22), is now equivalent to the following linear equations in ξ, η, ζ

$$\frac{\partial I}{\partial \xi} = -1\,, \qquad \frac{\partial I}{\partial \eta} = 0\,, \qquad \frac{\partial I}{\partial \zeta} = 0\,. \tag{24}$$

Our problem is therefore reduced to the solution of this set of equations. For the parameter ε the value $\varepsilon = \varkappa^2$ has been chosen. We shall see that the result is largely independent from this choice. Moreover, if also ε had been chosen as a variational parameter, a transcendental equation would have to be taken into account besides the three equations (24).

For a check on the accuracy of the solution use may be made of the exact relation (27). This can be obtained elementarily [4] if the equation

$$\left(\frac{\mathrm{d}^2}{\mathrm{d}r^2} + k^2\right) g_0(r) = 0\,, \tag{25}$$

with the solution

$$g_0(r) = \frac{\operatorname{sen} kr}{k}\,, \tag{26}$$

is considered besides (19) and (20). In fact, subtracting (19) multiplied by $g_0(r)$ from (25) multiplied by $f_0(r)$ and integrating over r, using (20) and (26), it follows

$$\frac{\operatorname{tg}\delta_0}{k} = -\int_0^\infty g_0(r)\,\mathrm{d}r\left[U(r)f_0(r) + \int_0^\infty \ldots f_0(r')\,\mathrm{d}r'\right]. \tag{27}$$

---

[4] N. F. Mott and I. N. Sneddon: *Wave Mechanics* (Oxford, 1948), p. 238.

Let us denote with Δ the value of tg δ_0/k calculated by means of (27) using for $f_0(r)$ the trial function (23) with the variational parameters given by the set (24). The ratio Δ/ξ will be nearly equal to one, if the function $f_0(r)$ used does actually represent a good approximation.

4. – Calculation of the phases $\delta_l (l \neq 0)$.

Because of the integral terms, the equation (14) for the component $F_l(\boldsymbol{r})$ cannot be separated, for $l \neq 0$, into two equations, one for the radial and one for the angular part. Therefore the calculation of the phases δ_l is practically impossible by ordinary methods, unless the phases are expected to be small. In this case use can be made of the Born approximation and a formula analogous to (27) can be applied. This formula can be deduced considering the equation (16), which we shall write in the form

$$(\Delta + k^2)F_l(\boldsymbol{r}) = U(r)F_l(\boldsymbol{r}) + \int \ldots F_l(\boldsymbol{r}')\,\mathrm{d}\boldsymbol{r}' , \tag{28}$$

with $F_l(\boldsymbol{r})$ having the asymptotic behaviour

$$F_l(\boldsymbol{r}) \simeq \frac{\operatorname{sen}\left(kr - l\frac{\pi}{2} + \delta_l\right)}{kr} P_l(\cos\vartheta) , \tag{29}$$

and the equation

$$(\Delta + k^2)G_l(\boldsymbol{r}) = 0, \tag{30}$$

with the solution

$$G_l(\boldsymbol{r}) = \sqrt{\frac{\pi}{2kr}}\, J_{l+1/2}(kr)P_l(\cos\vartheta) , \tag{31}$$

which behaves asymptotically as

$$G_l(\boldsymbol{r}) \simeq \frac{\operatorname{sen}\left(kr - l\frac{\pi}{2}\right)}{kr} P_l(\cos\vartheta) . \tag{32}$$

Subtracting now (28) multiplied by $G_l(\boldsymbol{r})$ from (30) multiplied by $F_l(\boldsymbol{r})$ and integrating over $\boldsymbol{r}$, wehave

$$\int \{ F_l(\boldsymbol{r})\nabla G_l(\boldsymbol{r}) - G_l(\boldsymbol{r})\nabla F_l(\boldsymbol{r}) \}\,\mathrm{d}S = -\int G_l(\boldsymbol{r})\,\mathrm{d}\boldsymbol{r} \left\{ U(\boldsymbol{r})F_l(\boldsymbol{r}) + \int \ldots F_l(\boldsymbol{r}')\,\mathrm{d}\boldsymbol{r}' \right\} , \tag{33}$$

where on the left hand side Green's theorem has been applied. Performing

the surface integral by use of (29) and (32), the identity

$$\text{sen}\,\delta_l = -\frac{k}{4\pi}(2l+1)\int G_l(\boldsymbol{r})\,d\boldsymbol{r}\left\{U(r)F_l(\boldsymbol{r}) + \int \ldots F_l(\boldsymbol{r}')\,d\boldsymbol{r}'\right\}, \tag{34}$$

follows. If the phases are expected to be small, the function $F_l(\boldsymbol{r})$ can be replaced by $G_l(\boldsymbol{r})$. In a different approach of the three body problem, an integral formula for the calculation of the phases has also been given by VERDE ([5]).

5. – Cross section for thermal energies.

For thermal energies ($k = 0$) only the phase δ_0 has to be considered. For $k = 0$ the function I can be easily calculated, because all integrals can be reduced to integrals of Gaussian type or to the following

$$\int_0^\infty \exp[-ar^2]\,\text{erf}(br)\,dr = \frac{1}{\sqrt{\pi a}}\,\text{arctg}\,\frac{b}{\sqrt{a}}\,. \tag{35}$$

The constants used are $\varepsilon = -2{,}20$ MeV for the binding energy of the deuteron, $\varkappa^{-1} = 2\cdot 10^{-13}$ cm for the range of the potential, $V_0 = 45$ MeV for the depth ([6]), and ([7]) $(a/\varkappa)^2 = 0{,}35$. As ratio between the potentials ^3S and ^1S of the deuteron the value $x = 0{,}6$ has been assumed.

Three types of forces have been considered: neutral forces (I) with $m = h = 0$, $b = (1/2)(1-x)$, $w = (1/2)(1+x)$; symmetrical forces (II) with $m = 2b = (1/3)(1+3x)$, $h = 2w = (1/3)(1-3x)$; a combination of Heisenberg and Majorana forces (III) with $b = w = 0$, $m = (1/2)(1+x)$, $h = (1/2)(1-x)$.

	I		II		III	
	D	Q	D	Q	D	Q
ξ	— 3,697	— 3,301	— 3,654	— 3,471	— 3,875	— 3,507
η	4,060	— 1,737	3,857	— 0,033	4,122	0,621
ζ	— 2,671	— 2,945	— 2,265	— 2,186	— 2,459	— 2,033
Δ/ξ	1,0246	0,8856	0,9961	1,0014	0,9993	1,0315
σ	1,485		1,569		1,653	

([5]) M. VERDE: *Helv. Phys. Acta*, **22**, 339 (1949).
([6]) L. ROSENFELD: *Nuclear Forces* (Amsterdam, 1948), p. 131.
([7]) E. GERJOUY and J. SCHWINGER: *Phys. Rev.*, **61**, 138 (1942).

The results are given in the table of pag. 192 with the cross section $\sigma = (4\pi/3)(\xi_D^2 + 2\xi_Q^2)$ in barns; the lengths are in units 10^{-13} cm. D and Q denote the doublet and quartet states respectively. The values given have been obtained by putting $\varepsilon = \varkappa^2$ in (23), but it has been verified that the results are modified by a few per cent for ε varying in the interval $\varkappa^2 \leqslant \varepsilon \leqslant 0{,}28\varkappa^2$.

The values of the cross section are rather low if compared with a recent experimental result of FERMI and MARSCHALL [8], who find for thermal energies a cross section of 3,44 barns. We come therefore to the conclusion that, at least for thermal energies and with the constants chosen, the Gauss potential cannot be used to describe the neutron-deuteron collision. Agreement with the experiment could be obtained with a range of the order $\varkappa^{-1}\sqrt{2}$. Such a value however could not possibly explain the nucleon-nucleon collision. The value of $|\xi|$ corresponds to the scattering length a of FERMI and MARSCHALL; experimentally the ratio a_4/a_2 is about 1, but for the incertitude in the measurements the previous authors give for this ratio a lower limit of 0,5 and an upper one of 2,3. According to our results this ratio is within 3 per cent 0,92 for all the types of forces; a contribution to the cross section of the same order by the doublet and quartet states is a characteristic feature already observed with Gaussian potential [9] for thermal energies and with exponential potential [1] for higher energies [10].

The author wishes to express his gratitude to Professor ROSENFELD for useful suggestions and interesting discussions. He is indebted to the British Council for a grant, which enabled him to stay at the University of Manchester.

---

[8] E. FERMI and M. MARSCHALL: *Phys. Rev.*, **75**, 578 (1949).

[9] K. OCHIAI: *Phys .Rev.*, **52**, 1221 (1937).

[10] Recently A. TRÖSCH and M. VERDE have found a cross section of 2,6 for neutral and 2,9 barns for symmetrical forces and a ratio $a_1/a_2 = 0{,}44$ for both types of forces. Their calculation is based on the method given by M. VERDE [5] and the values of the constants used by them practically coincide with ours. Although good agreement exists between their results and ours for the quartet state, their values for a_2 differ from ours by a factor two. Due to the difference in the method followed, it has not yet been possible to trace the origin of such a discrepancy. We are indebted to Dr. VERDE for sending us the paper before publication.

RIASSUNTO

La diffusione di neutroni termici da parte di deutoni viene trattata risolvendo l'equazione del moto per le onde S con metodo variazionale. Viene usata una funzione variazionale dipendente da tre parametri ed un potenziale gaussiano con una profondità di 45 MeV ed un range di $2 \cdot 10^{-13}$ cm. Il valore della sezione d'urto non dipende sensibilmente dai tipi di forze considerati (forze neutrali e simmetriche ed una combinazione di forze di Heisenberg e Majorana), ed i contributi da parte degli stati di quartetto e doppietto risultano dello stesso ordine. La sezione d'urto calcolata è inferiore a quella sperimentale per un fattore dell'ordine di due; la differenza fra il risultato teorico ed il dato sperimentale diminuisce aumentando il range del potenziale. Viene data infine una formula integrale per il calcolo delle fasi per le onde di ordine superiore.

Sulla distribuzione angolare dei rami delle stelle prodotte dalla radiazione cosmica nelle emulsioni fotografiche.

A. Manfredini

Istituto di Fisica dell'Università, Centro di Studio per la Fisica Nucleare del C.N.R. - Roma

(ricevuto il 20 Dicembre 1950)

Riassunto. — Si osserva la distribuzione angolare dei rami delle stelle con particolare riguardo alle stelle a 3, 4 e 5 rami. Utilizzando la distribuzione angolare dei nuclei di rinculo studiata da Harding, si può determinare un limite superiore per il contributo degli atomi pesanti alle stelle stesse. Tale limite è inferiore al 50%, in contraddizione con l'ipotesi che la sezione d'urto per la generazione delle stelle sia proporzionale alla sezione geometrica del nucleo.

1. – Diversi autori hanno studiato la distribuzione angolare dei rami delle « evaporazioni nucleari » generate in emulsioni fotografiche sia da particelle accelerate artificialmente (1), sia dalla radiazione cosmica (2) (3) (4). Per le evaporazioni prodotte dalla radiazione cosmica è stata anche studiata la distribuzione angolare dei nuclei di rinculo, da Harding (5), che si è valso delle sue misure per svolgere interessanti considerazioni sulla natura del fenomeno della evaporazione.

La difficoltà che si incontra nel caso della radiazione cosmica è che manca

(1) E. Gardner and V. Peterson: *Phys. Rev.*, **75**, 364 (1949).

(2) D. H. Perkins: *Nature*, **161**, 486 (1948).

(3) R. H. Brown, U. Camerini, P. H. Fowler, H. Heitler, D. T. King and C. F. Powell: *Phil. Mag.*, **40**, 862 (1949); U. Camerini, T. Coor, J. H. Davies, P. H. Fowler, W. O. Lock, H. Muirhead and N. Tobin: *Phil. Mag.*, **40**, 1073 (1949).

(4) M. D. Cosyns: Relazione al Congresso Internazionale di Como (Settembre 1949). Vedi *Suppl. Nuovo Cimento*, **6**, 397 (1949).

(5) J. B. Harding: *Phil. Mag.*, **40**, 530 (1949).

un vero e proprio asse di simmetria, in quanto la radiazione incidente non è monodirezionale, anzi tutto lascia notare che essa sia notevolmente sparpagliata intorno alla verticale, cosa che del resto ha una conferma diretta nelle stelle « doppie » osservate comunemente nelle lastre esposte in alta quota.

Tale difficoltà può essere superata se le singole stelle esaminate mostrano per loro natura una simmetria tale da poter ragionevolmente individuare la direzione del primario (esplosioni di alta energia, con parecchi rami al minimo di ionizzazione) [3] [4], oppure se si adotta un metodo di studio di tipo statistico tale che i risultati dipendano solo dal grado di anisotropia della distribuzione, e non dalla direzione del primario.

Un metodo di questo tipo è stato seguito da PERKINS [2] che ha studiato la distribuzione in lunghezza delle risultanti vettoriali che si possono associare alle stelle se ad ogni ramo si fa corrispondere un vettore di lunghezza unitaria avente la direzione del ramo stesso.

Un altro metodo dello stesso tipo è quello proposto da LOVERA [6] basato sulla misura degli s angoli formati fra le proiezioni delle s tracce di una stella sul piano della lastra. Rispetto al metodo di Perkins esso ha il pregio di richiedere solo misure relative a dette proiezioni e non misure in profondità. Queste ultime sono infatti meno sicure e molto più laboriose, il che dà ragione della scarsità della statistica raccolta da PERKINS.

2. – Scopo della presente ricerca è stato quello di raccogliere una statistica piuttosto estesa relativa alla distribuzione angolare delle stelle « cosmiche » in generale, ed esaminare le conclusioni che possono dedursi da tale materiale sperimentale. In questo studio ci si è proposti di fissare l'attenzione sui rami di bassa e media energia e particolarmente sulle stelle « piccole » (3, 4 5 rami) meno studiate dagli autori precedentemente citati.

Come si vedrà nel seguito i dati sperimentali che occorreva conoscere per ogni stella erano i numeri dei rami diretti verso il basso e rispettivamente verso l'alto. D'altra parte ci si proponeva di applicare il metodo di LOVERA [6] per studiare l'anisotropia in modo « intrinseco ». Pertanto, volendosi raccogliere un materiale abbastanza vasto, si è rinunziato alle misure di profondità e per ogni stella si sono misurati solo gli angoli rispetto alla verticale delle proiezioni dei rami sul piano della lastra (esposta verticalmente).

Le lastre usate erano Kodak NT4, esposte a 3500 m per 14 giorni, sia scoperte sia sotto piccoli spessori di Piombo (2 e 5 cm). Misure accurate eseguite sulla granulazione di tutte le tracce mesoniche più lunghe di 1000 μ hanno permesso di tarare le lastre, di determinare l'effetto del « fading » (che

---

[6] G. LOVERA: *Nuovo Cimento*, **6**, 233 (1949).

è risultato insensibile) e di stabilire che la minima ionizzazione registrata corrisponde a protoni di 200 ÷ 300 MeV. Dalla presente misura sono quindi esclusi tutti i rami dovuti a particelle di energia relativistica; nelle considerazioni seguenti si è supposto che la maggioranza dei rami osservati siano dovuti al solo processo di evaporazione.

Sono stati considerati come rami delle stelle tutte le tracce con lunghezza superiore ai 4 μ, ammettendo che le tracce di lunghezza inferiore fossero dovute ai nuclei di rinculo.

I risultati delle misure sono mostrati nelle figg. 1-5 in cui l'angolo 0° corrisponde alla direzione verticale verso l'alto. In esse (e nelle considerazioni che seguono) i dati relativi alle lastre scoperte e a quelle sotto piombo sono stati riuniti, perchè nessuna differenza significativa risultava nei due gruppi di misure. Gli istogrammi a tratto pieno si riferiscono alla totalità dei rami, quelli tratteggiati si riferiscono invece ai soli rami di energia maggiore di ~ 80 MeV.

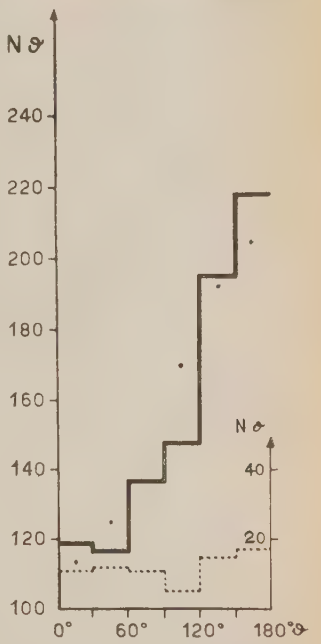

Fig. 1. – Distribuzione angolare rispetto alla verticale delle proiezioni dei rami nel piano della lastra. L'angolo 0° corrisponde alla verticale verso l'alto. Curva a tratto pieno (ordinate a sinistra): totalità dei rami. Curva tratteggiata (ordinata a destra): rami di alta energia ($\geqslant 80$ MeV). Punti: valori corrispondenti a una distribuzione del tipo: $1 - 0{,}3 \cos\theta$. Stelle a 3 rami.

3. – È evidente negli istogrammi figg. 1, 2, 3 l'esistenza di una notevole proiezione in avanti per stelle a 3, 4, 5 rami nonostante lo sparpagliamento della radiazione generante. Per le considerazioni che seguono è utile osservare che i dati raccolti in questi istogrammi si possono rappresentare abbastanza bene con una distribuzione differenziale del tipo

$$(1) \qquad N f(\theta)\,\mathrm{d}\theta = \frac{N}{\pi}(1 - a\cos\theta)\,\mathrm{d}\theta\,.$$

Nelle figg. 1, 2, 3 i punti indicano l'andamento teorico che avrebbero gli istogrammi per una funzione di questo tipo con $a = 0{,}3$ in tutti e tre i casi.

Per le stelle più grandi la proiezione in avanti appare invece molto meno pronunciata (figg. 4 e 5) e dovuta quasi esclusivamente ai soli rami di energia maggiore di ~ 80 MeV. Questi risultati coincidono con quelli di COSYNS [4] relativi alle stelle con più di 11 rami e si accorda con l'ipotesi che alla for-

mazione delle stelle medie e grandi concorra un certo numero di nucleoni di rinculo o prodotti dal riassorbimento dei mesoni, le cui tracce risultano ben distinte per distribuzione angolare e per energia da quelle dei rami di evaporazione.

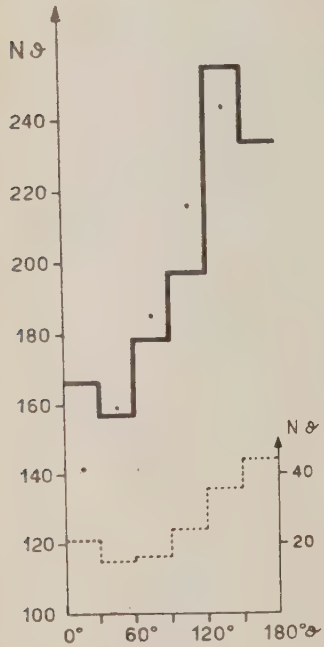

Fig. 2. – Stelle a 4 rami.

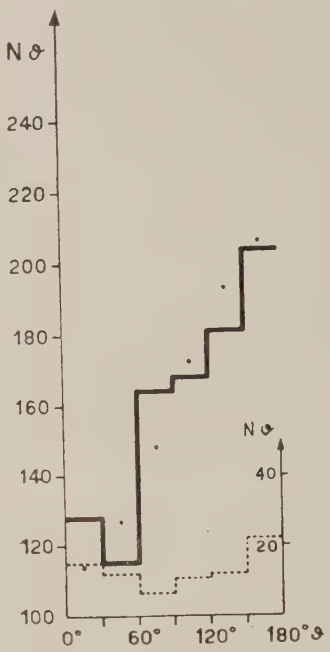

Fig. 3. – Stelle a 5 rami.

4. – Per eliminare dalle distribuzioni trovate l'effetto dello sparpagliamento dei primari si potrebbe ora pensare di applicare il metodo di LOVERA [6]. Disgraziatamente la distribuzione degli angoli fra tracce successive è quasi insensibile ad una modesta anisotropia. Tale distribuzione è data infatti da

$$g(\alpha) = (s-1)\int_0^{2\pi} f(\theta) f(\theta+\alpha)\left[1-\int_0^{\alpha} f(\theta+x)\,\mathrm{d}x\right]^{s-1}\mathrm{d}\theta\,,$$

essendo s il numero dei rami delle stelle considerate e $f(\theta)$ la distribuzione angolare rispetto alla verticale. Orbene, se si prendono per esempio le stelle a 3 rami, la $g(\alpha)$ relativa ad una distribuzione del tipo (1) scarta al massimo

da quella deducibile da una distribuzione isotropa per termini dell'ordine di $a^2/2$ (cioè $\sim 0{,}05$ per $a \sim 0{,}3$) rispetto all'unità.

Il metodo non appare quindi applicabile in questo caso a meno di esten-

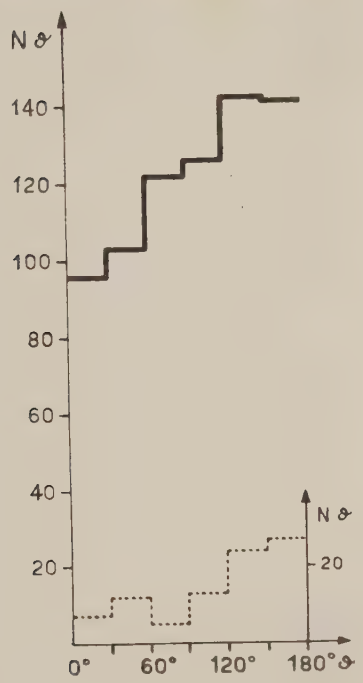

Fig. 4. – Stelle a $6 \div 11$ rami.

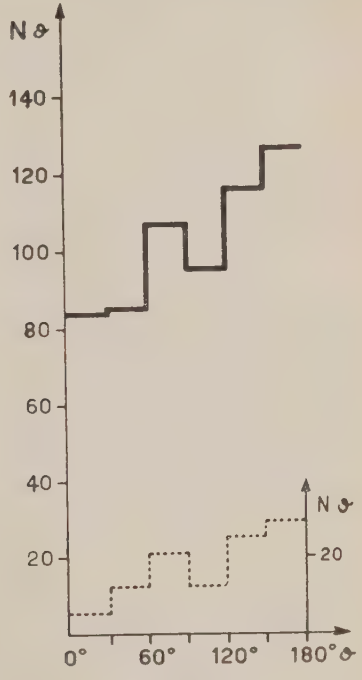

Fig. 5. – Stelle a numero di rami $\geqslant 12$.

dere enormemente la statistica, cosa che sarebbe criticabile per altro verso. perchè una certa frazione delle stelle a pochi rami è certo dovuta a fenomeni non di tipo evaporativo.

5. – Venuto così a mancare un metodo per lo studio « intrinseco » della distribuzione angolare ci si è dovuti accontentare dei dati relativi alla distribuzione rispetto alla verticale.

La circostanza che permette di ottenere qualche risultato interessante, pur prescindendo dalla apertura angolare dei primari, è che *nella evaporazione di un nucleo pesante la distribuzione angolare è poco diversa dalla distribuzione isotropa, per qualunque numero di rami*, purchè si eliminino dalla statistica quei rami « veloci » ($E \sim 80$ MeV) che non hanno generalmente origine nella fase evaporativa del processo.

Questa affermazione può essere precisata in modo quantitativo, sebbene con considerazioni abbastanza grossolane, nel modo seguente (7).

HARDING (5) discute la sua distribuzione angolare dei rinculi ammettendo che essa risulti dalla composizione vettoriale della velocità V_1, verticale verso il basso, dovuta alla cessione di momento al nucleo all'atto della eccitazione, con la velocità $(V_2)_R$ (a distribuzione isotropa) del rinculo rispetto al baricentro del nucleo eccitato. La distribuzione che ne risulta è del tipo

$$P(\theta)\,d\theta = K\left(1 - \frac{\pi}{2}\frac{V_1}{(V_2)_R}\cos\theta + \ldots\right)d\theta\,. \tag{2}$$

Integrando la (2) fra 0 e π e fra $\pi/2$ e π si ricava subito che

$$\frac{V_1}{(V_2)_R} = 2\left(\frac{N'}{N}\right)_R - 1\,, \tag{3}$$

essendo N il numero totale di tracce di rinculo osservate, ed N' quello delle tracce di rinculo dirette verso il basso ($\theta > \pi/2$), e dovendosi intendere per V_1 e $(V_2)_R$ i valori medi su un gran numero di stelle.

La equazione (2) è dello stesso tipo della $f(\theta)\,d\theta = K(1 - \cos\theta)$ trovata sperimentalmente nella presente misura e si può quindi tentare di interpretare in modo analogo il coefficiente di $\cos\theta$. In questa interpretazione vale, per i rami delle stelle, la relazione analoga alla (3)

$$\frac{V_1}{V_2} = 2\frac{N'}{N} - 1\,, \tag{4}$$

dove V_2 è la velocità, rispetto al baricentro, della particella ionizzante emessa nella evaporazione, N è il numero totale di tracce di un determinato tipo di stella, ed N' il numero totale delle tracce dirette verso il basso. Anche in questa relazione si intende naturalmente per V_1 e V_2 i valori medi su un gran numero di stelle.

Riferiamoci ora al sistema del nucleo dopo l'urto: se la distribuzione dei neutroni è analoga a quella delle particelle ionizzanti, se cioè la (4) si suppone valida anche per i neutroni, si può scrivere, indicando con n il numero delle particelle emesse:

$$|\,m_R(\boldsymbol{V}_2)_R\,| = |\,\Sigma\, m\boldsymbol{V}_2\,| = \sqrt{\frac{2}{3}}\sqrt{n}\,\overline{m}\,V_2\,, \tag{5}$$

---

(7) Considerazioni più precise sul fenomeno che dà origine alle stelle portano ad ammettere che le due fasi *A*) collisione diretta od indiretta, *B*) eccitazione ed evaporazione, sono spesso coesistenti. Di conseguenza si deve ammettere che ci sia una certa probabilità per la presenza di rami, di modesta energia, proiettati direttamente nella fase di collisione. Vedi M. L. GOLDBERG: *Phys. Rev.*, **74**, 1269 (1948) e G. BERNARDINI, G. CORTINI e A. MANFREDINI: *Phys. Rev.*, **79**, 952 (1950).

$\overline{m}$ rappresenta la massa media delle particelle emesse, e assume il valore di 1,6 masse protoniche se si tiene conto del rapporto sperimentale particelle-α/protoni e si ammette che il numero di neutroni emessi sia uguale a quello dei protoni, col che $n = (5/3)s$ (s essendo il numero dei rami delle stelle considerate). L'ultimo passaggio è valido nell'ipotesi che gli n vettori $m\boldsymbol{V}_i$ siano distribuiti a caso secondo una legge gaussiana.

Dalle (3), (4) e (5) si deduce subito

$$\frac{N'}{N} = \frac{1}{m_R}\left[\sqrt{\frac{2}{3}}\sqrt{n}\,\overline{m}\left(\frac{N'}{N}\right)_R + \frac{m_R - \sqrt{\frac{2}{3}}\sqrt{n}\,\overline{m}}{2}\right]. \tag{6}$$

Questa relazione è applicabile solo alle evaporazioni dei nuclei pesanti, perchè per i nuclei leggeri perde significato il parlare di nucleo di rinculo, come si dirà più oltre. Per i nuclei pesanti l'incertezza sperimentale su $(N'/N)_R$ disturba poco perchè il secondo termine risulta circa 20 volte maggiore del primo, fino ad $s \sim 20$.

Da essa risulta che N'/N è sempre molto prossimo ad 1/2 variando da 0,505 per $s = 3$ a 0,525 per $s = 20$.

6. – Come risulta dalle figg. 4 e 5 e dalla tab. I i dati sperimentali relativi alle stelle con $s \geqslant 6$ sono in accordo con le precedenti considerazioni se si eliminano i rami veloci, come già rilevato. Il lieve eccesso di rami verso il basso nelle stelle con numero di rami compreso fra 6 e 11 è dovuto in gran parte a fluttuazioni notevoli riscontrate nelle stelle a 9 e a 10 rami. Tuttavia una piccola prevalenza verso il basso è presente in tutti i gruppi di stelle e può dare una indicazione che al di sotto del limite scelto di 80 MeV è ancora presente una piccola percentuale (forse 2% o 3%) di rami non evaporativi.

TABELLA I. *Confronto tra la distribuzione sperimentale e una distribuzione isotropa.*
N = numero totale dei rami.
N' = numero dei rami diretti verso il gasso ($\theta > \pi/2$).

Stelle		$N/2$	N'
6 ÷ 11 rami	compresi i rami veloci	636	714 ± 27
	esclusi i rami veloci	514	553 ± 23
⩾12 rami	compresi i rami veloci	279	363 ± 19
	esclusi i rami veloci	143	160 ± 13
3 ÷ 5 rami	totale	2 790	3 305 ± 57
3 ÷ 5 rami	stelle con rinculo . . .	565	598 ± 24
4 ÷ 5 rami	stelle con rinculo . . .	343	350 ± 19

7. – Per quanto riguarda le stelle a $3 \div 5$ rami ([8]) si può anzitutto notare la netta differenza che la tab. I mette in evidenza tra la distribuzione della totalità delle stelle, evidentemente anisotropa, e quella relativa alle sole stelle con rinculo osservabile. Quest'ultima scarta dall'isotropia assai poco e quasi affatto nelle stelle a 4 e 5 rami. (È da osservare che per le stelle piccole l'anisotropia non è dovuta ai rami veloci come per le stelle con $s \geqslant 6$). Ciò si spiega se si considerano separatamente le varie possibilità perchè una stella a 3, 4 e 5 rami nasca dal C, O od N. Si vede allora che nella maggioranza dei casi il residuo del nucleo dopo la evaporazione ha una massa paragonabile alla massa dei singoli rami e quindi non può apparire nell'emulsione come un ramo distinguibile per lunghezza e ionizzazione degli altri rami della stella.

Possiamo quindi concludere che la quasi totalità delle stelle a 4 e 5 rami con rinculo non può essere generata che da nuclei pesanti, e lo stesso sarà per una forte percentuale delle stelle a 3 rami con rinculo.

Ciò fa comprendere perchè nel suo studio sulle tracce di rinculo Harding abbia trovato la stessa distribuzione per stelle piccole e grandi, cosa che è stata confermata anche da misure eseguite in questo laboratorio.

8. – Si possono ora utilizzare i dati relativi a tutte le stelle a 3, 4 e 5 rami per determinare quale percentuale di queste stelle provenga da nuclei pesanti (Ag e Br) e quale da nuclei leggeri.

Cerchiamo di ottenere un valore limite per tale dato.

Se tutte le stelle nascessero da nuclei pesanti e avessero quindi i rami distribuiti isotropicamente nello spazio, è possibile prevedere quante delle stelle ad s rami osservate dovrebbero avere K rami diretti verso il basso.

Nell'ipotesi della distribuzione istropa questo numero è proporzionale al coefficiente binomiale $\binom{s}{K}$. Precisamente, se indichiamo con A_s il numero di stelle osservate ad s rami, e con A_{sK} il numero delle stelle ad s rami con K rami diretti verso il basso, deve essere:

$$A_{sK} = \frac{1}{2^s}\binom{s}{K} A_s \,. \tag{7}$$

Gli scarti dalla relazione (7), che naturalmente sono significativi soprattutto per K piccolo ($K = 0$, $K = 1$), sono stati messi in evidenza nella tab. II.

([8]) Per la discussione delle stelle a $3 \div 5$ rami è stato necessario aumentare la statistica. Si sono usate per ciò lastre Ilford G5 le cui condizioni di esposizione e sviluppo erano equivalenti a quelle delle lastre Kodak NT4 usate nella prima parte della misura.

TABELLA II. – *Classifica delle stelle secondo il numero dei rami diretti verso il basso, per vari valori del numero totale s dei rami. Confronto tra la distribuzione sperimentale e quella isotropa per* $K = 0$ *e* $K = 1$.

s	$\frac{1}{2}\binom{s}{0} A_s$	A_{s0} osservato	$\frac{1}{2^s}\binom{s}{1} A_s$	A_{s1} osservato
3	80	$40 \pm 6{,}3$	240	201 ± 14
4	31,5	$13 \pm 3{,}6$	126	$65 \pm 8{,}1$
5	5	$3 \pm 1{,}7$	25	$18 \pm 4{,}2$

Da questi dati appare molto improbabile che più del 50% *di queste stelle possa nascere da nuclei pesanti.* E tale valore è un limite superiore non solo perchè la distribuzione è appiattita dallo sparpagliamento dei primari ma anche perchè il contributo dei nuclei leggeri ad A_{s0} ed A_{s1} non sarà probabilmente nullo.

Questo risultato è in contraddizione con l'ipotesi generalmente ammessa che la sezione d'urto per produzione di stelle sia proporzionale ad $A^{2/3}$, secondo cui, dalla composizione delle emulsioni usate, il contributo degli atomi pesanti alle stelle piccole dovrebbe essere di circa il 68% (74% per le lastre Kodak, e 64% per le lastre Ilford).

Una deviazione dalla legge $A^{2/3}$ nello stesso senso di quella trovata nella presente misura, fu già osservata da HARDING [9] confrontando il numero di stelle nate in emulsione con il numero di stelle nate in strati di gelatina interposti nella emulsione stessa.

HARDING trovava che la percentuale di stelle nate da atomi leggeri è del 36% anzichè del 27% calcolabile secondo la legge $A^{2/3}$ dalla composizione della sua emulsione.

La divergenza è minore di quella trovata da noi ma la lunga esposizione delle lastre di HARDING e il fatto che questo autore abbia trovato 11 stelle/cm³/giorno invece delle ~ 19 che si trovano alla stessa quota con esposizioni brevi, lasciano pensare che nella ricerca di HARDING una frazione non indifferente delle stelle piccole sia stata perduta. Se si correggono i dati basandosi sul troppo basso valore da lui trovato per la frequenza delle stelle, si trova una percentuale di stelle nate da nuclei leggeri di circa il 60%, in buon accordo con le precedenti considerazioni.

9. – La divergenza del risultato precedente dalla legge $A^{2/3}$ si può interpretare distinguendo tra sezioni d'urto per creazione di stelle e per assorbimento della radiazione « asterogena ».

---

[9] J. B. HARDING: *Nature* **163**, 440 (1949).

La legge $A^{2/3}$ risulta in discreto accordo con l'esperienza per quest'ultima sezione d'urto. Ma mentre nell'assorbimento della radiazione « asterogena » sembra certo [10] che il ruolo essenziale spetti ai nucleoni di 200 MeV o più, alla creazione delle stelle in una lastra possono partecipare in misura importante anche nucleoni più degradati.

Se allora si ammette, con FUJIMOTO e YALAGUCHI [11], che la sezione d'urto per l'evaporazione cresca con l'energia molto più lentamente per i nuclei pesanti che per quelli leggeri, se cioè si suppone che per far evaporare i nuclei pesanti occorrano nucleoni di energia piuttosto alta, si comprende come i due risultati possano divergere solo apparentemente.

Detta ipotesi sembra confermata dal lavoro di GARDNER e PETERSON [1] i quali lavorando con deutoni di varie energie (da 35 MeV a 190 MeV) trovano che al crescere dell'energia la proiezione in avanti diminuisce, come è da aspettarsi se al crescere dell'energia comincia ad intervenire nel fenomeno un numero crescente di nuclei pesanti.

La presente discussione è basata essenzialmente sulla ipotesi che tutti i rami osservati con energie minori di ~ 80 MeV, siano dovuti a particelle emesse nella fase di evaporazione del nucleo. Questa ipotesi è certo eccessivamente schematica in quanto, come è stato già accennato in nota [7], le considerazioni teoriche di GOLDBERG sulla interazione di neutroni di alta energia con nuclei pesanti, sulla energia trasferita al nucleo e sulla distribuzione angolare delle particelle uscenti dopo la collisione dal nucleo stesso, danno una apprezzabile probabilità per la presenza di particelle di bassa energia e proiettate nella direzione della radiazione incidente.

Su questa base si può dare una interpretazione qualitativa della distribuzione angolare delle stelle, indipendente da un diverso contributo degli atomi leggeri e pesanti alle stelle stesse (vedi G. BERNARDINI e coll. [7]).

Tuttavia i risultati sperimentali ottenuti nella presente misura sulle stelle a pochi rami con rinculo (la selezione dei rami classificati come rinculi è stata accuratamente controllata nel corso della misura) sembrano indicare che anche il contributo degli atomi leggeri abbia una parte non trascurabile nella distribuzione angolare osservata. Ulteriori misure sono in corso per decidere con un metodo più diretto quale sia il contributo degli atomi leggeri alla anisotropia della distribuzione angolare.

Sono lieta di esprimere la mia riconoscenza al prof. G. BERNARDINI per aver suggerita e indirizzata la presente ricerca e al dott. G. CORTINI per il suo contributo sostanziale al lavoro sperimentale e alla discussione dei dati.

---

[10] Vedi per esempio G. BERNARDINI, G. CORTINI e A. MANFREDINI: *Nuovo Cimento*, **6**, 456 (1949).

[11] Y. FUJIMOTO e Y. YAMAGUCHI: *Prog. Theor. Phys.*, **5**, 76 (1950).

SUMMARY

The angular distribution of the prongs of the stars produced by cosmic radiation in photographic emulsion has been measured, with particular reference to the stars with 3, 4 and 5 prongs. Using the angular distribution of the recoil nuclei studied by HARDING, un upper limit for the contribution to the observed stars due to heavy atoms in the emulsion can be determinated. This limit is less than 50% in contradiction with the hypothesis that the cross section for the generation of the stars is proportional to the geometrical cross section of the nucleus.

Un corps noir: étalon de brillance à température ajustable (*).

G.-A. Boutry

Professeur au Conservatoire National des Arts et Métiers - Paris

L. Le Blan

Chef de Service au Conservatoire National des Arts et Métiers - Paris

(ricevuto il 27 Novembre 1950)

Résumé (**). — Les Auteurs décrivent un nouvel appareillage mis à point au Conservatoire National des Arts et Métiers de Paris pour la détermination de l'intensité de brillance visuelle des sources lumineuses.

1. – Introduction.

A) Solution ancienne. – Rappelons brièvement comment se pose aujourd'hui le problème fondamental de la photométrie métrologique.

L'étalon d'intensité lumineuse a été longtemps constitué par un groupe de lampes à incandescence: ces lampes étaient assez nombreuses et les intercomparaisons entre elles assez fréquentes pour pouvoir détecter toute variation accidentelle. L'unité d'intensité lumineuse se trouvait alors définie par la moyenne des indications de ces lampes. L'instabilité et l'usure d'un tel étalon collectif représentait un danger négligeable tant que la température de couleur exigée restait basse. Il n'en est plus de même aujourd'hui parce que dans l'éclairage à incandescence la température de couleur usuelle monte jusqu'à 2 900 °K.

B) Solutions modernes. – De la nécessité d'en finir avec cette situation peu satisfaisante a résulté notre étude sur le corps noir considéré comme étalon de photométrie. On sait qu'au milieu de nombreuses difficultés expérimentales deux solutions distinctes du problème fondamental de la photométrie ont été envisagées:

1) *Corps noir à température fixe.* – On utilise un corps noir étalon fonctionnant à basse température, par exemple la température de solidification du platine (1 750 °C): C'est le cas de la réalisation du « Bureau of Standards » adoptée aujourd'hui comme étalon international de brillance. Si l'on fixe à priori la brillance d'un tel étalon (60 candélas/cm²) et si l'on admet comme

(*) Communication présentée au Congrès « A. Righi » de Bologne (Septembre 1950).
(**) *Aux soins de la Rédaction.*

données les constantes de la formule de Planck et la courbe de visibilité relative, le facteur M d'équivalent énergétique du lumen de visibilité maximum se trouve défini et on a donc la possibilité de calculer la brillance visuelle d'un autre corps noir à une température quelconque.

Dans cette solution, on utilise une opération de photométrie hétérochrome pour l'intercomparaison du corps noir primaire avec un groupe de lampes fonctionnant comme étalon à température de couleur différente; on peut d'ailleurs tourner la difficulté de cette opération hétérochrome en utilisant un filtre qui, intercalé sur le rayonemment de l'étalon primaire, transforme la composition spectrale de celui-ci dans le sens qui élève sa température de couleur. L'opération de photométrie hétérochrome est alors remplacée, au moins partiellement, par une opération de spectrophotométrie au prix d'une diminution de la brillance de l'étalon d'autant plus forte que la température de couleur à obtenir est plus élevée: d'où une perte de sensibilité qui n'est pas négligeable dans des conditions de mesures malaisées d'ailleurs.

En fait, l'opération de photométrie hétérochrome subsiste toujours car les températures des sources visuelles sont en continuelle élévation et la réalisation d'un filtre sur lequel l'accord international puisse se faire est toujours assez difficile pour que cet accord soit rarement tenté.

2) *Corps noir à température ajustable.* – Une solution différente consiste à faire usage comme étalon auxiliaire d'un corps noir à température ajustable. L'opération comprend alors:

— le chauffage du corps noir jusqu'à la réalisation de la meilleure homochromie avec la source à calibrer;

— la détermination de la température ainsi atteinte dans l'échelle absolue des températures.

On voit que, dans cette seconde solution, l'opération de photométrie hétérochrome a été remplacée par une opération pyrométrique. Ce fut le chemin suivi, entre autres, par FLEURY dans des recherches de très grand intérêt qui n'ont pas abouti à des applications pratiques parce que, à l'époque, la précision et la commodité d'emploi obtenues n'étaient pas entièrement satisfaisantes.

Nous avons repris un tel travail en utilisant les moyens fournis par l'électronique moderne: dans la construction des appareils, nous avons été guidés par le désir d'atteindre une bonne précision associée à une commodité et une sécurité d'emploi très grandes. Nous avons considéré le prix et l'encombrement comme accessoires, l'appareillage étant destiné aux grands Laboratoires de Métrologie primaire qu'entretiennent seuls les États souverains et quelques grandes compagnies industrielles.

Nous allons fixer pour commencer, l'ordre de grandeur de la précision à atteindre sur la connaissance de la température. Le corps noir étalon primaire fonctionne actuellement à la température de fusion du platine, et la très grande majorité des lampes à incandescence utilisées dans le monde travaillent à des températures de couleurs supérieures à 2 600 °K. On peut donc admettre que c'est dans le domaine de 2 500 à 3 000 °K que l'utilisation d'un étalon auxiliaire à température ajustable rendra les plus grands services.

Le tableau N. 1 donne pour quelques températures la brillance du corps noir exprimée en candélas/cm² et les variations relatives de cette brillance par °K.

TABLEAU I.

Température absolue T	Brillance B (candélas/cm²)	$\frac{1}{B}\frac{dB}{dT}$
2 250	178,5	$5 \cdot 10^{-3}$
2 500	541,6	$4 \cdot 10^{-3}$
2 750	1 345,4	$3{,}3 \cdot 10^{-3}$
2 850	1 853	$3{,}1 \cdot 10^{-3}$
3 000	2 883	$2{,}8 \cdot 10^{-3}$

Comme on le voit, cette variation relative dans le domaine qui nous intéresse est de 3 à 4/1 000 par degré. On s'imposera donc de faire en sorte que:

$$\Delta T \leqslant 1^{\circ}, \tag{1}$$

jusqu'à 3 000 °K. Cela est actuellement suffisant; les photométristes de l'avenir seront sans doute en droit d'exiger mieux. On verra dans la suite de ce mémoire qu'il n'est pas interdit d'espérer leur donner satisfaction. C'est pourquoi on a voulu que la précision avec laquelle la température du corps noir à réaliser se maintiendra dans le temps soit notablement supérieure, quelles que soient les fluctuations et les dérives possibles, à la précision actuellement imposée par la mesure de cette température.

En résumé, les conditions que nous avons désiré réaliser sont les suivantes:

— la température du corps noir pourra être fixée dans l'échelle internationale avec une incertitude inférieure où égale à 1 °K;

— la température du corps noir sera fixée dans le temps avec une incertitude égale à la moitié de l'incertitude précédente (0,5 °K).

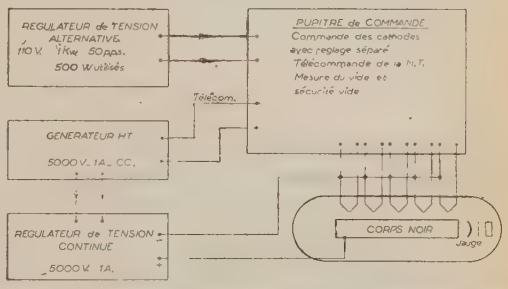

Fig. 1. – Schéma de principe pour le montage du corps noir.

2. – Description succincte de l'appareillage.

A) MODE DE CHAUFFAGE. – On a étudié un moment un corps noir chauffé par haute fréquence à cause des dispositions très symétriques et relativement très accessibles au calcul que cette méthode de chauffage permet d'employer. La solution a été finalement écartée à cause de la complexité de l'appareillage à mettre en œuvre et l'on a définitivement choisi le chauffage électronique.

La fig. 1. donne le schèma de l'installation. Le corps noir qui sera décrit un peu plus loin est placé dans le vide. Il est chauffé par bombardement électro-

nique, les électrons étant fournis par une cathode chaude. Le système de chauffage comprend donc:

— un générateur de courant alternatif destiné à chauffer les cathodes émissives;

— un générateur de haute tension continue destiné à accélérer les électrons qui tombent sur le corps noir.

Chacun de ces générateurs devant fournir une tension et un débit stables doit être muni d'un système de régulation.

B) Détails de réalisation. – Décrivons brièvement le corps noir proprement dit. C'est un crayon de tungstène dont la construction et la forme sont données par la fig. 2. Il a 60 mm de long et 8 mm de diamètre. Il est percé de

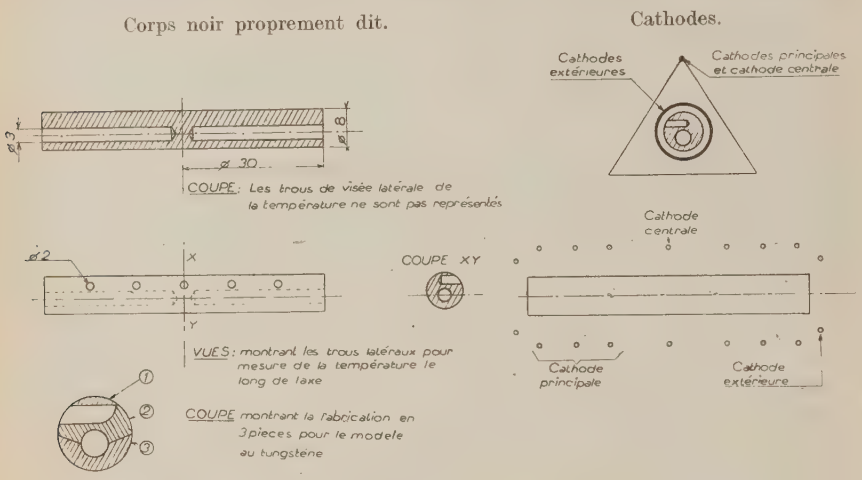

Fig. 2.

deux trous cylindriques de 3 mm de diamètre dont chacun constitue un étalon distinct. L'aire utile de ces étalons est d'environ 5 mm², ce qui correspond à une intensité disponible comprise entre 27 et 144 candélas entre 2 500 et 3 000 °K. On voit aussi, sur la fig. 2, que le cylindre de tungstène est percé à intervalles équidistants d'un certain nombre de petits trous qui fonctionnent comme des corps noirs auxiliaires et qui permettent de vérifier que le gradient de température le long du cylindre de tungstène est assez faible. On notera que cette condition n'est pas théoriquement nécessaire puisque c'est le fond du trou à température bien définie qui fournit le rayonnement étudié. Sa réalisation est cependant en pratique très désirable.

Il existe deux méthodes d'usinage d'un tel radiateur en tungstène. Dans la première, on part de lingots de tungstène pur tels qu'ils sont obtenus par concrétion dans la métallurgie de ce métal. On le travaille à la meule. Les différentes pièces de l'assemblage constituent le corps noir. Dans une seconde méthode, on part d'un alliage de tungstène et de cuivre a 95% de tungstène. L'usinage est fait avec cet alliage relativement facile à travailler. Une série

de préchauffages réalisés dans le vide évaporent le cuivre et laissent un lingot de tungstène pur. Le radiateur est, en général, légèrement déformé quand cette évaporation est terminée, ce qui est d'ailleurs sans importance.

La surface de rayonnement total d'un tel radiateur est d'environ 16 cm², ce qui représente une dépense d'énergie considérable. Le tableau n. 2 indique ces dépenses d'énergie, en admettant pour le tungstène, à la temperature d'utilisation, un pouvoir absorbant de 0,4:

TABLEAU II.

Température absolue	Puissance dissipée	
	Corps noir	Tungstène
2 000 °K	$91 \times 16 = 1\,500$ W	600 W
3 000 °K	$462 \times 16 = 7\,400$ W	3 000 W

Ce sont ces puissances considérables qui doivent être stabilisées.

C) PRÉCISIONS SUR LES TENSIONS D'ALIMENTATION. – Les tables relatives au rayonnement du tungstène montrent que l'on peut admettre que les fluctuations de température du radiateur seront, dans le domaine qui nous occupe, égales aux fluctuations de puissance divisées par 4,6:

$$\frac{\Delta T}{T} = \frac{1}{4{,}6}\frac{\Delta P}{P} \qquad (2)$$

Posons, conformément à ce qui précède, que ces variations de température ne dépasseront par 0°,5:

$$\frac{\Delta T}{T} \leqslant 0{,}5^{\circ}. \qquad (3)$$

Il vient de (2) et (3):

$$\frac{\Delta P}{P} \leqslant 4{,}6\,\frac{0{,}5}{3000} = 7{,}6 \cdot 10^{-4} \qquad (4)$$

à 3 000 °K, c'est-à-dire dans les conditions les plus défavorables.

Appelons V_A la tension de bombardement, I_C le courant fourni par les cathodes chaudes, courant très voisin du courant de saturation. On a:

$$\frac{\Delta P}{P} = \frac{\Delta V_A}{V_A} + \frac{\Delta I_C}{I_C} \leqslant 7{,}6 \cdot 10^{-4}. \qquad (5)$$

Quel est le poids qu'il convient de donner à chacun des deux termes de cette somme? On doit se souvenir que I_C sera fourni par une émission thermoionique: I_C dépend de la puissance P utilisée par le chauffage des cathodes, puissance qui dépend elle-même de la tension de chauffage de celle-ci V_C.

Supposons les cathodes également construites en tungstène. Après étude,

on a adopté pour obtenir un compromis entre un rendement et une vie moyenne suffisante, la température de fonctionnement 2 400 °K, pour laquelle on a:

$$\frac{\Delta I_C}{I_C} = 7{,}5\,\frac{\Delta V_C}{V_C}\,, \tag{6}$$

donc:

$$\frac{\Delta P}{P} = \frac{\Delta V_A}{V_A} + 7{,}5\,\frac{\Delta V_C}{V_C}\,. \tag{7}$$

L'identité de principe des 2 régulateurs utilisés permet d'obtenir:

$$\frac{\Delta V_A}{V_A} \# \frac{\Delta V_C}{V_C}\,. \tag{8}$$

En désignant la valeur commune de ces 2 rapports par $\Delta V/V$, (7) s'écrit:

$$\frac{\Delta P}{P} = 8{,}5\,\frac{\Delta V}{V}\,, \tag{9}$$

et en portant dans (5) il vient:

$$\frac{\Delta V}{V} \leqslant \frac{7{,}6}{8{,}5}\cdot 10^{-4} = 0{,}9\cdot 10^{-4}\,. \tag{10}$$

D) Précision sur la mesure photométrique. – Le repérage de la température dans l'échelle internationale, se fait par rapport à un point fixe de cette échelle (la solidification du platine) par comparaison entre la brillance de notre étalon et celle de l'étalon primaire. Après étude, nous avons décidé d'utiliser une méthode de pyrométrie optique monochromatique. Supposons que nous utilisons une longueur d'onde voisine de 5 000 Å, soit T la température à repérer et X le rapport des pouvoirs émissifs des deux corps noirs, on aura à 3000 °K:

$$\frac{\Delta T}{T} = \frac{1}{9{,}5}\,\frac{\Delta X}{X} \quad \text{donc} \quad \frac{\Delta X}{X} = 9{,}5\,\frac{\Delta T}{T}\,. \tag{11}$$

Pour définir la température de l'étalon auxiliaire à 1 °K près, il faut donc réaliser 1/300 sur X. Si on veut atteindre 0,5 °K, conformément aux conditions posées ci-dessus, il faudra savoir déterminer X à moins de 1/600 près.

On va maintenant décrire les parties de l'appareillage qui constituent une réalisation originale.

3. – Les régulateurs.

A) Généralités. – Ils sont d'un type particulier et reposent sur l'emploi d'un pont de Wheatstone qui joue le rôle d'un étalon de tension et qui fonctionne comme un bolomètre.

Le principe général de régulation que nous avons imaginé repose sur l'emploi d'un organe qui peut être considéré comme un étalon de tension.

Il s'agit d'un pont de Wheatstone constitué pour 2 des résistances, placées dans des branches opposées, de résistances en gros fil maintenues à une température sensiblement constante, et, pour les deux autres résistances, de fils fins en tungstène maintenus dans le vide. Un tel pont ne peut être accordé que pour une valeur donnée de la tension aux bornes, du fait que la résistance des fils de tungstène dépend du courant qui les traverse. Ce pont est alimenté par la tension à stabiliser (tension continue ou tension alternative) et l'effet régulateur est obtenu par un moyen convenable que nous décrirons plus loin à partir du déséquilibre du pont. Il convient d'insister sur les efforts apportés dans la réalisation de ce pont pour qu'il présente un caractère métrologique. L'ensemble du pont baigne dans du pétrole maintenu en circulation de façon que la température en soit uniforme et qu'il subisse un refroidissement continuel. Les résistances en tungstène se présentent sous la forme d'ampoules scellées et très soigneusement dégazées. Aucun contact serré ou vissé ne se présente dans la chaîne des résistances, les fils de tungstène (25 μ) se trouvant brasés sur des arrivées en molybdène. D'autre part, les fils de tungstène sont soutenus par des supports élastiques en mica, qui ont été étudiés spécialement de façon à maintenir les fils tendus malgré la dilatation dûe à l'échauffement. Ces fils travaillent, en effet, entre 300 et 400 °C. On a mesuré, d'autre part, individuellement, le coefficient de température des résistances en tungstène quand celles-ci sont traversées par leur courant normal d'utilisation et on a donné, à chaque résistance froide du pont, un coefficient de température égal, en les réalisant par deux métaux différents (nichrome et cuivre).

Pour exposer la suite du fonctionnement des régulateurs il convient de séparer le régulateur destiné au chauffage des cathodes de celui qui est destiné à la tension de bombardment.

B) Régulateur destiné au chauffage des cathodes. – Ce régulateur doit stabiliser une puissance alternative à la fréquence de 50 périodes par seconde, dont la valeur est de l'ordre de 600 W. Nous avons réalisé dans ce but un régulateur capable de stabiliser une puissance de 1 kW soit sensiblement 9 ampères sous 110 volts. Comme nous l'avons déjà indiqué, la tension est appliquée aux bornes d'un pont étalon (fig. 3). La tension qui sort de ce pont dans le cas où il n'est pas en équilibre, est amplifiée et appliquée à une sorte de rhéostat électronique placé en série sur le secteur d'alimentation. C'est l'action de ce rhéostat électronique qui a pour effet de produire une chute de tension compensant aussi exactement que possible les fluctuations du secteur d'alimentation. Ce rhéostat électronique est composé succinctement de triodes disposées symétriquement et attaquées à travers le transformateur par le circuit à réguler, tandis que leur grille est contrôlée par une tension amplifiée provenant du déséquilibre du pont. Il convient de signaler que, vu la valeur relativement faible de la fréquence, valeur faible par rapport à l'inertie des filaments des fils de tungstène, la résistance de ceux-ci se trouve modulée de façon notable à la fréquence de 100 périodes. Il s'en suit:

a) que la tension aux bornes de ces résistances de tungstène contient une composante notable à 150 périodes;

b) que cette tension contient également, même si le pont est à l'équilibre, une composante à 50 périodes qui n'est pas en phase avec la tension d'alimentation.

Il est alors nécessaire pour obtenir l'équilibre du pont d'introduire un terme

réactif dans l'une des branches sous la forme d'une capacité variable convenable. Il est également nécessaire, sur la chaîne amplificatrice, de prévoir un filtre destiné à arrêter du 150 périodes et d'autres tensions parasites de fréquences plus élevées pouvant être véhiculées par le secteur (par exemple, la tension pour la télécommande des divers relais de compteur). Diverses pré-

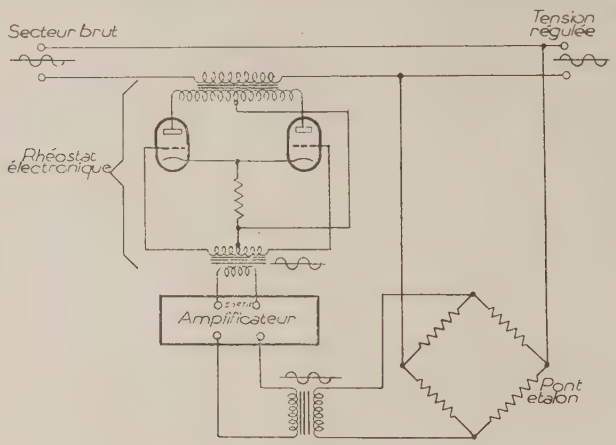

Fig. 3. – Régulateur de tension alternative. Schéma de principe.

cautions doivent être prises pour limiter ou corriger les déphasages le long de la chaîne amplificatrice, car ces déphasages provoquent, lorsqu'on augmente la fréquence et du même coup le coefficient de régulation de l'appareil, l'apparition d'oscillations entretenues qui ont pour effet de limiter la valeur du coefficient de régulation. Nous avons pu obtenir, au prix de réglages exceptionellement bien étudiés, avec ces régulateurs, des coefficients de régulation supérieurs à 1 000. En pratique, ils donnent couramment et en se tenant loin des conditions d'auto-oscillation, un coefficient de régulation égal à 500. Il convient de noter que ce régulateur stabilise la valeur efficace de la tension, ce qui est précisément le but cherché pour une tension de chauffage des cathodes. On voit qu'un coefficient de régulation de 500 permettra de maintenir la tension constante à $\pm 10^{-4}$ près, tant que la variation du secteur ne dépasse pas $\pm 5\%$.

En pratique, les variations rapides du secteur n'atteignent que très rarement ces valeurs et, en ce qui concerne les dérives lentes, si jamais, ce qui est peu probable, elles dépassaient $\pm 5\%$, il est possible de les corriger au moyen d'un auto-transformateur disposé sur l'appareil.

A vrai dire, l'instabilité essentielle de la tension obtenue avec un tel coefficient de régulation n'est guère dûe qu'aux fluctuations accidentelles de l'étalon de tension utilisé, c'est-à-dire le pont de résistances; aussi, un soin assez considérable a-t-il été apporté à la construction de ce pont et nous avons pu constater expérimentalement que ce régulateur était capable de stabiliser une puissance de 1 kW en ne laissant subsister que des fluctuations de tension se présentant sous forme rapide de l'ordre de 10^{-5}. Les dérives lentes que

l'on peut observer sont de l'ordre de $2 \cdot 10^{-4}$ à l'heure et, en outre, elles sont rigoureusement monotones, donc aisément corrigeables manuellement.

c) Régulateur pour la tension de bombardement. – Le régulateur pour la tension de bombardement est destiné à être inséré en série avec un générateur de tension continue susceptible de fournir 1 ampère sous 5000 volts. Dans l'ensemble, le principe de fonctionnement de ce régulateur est identique à celui que nous venons de décrire. Toutefois, quelques différences viennent, d'une part, de la tension de chauffage du pont qui est ici continue et, d'autre

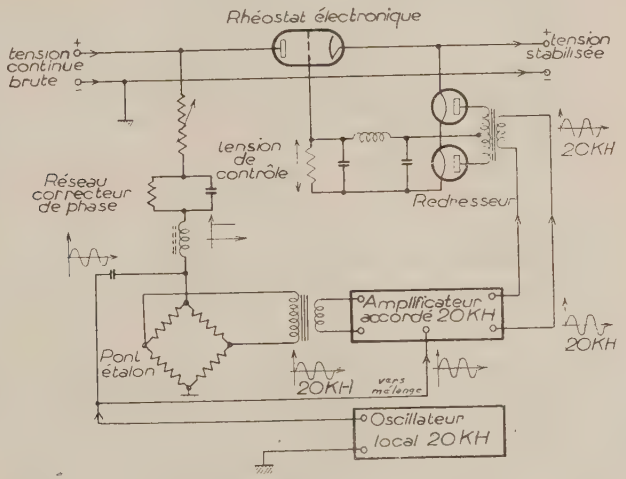

Fig. 4. – Régulateur de tension continue. Schéma de principe.

part, de la nature du rhéostat électronique à utiliser, ce rhéostat devant travailler en courant continu et non pas en courant alternatif (fig. 4). Pour déceler les déséquilibres du pont, une tension alternative fournie par un générateur auxiliaire à la fréquence de 20 kHz est superposée à la tension continue de l'alimentation. L'amplitude de cette tension auxiliaire a été choisie assez petite pour que les fluctuations éventuelles ne produisent pas des variations notables de la température des résistances du pont. La fréquence de travail étant assez élevée, un terme réactif de règlage, sous la forme d'une capacité variable, a été introduit sur l'une des branches du pont. On a dû prendre également pour constituer le transformateur de sortie du pont toutes les précautions nécessaires en un pareil cas, précautions qui ont d'ailleurs été également prises pour le pont du régulateur de tension alternative (fig. 5).

La tension provenant du déséquilibre du pont est amplifiée jusqu'à un niveau convenable et appliquée à un système qui joue le rôle de discriminateur de phase, de telle sorte que la tension redressée obtenue oscille autour d'une valeur moyenne dans un sens ou dans l'autre suivant le sens du déséquilibre du pont. La tension redressée ainsi obtenue est appliquée entre grille et cathode de tubes triodes placés en série sur la source à stabiliser. La variation de la

tension grille produit une variation de la chute de tension dans ces tubes qui doit compenser, aussi exactement que possible, les fluctuations de la source à stabiliser. Ici encore des précautions convenables ont été prises pour limiter ou diminuer le déphasage introduit dans la chaîne de régulation. La faculté que l'on a d'utiliser dans cet appareil une fréquence relativement élevée permet d'obtenir des valeurs du coefficient de régulation supérieures à celles qui étaient

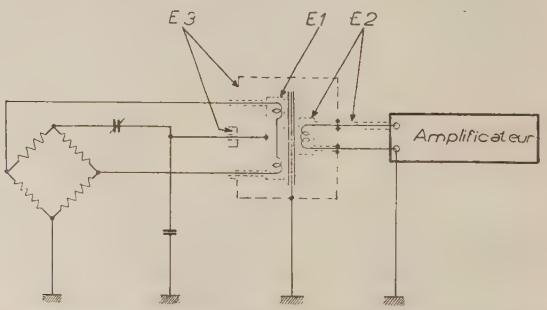

Fig. 5. – Schéma montrant la constitution du transformateur de liaison pont-amplificateur pour éliminer l'influence des capacités parasites.

fournies par le régulateur de tension alternative. Pour des réglages très soignés, on peut obtenir aisément un coefficient de régulation de 2 000 et, en fonctionnement normal et très éloigné des conditions d'auto-oscillation, on obtient couramment un coefficient de régulation de 1 000.

Les dérives et fluctuations propres à ce régulateur sont identiques à celles observées pour le régulateur de la tension de chauffage des cathodes.

On en conclut que chacun de ces régulateurs permet, moyennant une surveillance permettant la correction des grandes variations du secteur alternatif, de tenir largement la condition (10) au chapitre 2, paragraphe *C*.

4. – Mesures photométriques pour le répérage de la température.

Le principe fondamental du photomètre est de permettre la comparaison de deux flux à un rythme relativement très rapide, ce qui limite l'influence habituelle des dérives des sources d'alimentation, quand on utilise un détecteur photoélectrique. De plus, la comparaison, bien que s'effectuant à un rythme très rapide, est permanente, ce qui permet d'effectuer une mesure en autant de temps qu'on le veut, et par conséquent, de diminuer la bande passante de l'appareil de mesure final dans une proportion telle que le bruit de fond soit considérablement réduit.

L'appareil, se compose d'abord d'un système optique (fig. 6) qui permet d'amener simultanément les deux flux à comparer sur la cathode d'une cellule photoélectrique. L'un des flux est toujours en provenance d'une source auxiliaire que nous appelons « source tare ». Ce flux doit pouvoir varier dans

un rapport connu, aussi avons-nous adopté comme moyen de variation la loi des distances.

La lampe-tare est montée sur un banc d'optique et éclaire un diaphragme D.

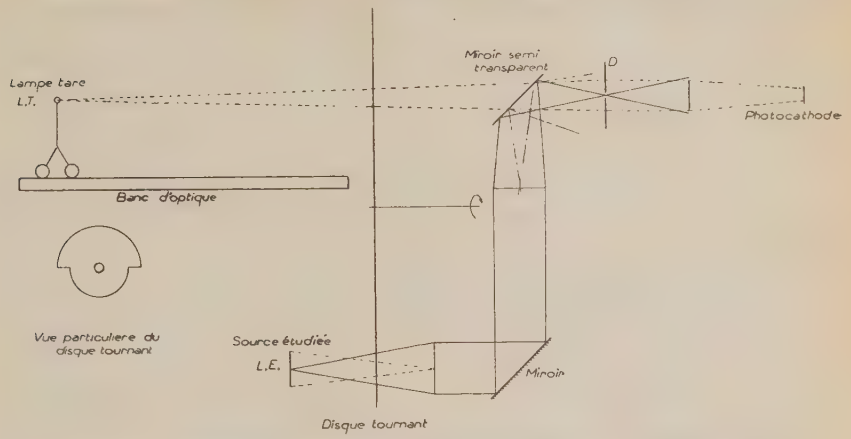

Fig. 6. – Disposition schématique de la partie optique du photomètre.

La suite de l'appareil est conçue de telle sorte que l'image de D soit formée sur la cathode photoélectrique, aucun diaphragme ultérieur ne limitant le flux envoyé par la lampe-tare LT à travers D. On peut exprimer cette dernière condition en disant que D est pupille d'entrée pour le système optique vis-à-vis

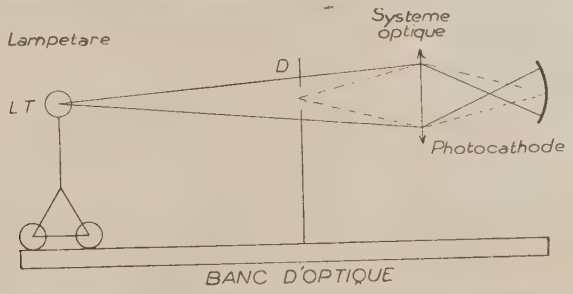

Fig. 7. – Schéma illustrant les propriétés de l'ensemble lampe tare/système optique photocathode.

de L.T., quoique cette expression soit, dans une certaine mesure, incorrecte du fait que le système optique n'a pas pour but de fournir en définitive une image de L.T. (fig. 7).

Le second flux provient de l'une des sources à comparer. Par un système optique convenable on forme sur D l'image de la source, de telle sorte que cette dernière recouvre entièrement D, et que de plus l'ouverture des faisceaux tombant sur D, en provenance d'un point de la source, soit supérieure à l'ouver-

ture des faisceaux issus de D et s'appuyant à la pupille d'entrée du système optique ultérieur. On voit que le diaphragme D joue ici, vis-à-vis de la source étudiée, le rôle de diaphragme de champ.

Un tel dispositif assure que le flux envoyé sur la cathode photoélectrique

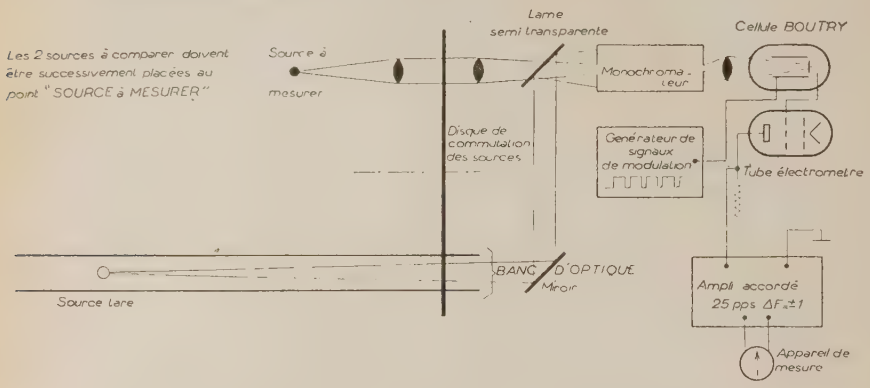

Fig. 7-*bis*. – Schéma de principe pour le photomètre.

par la source étudiée LE ne dépend que de la brillance de cette source, au facteur de transmission près de l'optique formant sur D l'image de LE.

Le photomètre ainsi monté optiquement permet donc la comparaison:

a) d'un flux en provenance d'une source tare, réglable en valeur relative;

b) d'un flux en provenance de l'une des sources à comparer, proportionnel

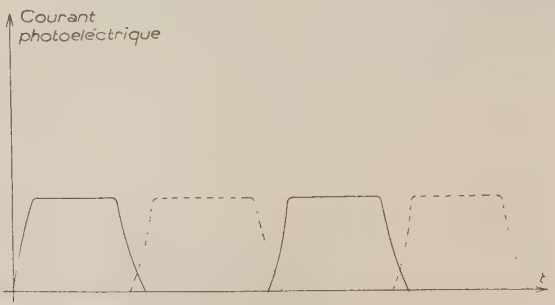

Fig. 8. – Allure du courant photoélectrique quand la cellule photoélectrique est alimentée sous tension continue.

à la brillance de cette source, le coefficient de proportionnalité étant une constante de l'appareil.

Nous allons décrire maintenant comment l'appareil permet de déceler l'égalité des courants photoélectriques provoqués séparément par les deux flux.

Un disque tournant permet l'occultation individuelle et périodique de

chaque source. Ce disque sera actionné par un moteur synchrone tournant à raison de N tours par seconde, par exemple 25.

On peut alors représenter grossièrement la forme du courant photo-électrique (fig. 8) dans le cas où la tension anodique de la cellule photoélectrique est une tension continue.

On obtient une série de paliers de courant qui auraient même ordonnée si les flux avaient la même action photoélectrique. Ces paliers sont séparés par des établissements de régime correspondant au cas où le disque coupe une partie d'un faisceau seulement. Ces régimes transitoires, quoique d'allures voisines, ne sont pas nécessairement identiques pour les deux flux, de telle sorte qu'on ne peut pas considérer que les lois de variation des courants en provenance des deux sources soient les mêmes.

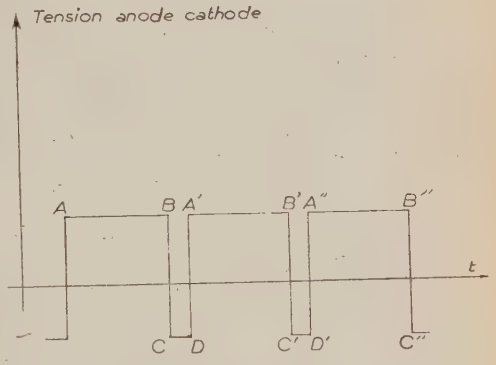

Fig. 9. – Tension d'alimentation de la cellule photoélectrique.

Or le fonctionnement de l'appareil réside, comme on le verra plus loin, dans le fait que les deux courants photoélectriques ont la même loi de variation en fonction du temps. Ce résultat est obtenu en appliquant à la cellule, entre anode et cathode, non pas une tension continue mais une tension en forme de signaux rectangulaires représentée par la fig. 9. Les paliers AB, $A'B'$, etc., sont contenus à l'intérieur des intervalles de temps pendant lesquels le disque tournant occulte entièrement l'un des faisceaux et leur sont inférieurs. Les paliers CD, $C'D'$, etc., contiennent entièrement les intervalles de temps pendant lesquels le disque occulte partiellement l'un des faisceaux. Il s'en suit que, pendant les intervalles de temps tels que CD, $C'D'$, etc., le courant photoélectrique est rigoureusement nul, tandis que le reste du temps il se présente sous des signaux rectangulaires, dûs à chacune des sources, qui sont rigoureusement identiques et les signaux peuvent être rendus superposables au moyen d'une affinité de rapport convenable par rapport à l'axe des temps.

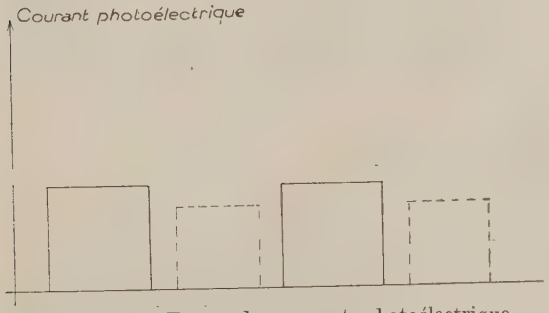

Fig. 10. – Forme du courant photoélectrique.

Les signaux rectangulaires appliqués comme tension d'alimentation de la cellule sont à la fréquence $2N$, soit pour l'exemple pris précédemment de 50 Hz (fréquence du secteur alternatif).

On voit aisément sur la fig. 10 que, si les effets photoélectriques des deux flux sont identiques, les rectangles successifs seront identiques, donnant un courant contenant un spectre de fréquences harmoniques dont le fondamental est $2N$. Si, au contraire, les deux effets sont différents, deux paliers successifs n'auront pas mêmes ordonnées et le fondamental sera N.

La détection de l'égalité des deux effets photoélectriques revient donc à déceler l'absence ou la présence, dans le courant photoélectrique, de la composante de fréquence N. Elle s'obtiendra par l'emploi d'un amplificateur accordé sur la fréquence N, de gain convenable.

Cet amplificateur sera terminé par un indicateur de niveau, et il pourra présenter une bande passante très étroite (1 à 2 périodes pour un ampli accordé sur 25 périodes). Il devra présenter une atténuation très élevée pour tous les harmoniques.

On voit que l'intérêt de ce photomètre réside dans les deux propriétés fondamentales suivantes:

1) Il compare, de façon quasi-instantanée, et à la façon d'un appareil de zéro. La comparaison entre les deux grandeurs étant directe, la dérive des appareils de mesure n'intervient pas, sauf sous la forme d'un bruit de fond de chaque grandeur (les deux courants photo-électriques).

2) La comparaison peut durer aussi longtemps qu'on le veut, ce qui permet d'accepter une durée notable de la mesure, d'où la possibilité pour l'appareil de mesure d'une bande passante très étroite, et de là une réduction importante du bruit de fond.

Voici très brièvement les résultats qu'on obtient avec cet appareil:

Il est parfaitement possible d'apprécier l'égalité des deux flux de l'ordre de 0,6 erg/s avec une erreur relative qui sera certainement inférieure à 10^{-4} et probablement même plus petite que 10^{-5}. Nous parlons ici de l'erreur inhérente à la partie proprement électrique de la chaîne cellule-amplificateur.

Un tel flux lumineux peut être obtenu à l'aide d'un corps noir à température de solidification du platine pourvu qu'on utilise un objectif d'ouverture raisonnable $O/F = 0{,}1$.

5. – Erreur sur la mesure de la température.

Pour étudier cette erreur, nous nous placerons par exemple dans le cas où il s'agit d'amener le corps noir à une température fixée d'avance.

Si nous utilisions pour le photomètre des flux rigoureusement monochromatiques, il nous suffirait de déterminer, par application de la formule de Planck, les valeurs de flux monochromatiques émis par le corps noir à la température désirée, d'une part, et par le corps noir à la température de fusion du platine, d'autre part. Il conviendrait alors, au moyen du photomètre, de s'assurer que la température du corps noir a bien été règlée de telle sorte que le rapport des flux ait la valeur calculée. En pratique, on utilisera une certaine largeur de bande (100 Å) et le calcul des rapports des actions photométriques des deux flux devra tenir compte de la sensibilité de la couche photoélectrique utilisée

à l'intérieur de la bande, ainsi que de la composition spectrale de l'énergie émise par le corps noir à l'intérieur de la bande. Outre la complication de calcul introduite par cette circonstance, il apparaît une erreur due à l'incertitude sur la courbe de réponse globale du système monochromateur-cellule. Il convient de noter que cette courbe de réponse pourra être établie au moyen du photomètre spécial lui-même et par conséquent être déterminée avec une

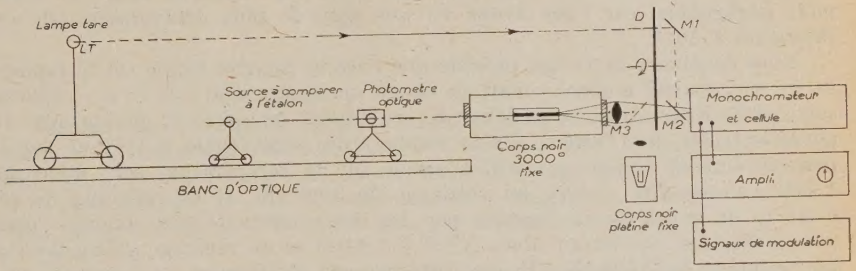

Dig. 11. – Montage pour l'utilisation normale du corps noir à température reglable.

précision notable. Nous avons admis que l'erreur sur le relevé de la courbe de réponse était, en valeur absolue, au plus égale à $\pm 2\%$ de la valeur maximum du coefficient de transmission relatif à cette courbe de réponse. En pratique, la mesure de la température se déroule comme suit:

1) Calcul du rapport des courants photoélectriques imputables au corps noir platine, d'une part, et au corps noir à ajuster, d'autre part, en admettant que ces corps noirs sont placés à la même distance d'un même diaphragme limitant les flux lumineux qu'ils envoient sur la cathode photoélectrique à travers le monochromateur. Ce calcul, comme nous l'avons dit, comporte un certain degré d'incertitude concernant la courbe de réponse globale monochromateur-cellule. Il s'en suit que le rapport ainsi défini, ne l'est qu'avec une certaine erreur dont le module est limité par une quantité ε_B. Nous appelons habituellement cette erreur « erreur due à la largeur de bande ». Nous avons effectué son calcul en prenant comme base d'erreur sur la courbe de réponse globale monochromateur-cellule, celle que nous venons de citer et dans le cas où le monochromateur a une courbe de réponse triangulaire, telle que la base du triangle corresponde à 200 Å (dans le langage des opticiens cela revient à une bande de 100 Å). Nous avons trouvé $\varepsilon_B = 0{,}0018$.

2) Ce calcul étant fait, on détermine les deux positions que doit occuper la source tare sur son banc d'optique, de façon qu'elle puisse équilibrer, sur la cathode photoélectrique, les flux provenant soit d'un corps noir, soit de l'autre. La source tare sera alors placée à chacune de ces positions suivant le cas. En pratique, une certaine erreur se produira sur la position de la source tare. Pour en juger, il convient de noter que sa distance au diaphragme doit varier dans le rapport 10, de telle sorte qu'elle sera située sensiblement, soit à 1 m soit à 10 m du diaphragme. Si nous considérons raisonnablement que sa distance au diaphragme peut être mesurée à 1 mm près, nous voyons que l'erreur relative sur les mesures de la distance sera de 10^{-3} dans le cas de la comparaison au corps noirs platine et de 10^{-4} dans le cas de la comparaison

au corps noir à 3 000 °K. L'erreur sur le flux lumineux envoyé sera le double de l'erreur sur la distance et il n'y a lieu de prendre en considération que celle qui intervient lors de la comparaison au corps noir platine, soit, ramenée au pouvoir émissif, une erreur $\varepsilon_T = 0{,}002$. Nous appelons cette erreur « erreur due à la source tare ».

3) Pour chacune des comparaisons source tare-corps noir, le zéro doit être détecté au photomètre. L'erreur introduite par l'appareil peut être tenue pour négligeable, car nous avons vu que dans le plus défavorable, elle est inférieure à 10^{-4}.

Nous concluons de ce qui précède que l'erreur relative totale sur le rapport du pouvoir émissif monochromatique est au maximum égal à $\varepsilon_B + \varepsilon_T = 0{,}0038$, soit: 1/260. Nous avons vu au début de cet exposé (chapitre 2, paragraphe *D*, équation (11)) que l'erreur sur la température était égale à l'erreur sur le pouvoir émissif divisée par 9,5. L'erreur sur la température sera donc de: 1/2500, c'est-à-dire $\pm$ 1°,2, au voisinage de 3 000 °K. Il est possible de réduire ε_B de moitié et ε_T d'autant par des déterminations très soignées, mais peu commodes. On aurait alors $\Delta T/T \leqslant 1/5\,000$ et un repérage voisin de 0°,6 au voisinage de 3 000 °K. Il est certainement intéressant de constater que dans cet appareil, pour la première fois, ce n'est plus la mesure des flux qui limite la précision des pointés.

RIASSUNTO (*)

Gli Autori descrivono una nuova apparecchiatura messa a punto al Conservatoire National des Arts et Métiers di Parigi per la determinazione dell'intensità di brillanza visuale delle sorgenti luminose.

(*) *A cura della Redazione.*

INFORMAZIONI

Aderendo ad una richiesta del prof. Bruno Borghi, Presidente del Comitato promotore per le onoranze a Gaspare Barbèra in occasione del 1° centenario della fondazione della Casa editrice omonima, s'informano i lettori che detto Comitato ha aperto un *Concorso nazionale per testi scolastici* nelle varie discipline e, in particolare, per la Fisica (premio L. 500 000). Il tempo utile per la presentazione dei lavori è fino al 31 Marzo 1952.

Inoltre è stata costituita la « Fondazione Gaspare Barbèra » con le seguenti finalità: promuovere, con relazioni e discussioni e con la pubblicazione di scritti, lo studio dei problemi della Scuola e della formazione culturale, umanistica e tecnica, degli studenti italiani; contribuire, con borse di studio e con l'offerta di libri, ad aumentare le possibilità di accedere e di seguire i vari corsi di studi per i giovani più meritevoli e di disagiata condizione economica.

Infine la Casa editrice Barbèra, aderendo all'invito del Comitato, per onorare la memoria del suo fondatore e per contribuire tangibilmente alla benemerita iniziativa, ha destinato, come sede della Fondazione, la storica Villa della Cisterna in Firenze, restituendola all'antica dignità e alle sue tradizioni patrie e umanistiche.

Chi voglia avere maggiori informazioni circa queste iniziative fiorentine, si rivolga direttamente alla Segreteria del Comitato per le onoranze a Gaspare Barbèra, presso l'Università degli Studi di Firenze - Piazza S. Marco, 4.

Direttore responsabile: G. POLVANI

Tipografia Compositori - Bologna

Questo fascicolo è stato licenziato dai torchi il 23-II-1951